

# Molecular Plant

## Robust transcriptional indicators of immune cell death revealed by spatio-temporal transcriptome analyses

--Manuscript Draft--

|                                    |  |
|------------------------------------|--|
| <b>Manuscript Number:</b>          | MOLECULAR-PLANT-D-21-00855R2   |
| <b>Full Title:</b>                 | Robust transcriptional indicators of immune cell death revealed by spatio-temporal transcriptome analyses  |
| <b>Article Type:</b>               | Resource Article   |
| <b>Manuscript Classifications:</b> | 2.27: programmed cell death / apoptosis; 3.11: gene expression; 5.08: plant-microbe interactions   |
| <b>Keywords:</b>                   | Arabidopsis thaliana; Cell Death Indicator; Effector-Triggered Immunity; hypersensitive response; pattern-triggered immunity; plant immunity; Pseudomonas syringae   |
| <b>Corresponding Author:</b>       | Núria Sanchez Coll, PhD<br>Centre for Research in Agricultural Genomics<br>Cerdanyola del Vallès, Barcelona SPAIN  |
| <b>First Author:</b>               | Jose Salguero-Linares  |
| <b>Order of Authors:</b>           | Jose Salguero-Linares<br>Irene Serrano<br>Nerea Ruiz-Solani<br>Ujjal Jyoti Phukan<br>Víctor Manuel González<br>Martí Bernardo-Faura<br>Marc Valls<br>David Rengel<br>Núria Sanchez Coll, PhD   |
| <b>Abstract:</b>                   | <p>Recognition of a pathogen by the plant immune system often triggers a form of regulated cell death traditionally known as the hypersensitive response (HR). This type of cell death occurs precisely at the site of pathogen recognition, and it is restricted to a few cells. Extensive research has shed light into how plant immune receptors are mechanistically activated. However, a central key question remains largely unresolved: how does cell death zonation take place and what are the mechanisms that underpin this phenomenon? Consequently, bona fide transcriptional indicators of HR are lacking, which prevents gaining a deeper insight of its mechanisms before cell death becomes macroscopic and precludes any early or live observation. We addressed this question using the paradigmatic <i>Arabidopsis thaliana</i> – <i>Pseudomonas syringae</i> pathosystem, by performing a spatio-temporally resolved gene expression analysis that compared infected cells that will undergo HR upon pathogen recognition vs bystander cells that will stay alive and activate immunity. Our data revealed unique and time-dependent differences in the repertoire of differentially expressed genes, expression profiles and biological processes derived from tissue undergoing HR and that of its surroundings. Further, we generated a pipeline based on concatenated pairwise comparisons between time, zone and treatment that enabled us to define 13 robust transcriptional HR markers. Among these genes, the promoter of an uncharacterized AAA-ATPase has been used to obtain a fluorescent reporter transgenic line, which displays a strong spatio-temporally resolved signal specifically in cells that will later undergo pathogen-triggered cell death. In sum, this valuable set of genes can be used to define those cells that are destined to die upon infection with HR-triggering bacteria, opening new avenues for specific and/or high-throughput techniques to study HR processes at a single-cell level.</p> |
| <b>Suggested Reviewers:</b>        | Kenichi Tsuda  |

|                                  |   |
|----------------------------------|---|
|                                  | <p>Huazhong Agricultural University<br/> tsuda@mail.hzau.edu.cn<br/> Expert in plant-pathogen interactions, specialized in transcriptomic networks and gene expression analysis</p>   |
|                                  | <p>Moritz Nowack<br/> VIB-UGENT Center for Plant Systems Biology: Vlaams Instituut voor Biotechnologie<br/> Department of Plant Systems Biology<br/> Moritz.Nowack@psb.vib-ugent.be<br/> Expert in plant programmed cell death, gene expression networks, transcriptomics</p> |
|                                  | <p>Daniel Hofius<br/> Swedish University of Agricultural Sciences<br/> Daniel.Hofius@slu.se<br/> Expert in plant programmed cell death and plant-pathogen interactions</p>  |
|                                  | <p>Farid El Kasmi<br/> University of Tuebingen ZMBP<br/> farid.el-kasmi@zmbp.uni-tuebingen.de<br/> Expert in plant-pathogen interactions and plant programmed cell death</p>  |
| <p><b>Opposed Reviewers:</b></p> |   |

[Click here to view linked References](#)

# Robust transcriptional indicators of immune cell death revealed by spatio-temporal transcriptome analyses

**Running title: Plant HR indicators**

**Short summary:** Our work provides a detailed overview of the spatio-temporal transcriptomic landscape of the hypersensitive response (HR), a form of plant-specific immune cell death. Further, a set of robust transcriptional marker genes of the cells that will undergo HR is provided.

Jose Salguero-Linares<sup>a,#</sup>, Irene Serrano<sup>b, #,†</sup>, Nerea Ruiz-Solani<sup>a</sup>, Marta Salas-Gómez<sup>a</sup>, Ujjal Jyoti Phukan<sup>a</sup>, Victor Manuel González<sup>a</sup>, Martí Bernardo-Faura<sup>a</sup>, Marc Valls<sup>a,b</sup>, David Rengel<sup>b,c,¥,§,\*</sup>, Nuria S. Coll<sup>a,d,§,\*</sup>

<sup>a</sup> *Centre for Research in Agricultural Genomics (CRAG), CSIC-IRTA-UAB-UB, Campus UAB, Bellaterra, Barcelona, 08193, Spain*

<sup>b</sup> *LIPM, Universite de Toulouse, INRA, CNRS, 84195 Castanet-Tolosan, France*

<sup>c</sup> *INRAE, GeT-PlaGe, Genotoul, 31326 Castanet-Tolosan, France (doi: 10.15454/1.5572370921303193E12)*

<sup>d</sup> *Department of Genetics, Universitat de Barcelona, 08028 Barcelona, Spain*

<sup>e</sup> *Consejo Superior de Investigaciones Científicas (CSIC), Barcelona, Spain*

<sup>#,§</sup> *Equal contributions*

<sup>†</sup> *Current address: Department of Plant Molecular Biology and Physiology, Albrecht-von-Haller-Institute for Plant Sciences, University of Göttingen, Julia-Lermontowa-Weg 3, D-37077 Göttingen, Germany.*

‡ *Current address: Institut de Pharmacologie et de Biologie Structurale, IPBS, Université de Toulouse, CNRS, UPS, Toulouse, France*

\* *To whom correspondence should be addressed:*

*e-mail: [nuria.sanchez-coll@cragenomica.es](mailto:nuria.sanchez-coll@cragenomica.es)*

*Centre for Research in Agricultural Genomics (CRAG), CSIC-IRTA-UAB-UB*

*Campus UAB*

*Bellaterra, 08193*

*Spain*

*e-mail: [david.rengel@ipbs.fr](mailto:david.rengel@ipbs.fr)*

*Institut de Pharmacologie et de Biologie Structurale*

*BP 64182*

*205 route de Narbonne*

*31077 Toulouse Cedex 04*

*France*

**Conflict of interest statement:** The authors declare no conflict of interest.

## Abstract

Recognition of a pathogen by the plant immune system often triggers a form of regulated cell death traditionally known as the hypersensitive response (HR). This type of cell death occurs precisely at the site of pathogen recognition, and it is restricted to a few cells. Extensive research has shed light into how plant immune receptors are mechanistically activated. However, a central key question remains largely unresolved: how does cell death zonation take place and what are the mechanisms that underpin this phenomenon? Consequently, *bona fide* transcriptional indicators of HR are lacking, which prevents gaining a deeper insight of its mechanisms before cell death becomes macroscopic and precludes any early or live observation. We addressed this question using the paradigmatic *Arabidopsis thaliana*–*Pseudomonas syringae* pathosystem, by performing a spatio-temporally resolved gene expression analysis that compared infected cells that will undergo HR upon pathogen recognition *vs* by-stander cells that will stay alive and activate immunity. Our data revealed unique and time-dependent differences in the repertoire of differentially expressed genes, expression profiles and biological processes derived from tissue undergoing HR and that of its surroundings. Further, we generated a pipeline based on concatenated pairwise comparisons between time, zone and treatment that enabled us to define 13 robust transcriptional HR markers. Among these genes, the promoter of an uncharacterized AAA-ATPase has been used to obtain a fluorescent reporter transgenic line, which displays a strong spatio-temporally resolved signal specifically in cells that will later undergo pathogen-triggered cell death. In sum, this valuable set of genes can be used to define those cells that are destined to die upon infection with HR-triggering bacteria, opening new avenues for specific and/or high-throughput techniques to study HR processes at a single-cell level.

**Keywords:** *Arabidopsis thaliana*, Cell Death Indicator, Effector-Triggered Immunity, Hypersensitive Response, Pattern-Triggered Immunity, Plant Immunity, *Pseudomonas syringae*.

## 1 INTRODUCTION

2

3 Plants are rich sources of nutrients for pathogens with contrasting lifestyles (Dangl et al., 2013).

4 As opposed to animals, plants do not possess a circulatory system with mobile cells specialized

5 in pathogen defense (Jones and Dangl, 2006). Since their cells are fixed by their cell walls,

6 plants rely on each cell's autonomous immunity and on systemic signals emanating from

7 infection sites to distal cells to prime the plant for future pathogen encounters (Ausubel, 2005).

8 Moreover, instead of a somatic adaptive immune system that produces antigen receptors on

9 demand, plant cells are equipped with extracellular pattern-recognition receptors (PRRs) and

10 intracellular nucleotide-binding leucine-rich repeat immune receptors (NLRs) that recognize

11 microbe-associated microbial patterns (MAMPs) and pathogen effectors required for

12 virulence, respectively (Couto and Zipfel, 2016). PRR activation brings about a broad defense

13 response named pattern-triggered immunity (PTI), while NLR activation triggers a potentiated

14 and prolonged immune response named effector-triggered immunity (ETI) that reinforce

15 defense outputs observed during PTI (Yuan et al., 2021a; Ngou et al., 2021b). ETI often

16 culminates in a macroscopic localized cell death at the attempted pathogen ingress site known

17 as hypersensitive response (HR)-cell death or immune-related cell death (Olvera-Carrillo et al.,

18 2015; Balint-Kurti, 2019; Salguero-Linares and Coll, 2019).

19

20 Regulated cell death has a crucial role in both animals and plant immune responses. Extensive

21 research in the animal field supports the notion that the immune system is highly dependent on

22 cell death for a robust and tightly controlled immune response to occur (Lu et al., 2014; Nagata

23 and Tanaka, 2017) . In plants, our knowledge about the biochemical and genetic pathways

24 regulating cell death, particularly in the context of immunity, is still very limited. As an attempt

25 to shed light into how HR is orchestrated in plants, most efforts have been directed towards

26 understanding how NLRs are mechanistically activated, as well as identifying molecular  
27 components upstream or downstream of NLRs that are required for HR to occur (Dangl and  
28 Jones, 2019; Wang et al., 2019a; Wang et al., 2019b; Ma et al., 2020; Ngou et al., 2021a)

29

30 Plant NLRs can be broadly classified into TNLs and CNLs based on their domain composition:  
31 TNLs contain a Toll/Interleukin-1 Receptor (TIR), whereas CNLs harbor a coiled-coiled  
32 domain at their N-terminal end (Jones et al., 2016). Groundbreaking research has shown that  
33 in plants, pathogen perception leads to NLR oligomerization, which ultimately will result in  
34 cell death and immunity (Wang et al., 2019a; Wang et al., 2019b; Ma et al., 2020; Förderer et  
35 al., 2022). Oligomerized forms of CNLs can form pores at the plasma membrane that act as  
36 Ca<sup>2+</sup>-permeable channels (Wang et al., 2019a; Wang et al., 2019b; Jacob et al., 2021). Some  
37 TNLs, in turn, can oligomerize upon activation to reconstitute a holoenzyme that triggers cell  
38 death by a mechanism that is not fully elucidated but that may involve their NAD<sup>+</sup> hydrolase,  
39 as well as their 2',3'-cAMP/cGMP synthetase activities (Ma et al., 2020; Martin et al., 2020;  
40 Yu et al., 2021). How oligomerization translates to immune signaling and HR remains to be  
41 defined.

42

43 In the context of signaling downstream NLR activation or ETI, large-scale transcriptional  
44 studies have highlighted the importance of phytohormone networks for high-amplitude  
45 transcriptional reprogramming to mount a fast and efficient response (Mine et al., 2018).  
46 Comparisons between host transcriptional responses elicited by PTI and ETI suggest minor  
47 qualitative differences in the repertoire of genes differentially expressed (Navarro et al., 2004;  
48 Mine et al., 2018). These studies also support the recently evidenced assumption that ETI and  
49 PTI share immune signaling components (Pruitt et al., 2021; Yuan et al., 2021a; Ngou et al.,  
50 2021b). However, a central key question remains unexplored: which early transcriptional



51 signatures differentiate cells that recognize the pathogen and will undergo HR from by-stander  
52 cells that will remain alive and will activate defenses to fight the pathogen? In recent literature,  
53 a few studies underscore the importance of zonation during HR (Betsuyaku et al., 2018; Giolai  
54 et al., 2019; Lukan et al., 2020). At the hormonal level, it has been shown that salicylic acid  
55 (SA) plays a major role at pathogen-inoculated spots that will later undergo HR, while the  
56 jasmonic acid (JA) signaling pathway is activated in the cells surrounding the central SA-active  
57 cells (Dorey et al., 1997; Betsuyaku et al., 2018). Furthermore, precision transcriptomics during  
58 the immune response elicited by the potato Ny-1 gene against potato virus Y (PVY) revealed  
59 the importance of SA accumulation and genes involved in the generation of reactive oxygen  
60 species (ROS) for efficient confinement of macroscopic cell death lesions caused by PVY  
61 (Lukan et al., 2020). The cell wall polymer lignin has also been shown to participate in HR  
62 zonation, by forming a physical barrier around the infection site upon pathogen recognition  
63 that presumably contributes to confine the invading agents and restricts colonization (Lee et  
64 al., 2019). A transcriptional meta-analysis of developmental *vs* HR-cell death in plants could  
65 only reveal robust indicators for developmental cell death but not for HR-cell death (Olvera-  
66 Carrillo et al., 2015) . We realized that the limitation of previous large-scale transcriptomic  
67 analysis lacked the spatial dimension of HR (Lewis et al., 2015; Mine et al., 2018), as dying  
68 cells were not compared to by-stander cells, and the focus was not placed on identifying  
69 specific cell death markers, but rather bulk-analyzing the ETI response at the inoculated area.

70

71 A systematic gene expression analysis of the zonation of HR overtime would help  
72 understanding the process of HR at the molecular level and importantly, would allow defining  
73 *bona fide* transcriptional markers of the process. With this purpose, we generated RNA-  
74 sequencing (RNA-seq) data to systematically analyze and compare the transcriptional  
75 programs taking place at the zone of inoculation/pathogen recognition that will undergo HR vs

76 the surrounding area that will stay alive and activate immunity. We show unique and time-  
77 dependent differences in the repertoire of differentially expressed genes (DEGs) and  
78 expression profiles derived from tissue undergoing HR and that of its surrounding tissues.  
79 Furthermore, we generated a pipeline based on pairwise comparisons between time, zone and  
80 treatment that enabled us to define 13 robust transcriptional HR markers and a fluorescent  
81 transgenic reporter line. These valuable set of genes can be used to define those cells that are  
82 destined to die upon pathogen recognition before the onset of cell death becomes  
83 macroscopically visible, opening new horizons to study the processes therein by live, cell-  
84 specific and/or high-throughput techniques.

85

## 86 **RESULTS**

87

### 88 **Zonally dissected Arabidopsis transcriptomes upon *Pto AvrRpm1* infection reveal unique** 89 **spatio-temporal gene expression.**

90 In our experiments we used the paradigmatic interaction between *Arabidopsis thaliana* Col-0  
91 (hereafter Arabidopsis) and the bacterial pathogen *Pseudomonas syringae* pathovar tomato  
92 (*Pto*) carrying the effector *AvrRpm1* (hereafter *Pto AvrRpm1*), which triggers restricted HR at  
93 the site of inoculation upon recognition by the CNL RPM1 (RESISTANCE TO  
94 PSEUDOMONAS SYRINGAE PV MACULICOLA 1) (Mackey et al., 2002). In order to  
95 zonally dissect HR and its surrounding, we syringe-infiltrated a limited area (roughly 3-4 mm)  
96 at the side edge of Arabidopsis leaves with either a mock solution or *Pto AvrRpm1*. Collected  
97 tissue from this area was designated as the “IN” zone. To ensure proper separation between IN  
98 and OUT zones, a buffer zone expanding 1 mm next to the IN area was discarded, and a parallel  
99 region expanding 1 to 2 mm towards the vein was designated as “OUT” (**Figure 1A**). We  
100 collected tissue at 0, 1-, 2-, 4- and 6-hours post-inoculation (hpi), extracted RNA and assessed

101 transcript abundance by RNA-seq. Under these conditions, macroscopic cell death started  
102 appearing at 4 hpi in the *Pto AvrRpm1*-inoculated samples, as visualized by trypan blue staining  
103 (**Figure 1B**). As expected, this cell death is concomitant with a dramatic drop in photosynthetic  
104 efficiency of photosystem II (Fv/Fm ratio) and electron transport rate (ETR) at the IN area  
105 (**Figure 1C**) (Berger et al., 2007).

106

107 To determine whether the obtained RNA-seq data complied with our working hypothesis of  
108 spatio-temporal gene expression regulation we performed a Principal Component Analysis  
109 (PCA) (**Figure S1A-B**). We observed that at the IN area, *Pto AvrRpm1*-treated samples  
110 separated from their mock controls from 2 hpi onwards. At the OUT area, however, only *Pto*  
111 *AvrRpm1*-treated samples at 4 and 6 hpi separated from mock controls. Overall, the PCA  
112 confirms that the biggest changes in gene expression are produced at IN, particularly at 4 and  
113 6 hpi, whereas at OUT there is a subtler modulation that is most pronounced at 4 hpi.

114

115 Next, we identified differentially expressed genes (DEGs) between bacteria and mock-  
116 inoculated samples (DEGs; false discovery rate (FDR) < 0.05 and  $|\log_2FC| > 2$ ), thereby  
117 characterizing the transcriptional changes occurring at each tissue area at every time point. We  
118 found a total of 5,495 DEGs at the IN zone and 1,785 at the OUT zone (**Figure 2A, Table S1**).  
119 Enrichment of Gene Ontology (GO) terms was examined in every group of DEGs at each  
120 specific time point (**Figure S2, Table S2**). Upregulated genes at the IN area were enriched in  
121 immunity- and phytohormone-associated processes (**Figure S2A**). Immunity-related GO terms  
122 associated with PTI and ETI such as “plant-type hypersensitive response” and “pattern  
123 recognition receptor signalling pathway” appeared at initial stages of infection (1 and 2 hpi),  
124 while at later stages (from 2 hpi onwards) there is enrichment of GO terms associated with  
125 more general defense and abiotic stress processes such as “defense response to bacteria” and

126 “response to wounding”, respectively (**Figure S2A**). Regarding phytohormone-related  
127 processes, we observed an enrichment in SA-related GO terms from 1 hpi onwards, confirming  
128 the importance of SA at the HR/IN area (Dorey et al., 1997; Zheng et al., 2015). In contrast,  
129 GO terms associated with JA were particularly overrepresented at later time points (4 and 6  
130 hpi), in accordance with previous findings demonstrating that SA can activate JA signaling  
131 through a non-canonical pathway promoting ETI (Liu et al., 2016). GO terms related to other  
132 defense/stress-related phytohormones such as ethylene (ET) and abscisic acid (ABA), were  
133 also enriched at 4 and 6 hpi (**Figure S2A**).

134

135 Among downregulated genes at the IN zone, an enrichment in GO terms related to  
136 photosynthesis and chloroplast biology occurred at late time points (4 and 6 hpi) (**Figure S2B**).  
137 This correlates with the drop in photosynthetic efficiency shown in **Figure 1C**, which is part  
138 of the defense/yield trade-off to derive resources to immune responses and shut down  
139 production of sugars and nutrients, as they might serve as a source for pathogen survival and  
140 multiplication (Lu and Yao, 2018).

141

142 Strikingly, at the OUT area we only observed differential expression at late time points (4 and  
143 6 hpi), with an overall reduction in the number of DEGs compared to the IN area (**Figure 2A**).  
144 Upregulated genes were enriched in GO terms associated with hormonal regulation,  
145 particularly to the JA signaling pathway (**Figure S2C**). Downregulated genes at the OUT area  
146 did not show any enriched GO term, possibly due to the low number of genes.

147

148 To identify genes exclusively upregulated ( $FDR < 0.05$  and  $|\log_2FC| > 2$ ) at either the IN or  
149 OUT areas we first generated Venn diagrams representing the number of genes modulated at  
150 each time point upon infection (**Figure S3**). This analysis confirmed that upregulation at both

151 IN and OUT mainly occurs at 4 or 6 hpi (**Figure S3**) and therefore, we selected these two time  
152 points to further identify genes that are exclusively upregulated at each tissue area (**Figure 2B**).  
153 Specifically, we found a total of 1,840 genes being upregulated exclusively at IN, 1,117 genes  
154 upregulated at both IN and OUT and 221 genes being exclusively upregulated at OUT (**Figure**  
155 **2B, Table S3**). Among the overrepresented GO terms found in genes exclusive for the IN area  
156 were “defense response to bacterium”, “response to molecule of bacterial origin” or “response  
157 to salicylic acid”. We also found various GO terms associated with responses to several other  
158 stresses such as salt, oxygen-containing compounds, sulfur compounds, heat and hydrogen  
159 peroxide (**Figure 2C, Table S4**), which is not surprising, considering that the tissue is  
160 undergoing cell death. In contrast, overrepresented GO terms in genes exclusively upregulated  
161 at the OUT area included “regulation of defense response” and, interestingly, “response to  
162 wounding” and “response to jasmonic acid” (**Figure 2C, Table S4**). These JA-related genes  
163 follow a very distinct expression pattern, with an early peak at 1 hpi both at the IN and OUT  
164 areas, and a second peak at 4 hpi of higher intensity in the OUT zone (**Figure S5, Table S4**).  
165 Although further experimental validation would be required, these data reveal expression  
166 patterns of a set of genes that could potentially be used as OUT markers along with previously  
167 reported markers such as VSP1 (Chung et al., 2008; Betsuyaku et al., 2018). To better visualize  
168 the behavior of the remaining OUT specific genes throughout the course of the infection, we  
169 generated heatmaps representing their differential expression at IN and OUT areas (**Figure**  
170 **S4**).

171

## 172 **Clustering of gene expression profiles reveals distinct expression patterns at the IN and** 173 **OUT areas over time**

174 Next, we set out to determine whether genes at the IN and OUT areas followed specific  
175 expression patterns and if particular biological processes were associated to those patterns. For

176 this, we first analyzed gene expression profiles using Fuzzy c-means, a soft partitioning  
177 algorithm which offers robust clustering with regards to noise by variation of a fuzzification  
178 parameter that limits the contribution of ill-behaved profiles to the clustering process (Olsen et  
179 al., 2006; Kumar and Futschik, 2007). Based on this, we could define three and five distinct  
180 and non-overlapping clusters for *Pto AvrRpm1*-treated samples in the IN and OUT areas,  
181 respectively (**Figure 3, Figure S8 and Table S6-S7**). Genes within each cluster were  
182 subsequently re-clustered in mock-treated samples, producing two distinct sub-clusters  
183 (**Figures 3, Figure S8 and Table S6-S7**). This procedure provided a more detailed overview  
184 of the differences and similarities of trajectories between treatments over time and reflected  
185 the well-documented wound response that takes place in mock-treated tissue (Mine et al., 2018;  
186 Giolai et al., 2019; Vega-Munoz et al., 2020).

187

188 At the IN area of infection, cluster I exhibited a pattern of upregulation from 0 to 2 hpi and  
189 mild downregulation from 2 to 6 hpi (**Figure 3A**). Genes near to its centroid ( $MSV > 0.7$ ; **see**  
190 **Materials and Methods**) are mainly associated with immune-related GO terms (**Figure S6A,**  
191 **Table S8**). Genes in this cluster followed two distinct trajectories in the mock-treated samples:  
192 while mock sub-cluster 1.1 showed a steady increase throughout the experiment, mock sub-  
193 cluster 1.2 exhibited a typical wounding immune-related response common with infected  
194 samples, peaking at 1 h and rapidly returning to steady-state levels (Savatin et al., 2014).

195

196 Cluster II-IN includes genes with a sharp increase of expression at 4 hpi (**Figure 3A**). Many  
197 of the genes following that trajectory are involved in protein degradation processes (autophagy,  
198 protein targeting to the vacuole, proteasome mediated degradation) taking place in response to  
199 infection (**Figure S6A and Table S8**). Sub-clusters from mock-treated samples predominantly  
200 followed a similar steady trajectory throughout the experiment, which points to an infection-

201 specific effect of upregulation on protein turnover due to infection at the IN area (**Figure 3A,**  
202 **Figure S7A and Table S10**).

203

204 Cluster III-IN exhibits an expression pattern of steady downregulation from 0 to 4 hpi, followed  
205 by a slight recovery of expression from 4 to 6 hpi (**Figure 3A**). This cluster includes mostly  
206 genes belonging to GO terms related to photosynthesis (**Figure S6A and Table S8**). In this  
207 case, mock-treated samples sub-cluster into two distinct patterns of expression: sub-cluster 3.1  
208 follows a similar pattern as infected samples, while sub-cluster 3.2 shows a transient decrease  
209 of expression at 1 h followed by a recovery phase from 2 to 6 hpi (**Figure 3A**). Our data show  
210 that only certain components of the photosynthetic machinery are specifically affected by the  
211 pathogen treatment (**Figure S6A, Figure S7A and Table S10**).

212

213 At the OUT area of infection, cluster I includes genes that display a sharp peak of expression  
214 at 4 hpi (**Figure 3B**). From this cluster, genes near the centroid belong to GO terms associated  
215 with metabolism, hormonal regulation, and wounding response, among others (**Figure S6B**  
216 **and Table S9**). Interestingly, JA- and SA-responsive genes, which are known to act  
217 antagonistically and cooperatively during ETI (Liu et al., 2016; Betsuyaku et al., 2018), seem  
218 to be highly enriched in the OUT area. Genes comprising the mock-derived sub-clusters follow  
219 a similar trend of steady expression throughout the time course of the experiment, suggesting  
220 that the peak of high expression is a specific response to the bacterial infection in the  
221 surrounding area (**Figure 3B, Figure S7B and Table S11**).

222

223 Cluster II-OUT in *Pto AvrRpm1*-treated samples follows an expression pattern with two sharp  
224 upregulation peaks at 1 and 4 hpi (**Figure 3B**). These trajectories are followed by genes  
225 associated with JA-related processes and wounding, and is a very specific pattern exclusively

226 found at the OUT zone (**Figure 3, Figure S6B and Table S9**). The early peak at 1 hpi shared  
227 between mock and infected samples could account for a wounding response elicited early at  
228 the area surrounding the syringe-infiltrated area, while the peak at 4 hpi appears as a late  
229 response that occurs specifically at the tissues surrounding the pathogen inoculation area  
230 (**Figure 3, Figure S6 and Table S11**).

231

232 In cluster III-OUT, the trajectory of genes from *Pto AvrRpm1*-treated samples does not  
233 remarkably differ from mock treatment (**Figure 3B**). Genes that comprise this cluster mainly  
234 fall into GO terms associated with the photosynthetic machinery (**Figure S6B and Table S9**).  
235 These data indicate that photosynthesis at the OUT area of infection does not seem to be altered  
236 by pathogen infection as opposed to the IN area (**Figure 3B and Figure S6-S7**) correlating  
237 with zonal photosynthesis efficiency values shown in **Figure 1C** and as previously reported  
238 (Berger et al., 2007).

239

#### 240 **Novel zonal HR transcriptional indicators can be elucidated from pairwise comparisons** 241 **between time, treatment and area**

242 In order to identify robust HR markers that are exclusively upregulated at the site of cell death  
243 (IN area) we conducted a pipeline of differential expression analysis that consisted of  
244 concatenated pairwise comparisons considering the three variables in our experimental design:  
245 time, treatment and area (**Figure 4A**). Since the highest degree of differential expression  
246 between treatments took place at 4 and 6 hpi (**Figure 2A**), we carried out the comparisons at  
247 these two time points independently. Firstly, we focused on the time variable and selected  
248 genes that were confidently upregulated at the IN area of *Pto AvrRpm1*-infected plants, either  
249 at 4 and/or 6 hpi, compared to 0 hpi (1<sup>st</sup> filter: FDR < 0.05 and log<sub>2</sub>FC > 2). Secondly, we  
250 removed genes also upregulated at 4 and/or 6 hpi at the IN area in mock controls (2<sup>nd</sup> filter:



251 FDR < 0.05 and  $\log_2FC > 2$ ). Since we aimed to find genes only upregulated at the IN/cell death  
252 area, next, we removed the genes that were upregulated by bacterial inoculation at the OUT  
253 area at least to half of the levels than in the IN zone (3<sup>rd</sup> filter: FDR < 0.05 and  $\log_2FC < 1$ ).  
254 Finally, from the genes that met those three criteria, we kept those that were differentially  
255 upregulated at IN compared to the OUT area in *Pto AvrRpm1*-infected plants (4<sup>th</sup> filter: FDR  
256 < 0.05 and  $\log_2FC > 2$ ) (**Figure 4A**).

257

258 A total of 32 genes passed all 4 filters, constituting a set of potential HR indicators (**Figure**  
259 **S9**). From these, 24 were extracted from the 4 hpi dataset and 11 from the 6 hpi dataset and 3  
260 from both time points (**Figure S9**). Of note, due to the stringency of the filters none of these  
261 genes passed all the filters at 1 or 2 hpi, although 7 of them were upregulated after infection at  
262 the IN zone at these early time points (M5, M6, M7, M8, M9, M11 and M12). The expression  
263 profiles of this putative HR indicators can be visualized as DESeq2 pseudo-counts as a function  
264 of time at both areas of infection in **Figure S10**. The expression patterns of these 32 genes at  
265 0 and 4/6 hpi were validated by real time quantitative PCR (RT-qPCR) using newly obtained  
266 biological samples (**Figure S11**). To ensure that the potential markers were exclusively  
267 upregulated as part of the HR response triggered by effector-mediated bacterial recognition  
268 and not as part of the defense responses triggered by disease-causing bacteria, we also included  
269 samples inoculated with *Pto* DC3000 EV (*Pto* EV), a strain that causes disease but does not  
270 trigger HR in Arabidopsis Col-0. Among the 32 genes tested, a total of 13 (10 of them at 4 hpi,  
271 4 at 6 hpi, with one at both time points), behaved as *bona fide* HR indicators (**Figure 4B-C**),  
272 showing a distinctive upregulation specifically triggered at the IN area by an HR-causing  
273 bacterium.

274

275 **The AAA-ATPase *At5g17760* promoter specifically drives expression of GFP to the IN**  
276 **area of infection, constituting a robust transcriptional live marker of HR**

277 In order to generate much needed tools to extend our understanding of how HR unfolds at the  
278 infection site and its surrounding tissue, we generated stable transgenic Arabidopsis plants  
279 expressing green fluorescent protein (3xGFP) under the control of the promoters of each of the  
280 13 identified putative HR marker genes. A nuclear localization signal (NLS) was fused to GFP  
281 to concentrate the signal in the nucleus and facilitate detection, which enabled us to distinguish  
282 promoter-driven fluorescence from the auto-fluorescence derived from HR (Bennett et al.,  
283 1996).

284

285 We focused our analysis on plants expressing *pAT5G17760:NLS-3xGFP* (corresponding to  
286 M13), as they showed high, cell-specific, robust and clear GFP signal in the nuclei of the leaf  
287 regions infected with *Pto AvrRpm1* (**Figure 5B, Figure S12**). In several independent transgenic  
288 lines, activation of *pAT5G17760* was limited to the syringe-infiltrated area and could not be  
289 detected in the surrounding tissues (**Figure S13**). In all *pAT5G17760:NLS-3xGFP* marker lines  
290 the GFP signal appeared concomitantly with cell death, as shown by trypan blue staining  
291 (**Figure 5B, Figure S12 and S13**). A clear GFP signal was not detected in all other marker  
292 lines tested.

293

294 In addition to *Pto AvrRpm1*, we also analyzed the response of *pAT5G17760:NLS-3xGFP* plants  
295 to *Pto* expressing *AvrRpt2* (*Pto AvrRpt2*), which induces HR in Col-0 plants via the CNL  
296 RESISTANT TO P. SYRINGAE 2 (RPS2) (Mackey et al., 2003) and to *Pto* expressing  
297 *AvrRps4* (*Pto AvrRps4*), where HR is mediated by the TNL-pair RPS4/RRS1 and requires  
298 helper NLRs (Gassmann et al., 1999; Narusaka et al., 2009). The same pattern was observed  
299 after infiltration with *Pto AvrRpt2* or *Pto AvrRps4* (**Figure 5B**), which indicates that

300 *pAT5G17760* robustly responds to pathogen-mediated activation of different classes of NLR  
301 receptors. As controls, we included mock, *Pto* EV and a non-pathogenic mutant strain secreting  
302 no effectors (*Pto hrcC*) (Alfano et al., 2000). Importantly, infiltration with the mock solution  
303 or with non-HR causing bacterial strains did not activate *pAT5G17760*. It is worth noting that  
304 for microscopy imaging experiments we used a lower bacterial inoculum (O.D<sub>600</sub> 0.01) to  
305 mimic more natural infection conditions and to delay the onset of HR and tissue collapse  
306 (**Figure 5A**), which was necessary for microscopic detection of GFP. At higher inoculum, rapid  
307 accumulation of phenolic compounds at the site of infection results in extremely high auto-  
308 fluorescence levels that hamper imaging.

309

310 Since pathogens with contrasting lifestyles can trigger HR or HR-like cell death in plants, we  
311 tested whether this reporter line can be employed in a broader sense. For this, we infected adult  
312 *Arabidopsis* leaves by drop inoculation with *Botrytis cinerea*, a necrotrophic pathogen that kills  
313 plant tissue prior to feeding, using a range of toxic molecules (Muckenschnabel et al., 2002).  
314 At 3 dpi, we observed GFP expression in the nuclei of cells at the region inoculated with the  
315 pathogen as opposed to mock-inoculated plants (**Figure S14**). Together, our observations  
316 indicate that *pAT5G17760* activity is spatially regulated and confined to the area undergoing  
317 HR elicited by hemibiotrophic (*P. syringae*) and necrotrophic (*B. cinerea*) pathogens. Thus,  
318 the transgenic reporter line *pAT5G17760:NLS-3xGFP* constitutes a very useful tool to monitor  
319 this process *in planta*.

320

321 The *AT5G17760* gene encodes a putative AAA ATPase of unknown function. A knock-out  
322 mutant of this gene did not show any alteration in HR or pathogen growth restriction compared  
323 to wild-type plants (**Figure S14**). The lack of phenotype could be due to functional  
324 redundancy/compensation, a very common masking phenomenon in plants.

325

326 **HR markers and particularly *At5g1776* are highly upregulated in other RNA-seq data**  
327 **sets from plants undergoing ETI and autoimmunity**

328 We looked at the behavior of *At5g17760* and the rest of marker genes in already published  
329 RNA-seq data sets from either plants undergoing ETI or autoimmune mutant plants displaying  
330 constitutive defense responses and runaway cell death (**Figure S16**) (Mine et al., 2018; Yang  
331 et al., 2020; Barragan et al., 2020; Chantarachot et al., 2020). Fold changes from marker genes  
332 with significant p values (FDR < 0.05) in these data sets were plotted as heatmaps to reveal  
333 their level of upregulation (**Figure S16**). As expected, most gene markers are significantly  
334 (FDR < 0.05) upregulated during ETI triggered by *Pto AvrRpm1* and *Pto AvrRpt2* at 4, 6 and  
335 9 hpi in Mine et al., (2018) (**Figure S16A**). Interestingly, *At5g17760* is the highest upregulated  
336 gene in *hos15-4* and *rh6812* mutant plants undergoing autoimmunity (Yang et al., 2020;  
337 Chantarachot et al., 2020). Likewise, upregulated genes from data sets of incompatible  
338 Arabidopsis F1 hybrids (*Cdm-0 x TueScha-9*) exhibiting autoimmunity comprised most HR  
339 markers found in this study with *At5g17760* being the highest upregulated gene (Barragan et  
340 al., 2020)(**Figure S16B**).

341

342 **DISCUSSION**

343 **Zonation of HR in plants is underscored by distinct gene expression patterns and**  
344 **processes in dying vs by-stander cells**

345 In plants, pathogen recognition via intracellular NLR receptors often results in an HR reaction  
346 that helps preventing pathogen proliferation (Pitsili et al., 2020). This is a highly zonal response  
347 that takes place at the site of infection, whereby dying cells send signals to the surrounding  
348 tissues to activate defenses and block pathogen invasion. Traditionally, the plant immune  
349 system was considered strictly two-branched, with PTI being elicited by recognition of

350 conserved pathogen patterns via cell surface receptors, and ETI recognizing pathogen effector  
351 proteins secreted into the plant cell via intracellular NLR receptors (Jones and Dangl, 2006).  
352 Over the last decades, many efforts have been directed towards understanding the  
353 transcriptional reprogramming elicited during PTI and ETI (Tao et al., 2003; Lewis et al., 2015;  
354 Bozso et al., 2016; Mine et al., 2018; Duan et al., 2020). One of the major conclusions drawn  
355 from these studies is that whilst the repertoire of differentially expressed genes in the host is  
356 largely similar, ETI leads to a faster and more robust transcriptional response than PTI (Tao et  
357 al., 2003; Mine et al., 2018; Yuan et al., 2021a; Yuan et al., 2021b; Ngou et al., 2021b). These  
358 findings, together with emerging evidence showing additional levels of synergy and crosstalk  
359 between PTI and ETI has somewhat blurred the traditional PTI-ETI dichotomy (Dongus and  
360 Parker, 2021; Ngou et al., 2021a; Pruitt et al., 2021). However, despite the large amount of  
361 time-resolved transcriptomic data produced (Tao et al., 2003; Lewis et al., 2015; Hillmer et al.,  
362 2017; Mine et al., 2018), the spatial consideration of HR upon ETI activation has been partly  
363 overlooked, with only few studies pointing to its importance in regulating the process (Dorey  
364 et al., 1997; Betsuyaku et al., 2018; Giolai et al., 2019; Lukan et al., 2020). It remains unclear  
365 whether and to what extent transcriptional reprogramming takes place at the vicinity of cell  
366 death compared to that occurring at the infected area upon bacterial infection.

367

368 Our experimental design (**Figure 1A**) considered the spatio-temporal angle of plant HR to gain  
369 a better understanding of how this process is restricted to a few cells upon pathogen recognition  
370 and to define robust markers of the dying area over time. This is particularly important since  
371 in plants, cell death characterization has largely relied on biochemical and morphological  
372 hallmarks most of which are *post-mortem* and which in most cases do not provide unequivocal  
373 criteria (van Doorn, 2011; van Doorn et al., 2011). We currently lack a set of genes that can be  
374 employed as gene indicators of cell death triggered by pathogens. *In silico* comparisons of

375 transcriptome profiles at different developmental stages and upon environmental stresses  
376 leading to cell death, enabled identification of cell death indicators of developmentally  
377 regulated programmed cell death that can be used to detect or even isolate cells that are ready  
378 to die (Olvera-Carrillo et al., 2015). The same approach did not lead to identification of reliable  
379 HR markers, partly because the available datasets were not obtained on zonally resolved  
380 samples (Olvera-Carrillo et al., 2015).

381

382 Here, differential expression analysis and clustering of genes based on expression profiles over  
383 time enabled us to infer biological processes taking place at each tissue area (IN/OUT) upon  
384 bacterial infection, giving us hints on how HR can be spatially restricted. At the IN area, genes  
385 involved in a local immune response to ETI-triggering bacteria are greatly induced from 1 hpi  
386 onwards (cluster I) (**Figure 2A and Figure S2A, Figure 3A**). Tissue from the IN area, also  
387 contains a set of genes that show a peak of upregulation from 2 to 4 hpi (cluster II), involved  
388 in diverse biological processes ranging from regulation of immunity, responses to JA and SA  
389 or protein turnover (**Figure S6A**). It is now well established that proteasome activity is strongly  
390 induced during bacterial infection and that certain subunits of the proteasome are required for  
391 efficient fine-tuning of immune responses in plants (Misas-Villamil et al., 2013; Ustun et al.,  
392 2016; Ustun et al., 2018). Finally, we identified a strong transcriptional repression of  
393 photosynthetic genes at 4 hpi at the IN area (cluster III) (**Figure 2B, Figure S2B, Figure 3A**  
394 **and Figure S6A**), in accordance with the previously established notion that infection results  
395 in a global downregulation of genes associated with the photosynthetic machinery (Bilgin et  
396 al., 2010). This specific decrease in photosynthesis is particularly interesting in light of recent  
397 reports of the interplay between bacterial effectors and the chloroplast, whereby certain  
398 effectors can suppress chloroplast functions and in turn, chloroplasts can adopt immune

399 functions to fight off pathogens (Kachroo et al., 2021; Littlejohn et al., 2021; Savage et al.,  
400 2021).

401

402 Our results also show that transcriptional reprogramming in host cells surrounding the infection  
403 area (OUT area) is less extensive with a lower number of differentially expressed genes than  
404 at the IN area, and starts later mostly from 4 hpi onwards (**Figure 2A**). Remarkably,  
405 photosynthesis is not significantly affected at the OUT area, corroborating our *in vivo*  
406 measurements (**Figure 1C**) and previous findings (Bilgin et al., 2010). A relatively functional  
407 photosynthetic machinery may be key to maintain effective defense mechanisms and prevent  
408 these cells from dying as their neighbors. This finding might have been masked in previous  
409 transcriptional studies that have not taken into account the zonal nature of HR, and reveals that  
410 the defense-growth trade-off may also have a marked spatial component that needs to be taken  
411 into account in future research. Besides photosynthesis, the OUT zone was characterized by a  
412 marked upregulation of wound/JA-related genes at 4 hpi (**Figure 2C, Figure 3B and Figure**  
413 **S2C**). This response can also be observed at the IN zone but the level of upregulation at the  
414 OUT zone is remarkably higher (**Figure S4**), indicating an amplification in JA signaling at the  
415 cells surrounding the death zone. In addition, some of the JA-related genes are among those  
416 genes exclusively upregulated at OUT at 4/6 hpi, which indicates that they could potentially  
417 be used as zonal markers of the surrounding area (**Figure 2B-C and Figure S5**). *In vivo*  
418 imaging of marker gene promoter activities of SA and JA signaling during ETI discerned two  
419 spatially distinct domains around the infection site, where JA signaling is thought to be  
420 important for regulating over-activation of SA signaling (Betsuyaku et al., 2018). Future  
421 studies that include mutants deficient in JA could provide mechanistic insights into how JA  
422 signaling contributes to the confinement of plant HR. Our analysis also shows that some SA-  
423 signaling genes are among the upregulated IN-specific genes at late time points (**Figure 2B-C**

424 **and Table S4**). Although originally considered antagonistic hormones required for immunity  
425 against pathogens with contrasting lifestyles (Spoel et al., 2007), the interplay and synergism  
426 of these two phytohormones is now well established during ETI (Liu et al., 2016).

427

428 **Zonally resolved transcriptomic analysis of HR in plants allows for the identification of**  
429 **robust biomarkers of the process**

430

431 Robust biomarkers are essential to gain mechanistic knowledge of cell- or tissue-specific  
432 processes. In mammals, the extensive mechanistic knowledge of molecular constituents  
433 underlying regulated cell death has enabled the use of biomarkers for detection of tumor cells  
434 or aberrant cell death processes in cancer patients (Abu-Qare and Abou-Donia, 2001; Ward et  
435 al., 2008). The field of HR in plants is gaining momentum thanks to recent major discoveries  
436 that in one hand are leading to a redefinition of the PTI-ETI relationship and on the other, have  
437 provided mechanistic insight into how NLRs become activated and form supramolecular  
438 complexes that mediate cell death (Wang et al., 2019a; Wang et al., 2019b; Martin et al., 2020;  
439 Bi et al., 2021; Jacob et al., 2021; Pruitt et al., 2021; Tian et al., 2021; Yuan et al., 2021a; Ngou  
440 et al., 2021b; Förderer et al., 2022). However, amidst this exciting scenario, the conceptual  
441 framework of HR zonation is scarcely defined and will be key to understand its execution,  
442 spatial restriction mechanisms and define *bona fide* indicators of the process.

443

444 One of the main goals of our analysis was to define new markers of HR. We made use of the  
445 RNA-seq data generated from IN and OUT areas to pinpoint gene indicators of HR that can be  
446 used either as transcriptional markers or gene promoter markers for *in planta* detection of cells  
447 destined to die using live imaging. Applying stringent filters to our dataset we identified 13  
448 genes that can be used as unequivocal transcriptional markers of zonally restricted cells that



449 have activated a death program in response to pathogen perception via NLR activation (**Figure**  
450 **4C**).

451

452 This marker set includes genes involved or putatively involved in various processes such as  
453 ion transport across the plasma membrane (M1), cell detoxification (M2, M3), lipid  
454 metabolism (M5, M6), cell wall remodeling (M7, M8, M9), protein degradation (M10),  
455 glycolysis (M11, M12), whereas one of these genes remains largely uncharacterized (M13) and  
456 encodes an AAA+ ATPase of unknown function. Interestingly, all these predicted functions  
457 are consistent with processes expectedly taking place on cells destined to die or that have  
458 started dying, although the function of most of these genes remains to be fully determined. This  
459 set of genes provide a glimpse of transcriptional regulation of HR at the site of infection, the  
460 tip of the iceberg of the multi-level regulation of the process. For example, the fact that several  
461 genes are involved in cell wall remodeling highlights the importance of processes taking place  
462 in this extracellular compartment. In line with this, an increase of lignification at the edge of  
463 cells undergoing HR was shown in the past and provided a clear picture of the zonal nature of  
464 this process (Lee et al., 2019). Interestingly, our transcriptome data clearly shows that many  
465 lignin biosynthetic genes are strongly and specifically upregulated at the IN zone at certain  
466 time points (**Figure S15**). How this cell wall lignification is regulated upon pathogen  
467 perception remains to be clarified and will be an interesting topic of research in the future.

468

469 Our data also reinforces the idea that the proteases involved in degradation of cell components  
470 during HR are not particularly regulated at the transcriptional level. We observe specific  
471 upregulation of degradative processes at the IN zone such as autophagy, vacuolar degradation,  
472 and proteasome-mediated processes and in fact, one of the marker genes is a proteasome  
473 subunit (**Figure 3 and Figure 4B**). However, we did not find any protease specifically

474 upregulated at the IN zone, nor did any of them pass the filters that constitute a marker gene in  
475 our study.

476

477 In parallel, the changes observed in marker genes involved either in ion transport across the  
478 plasma membrane or cell detoxification may be somewhat related with the predicted formation  
479 of a pore at the plasma membrane by pathogen-mediated activation of certain NLRs (Bi et al.,  
480 2021; Jacob et al., 2021; Förderer et al., 2022). Although crucial pieces of this mechanism have  
481 been unveiled, knowledge is still scattered and we lack a more integrated picture that combines  
482 NLR activation with downstream processes, including cell death execution. Interestingly, 7 out  
483 of the 32 gene markers (*M5*, *M6*, *M7*, *M8*, *M9*, *M11* and *M12*) that pass our filters exhibit an  
484 early upregulation at 2 hpi compared to mock controls according to the RNA-seq data (**Figure**  
485 **S10**). Although these genes did not pass the stringent 4-tier filtering applied (**Figure 4A**) at 2  
486 hpi, the expression profiles of these genes could be compatible with their potential use as earlier  
487 markers of HR at the IN area.

488 In sum, our data provides a snapshot of how infected cells respond to pathogen recognition at  
489 the transcriptional level, compared to their neighbors, that are not directly exposed to the  
490 pathogen but respond to it. Importantly, this analysis has revealed a set of genes that are  
491 specifically upregulated at the IN zone and constitute robust markers of HR, opening new paths  
492 to deepen our knowledge on the process.

493

494 Importantly, we present an *Arabidopsis* HR reporter line stably expressing GFP under the  
495 control of the AAA+ ATPase *At5g17760* (*M13*), which shows extremely clear and strong  
496 expression exclusively at the inoculated area where pathogen recognition takes place via ETI,  
497 before the onset of cell death becomes apparent (**Figure 5A-B** and **Figure S12**). The other  
498 genes (*M1-M12*) constituted very clear qPCR markers but GFP promoter fusions did not result

499 in clear GFP expression. This can be attributed to the limitations from defining an active  
500 promoter sequence.

501

502 Interestingly, expression of the marker *pAt5g17760:NLS-3xGFP* is similarly regulated by  
503 different classes of NLRs (CNLs and TNLs) revealing conservation of the process (**Figure**  
504 **5A**). Moreover, the marker is also induced zonally by necrotrophic pathogens such as *B.*  
505 *cinerea* that cause an HR-like phenotype (**Figure 5C**). Thus, this transgenic line constitutes a  
506 robust *in planta* biomarker of HR triggered by activation of different NLRs upon infection with  
507 pathogens with contrasting lifestyles.

508

509 Future in-depth analysis of all HR marker genes identified in this work, including  
510 combinatorial genetics, will contribute to a better understanding of HR. This set of genes  
511 constitutes an invaluable tool to zonally discriminate cells undergoing pathogen-triggered cell  
512 death and mechanistically dissect this process. Of particular interest will be to sort GFP-  
513 expressing cells of the *pAt5g17760:NLS-3xGFP* transgenic line upon infection and adapt high-  
514 throughput cell death monitoring equipment used so far for animal cell death to describe and  
515 quantify the features and regulatory networks that define HR in plants at a single-cell level.

516

## 517 **MATERIALS AND METHODS**

### 518 **Plant and bacteria materials and growth**

519 The *Arabidopsis thaliana* accession Col-0 was used for all experiments carried out in this study  
520 expect for electrolyte leakage. For electrolyte leakage, Col-0, *rpm1-3* (Grant et al., 1995)  
521 mutant of the NLR RPM1 and *at5g17760* mutant (GABI-KAT line 592F04\_1) which carries  
522 T-DNA insertion in exon two, were used. Primers used for identifying the T-DNA mutant and  
523 for corroboration null expression by RT-qPCR are listed in **Table S12**.

524

525 Seeds were sown on ½ Murashige and Skoog (MS) media supplemented with 1% sucrose and  
526 stratified at 4°C for two days. Plants were grown in a controlled chamber with a photoperiod  
527 of 9 h light and 15 h dark with white fluorescent lamps under 65% relative humidity. Seeds  
528 were germinated on plates and grown for 10-7 days, then individually transplanted to Jiffy  
529 pellets and grown for 3 additional weeks.

530

531 *Pseudomonas syringae* pathovar tomato (*Pto*) strains *Pto AvrRpm1*, *Pto AvrRpt2*, *Pto AvrRps4*,  
532 *Pto hrpC*- and *Pto* empty vector pVSP61 (EV) were grown on selective King's B (KB) medium  
533 plates for 48 h at 28 °C. Bacteria was then resuspended in 10 mM MgCl<sub>2</sub> and the OD<sub>600</sub> adjusted  
534 to the appropriate inoculum.

535

#### 536 **Bacterial inoculation and RNA-seq data collection.**

537 Bacteria were resuspended and the concentration was adjusted at  $5 \times 10^7$  colony-forming units  
538 or to an optical density measured at a wavelength of 600 nm (OD<sub>600</sub>) of 0.05. Fully expanded  
539 7<sup>th</sup> or 8<sup>th</sup> rosette leaves were used for infiltration with either a mock solution (10 mM MgCl<sub>2</sub>)  
540 or *Pto AvrRpm1*. We syringe-infiltrated an area of roughly 3-4 mm at the side edge of leaves.  
541 Upon infiltration, the edge of the infiltrated area was underlined using India ink, and the total  
542 area infiltrated designated as "IN". A 1 mm buffer zone next to the IN area was discarded and  
543 used as a reference to properly separate between the IN and the OUT zone, that expanded 1-2  
544 mm towards the vein. Leaf tissue was separately collected from the IN and OUT area of  
545 infiltration at 5 different time points: 0, 1, 2, 4 and 6 hours by making use of a sterile scalpel.  
546 Leaf tissue was stored in 2 mL Eppendorf tubes and snapped-frozen in liquid nitrogen until the  
547 time of RNA extraction. Each sample collected consisted of tissue from six leaves derived from  
548 three different plants. For generation of three biological replicates from each condition (area,

549 treatment and time), three independent experiments were performed. total sum of 60 samples  
550 -2 treatments (mock/infected), 5 time points (0, 1, 2, 4 and 6 hpi), 2 areas (IN/OUT) and 3  
551 biological replicates- were used for RNA-sequencing.

552

553 For RNA library preparation, 1 µg of RNA from each sample was isolated using the  
554 NucleoSpin® RNA isolation kit (Macherey-Nagel, Hoerd Cedex, France) following the  
555 manufacturer's instructions. RNAseq was performed at the GeT-PlaGe core facility, INRA  
556 Toulouse. RNA-seq libraries have been prepared according to Illumina's protocols using the  
557 Illumina TruSeq Stranded mRNA sample prep kit to analyze mRNA. Briefly, mRNA was  
558 selected using poly-T beads. Then, RNA was fragmented to generate double stranded cDNA  
559 and adaptors were ligated to be sequenced. 11 cycles of PCR were applied to amplify libraries.  
560 Library quality was assessed using a Fragment Analyzer and libraries were quantified by qPCR  
561 using the Kapa Library Quantification Kit (Kapa Biosystems, Inc, Wilmington, MA, USA).  
562 RNA-seq experiments have been performed on an Illumina HiSeq3000 using a paired-end read  
563 length of 2x150 bp with the Illumina HiSeq3000 sequencing kits.

564

### 565 **Read mapping and differential expression analysis**

566 "FastQC" and "TrimGalore!" software was used for raw Illumina reads quality control analysis  
567 and trimming of reads containing adaptor- or vector-derived sequences, respectively  
568 (Babraham Bioinformatics - FastQC A Quality Control tool for High Throughput Sequence  
569 Data, 2021). rRNA was detected and removed using "SortMeRNA 2.1b" software (Kopylova  
570 et al., 2012). Cleaned reads together with the transcriptome of *Arabidopsis thaliana* (as of 30  
571 August 2018), including ncRNA, were used to quantify gene expression at transcript level  
572 using the software "Salmon v0.11.3" (Patro et al., 2017). Raw counts aggregated by gene were  
573 obtained using "tximport v1.14.2" and the result was used as input to "DESeq2" v1.26.0 (Love

574 et al., 2014; Sonesson et al., 2015) to perform differential expression analysis. Then, genes  
575 adding up to less than 10 counts across all 60 samples were removed. The pre-filtered DESeq2  
576 object contained 32,865 rows that turned to 23,986 after filtering. Counts normalized for  
577 sample size and regularized-logarithm transformed were used to produce PCAs.

578

579 Raw counts together with sample size information were used as input for DESeq2's differential  
580 expression analysis. Simple pairwise comparisons based on a single factor were performed  
581 using DESeq2's "result" function while time course differential expression results were  
582 obtained using a likelihood ratio test as previously described (Love et al., 2015). Genes with  
583 FDR below 0.05 and  $|\log_2FC|$  higher than 2 were considered as differentially expressed. FDR  
584 was calculated according to the Benjamini and Hochberg's (BH) method (Benjamini and  
585 Hochberg, 1995).

586

### 587 **Gene clustering**

588 Gene clustering was performed using Mfuzz v2.46.0 package under the R environment (Kumar  
589 and Futschik, 2007; RStudio | Open source & professional software for data science teams,  
590 2021) which is based on fuzzy c-means clustering algorithms. IN and OUT samples were  
591 independently analyzed. After time course differential expression analysis using DESeq2, only  
592 genes with an FDR <0.05 in the likelihood ratio test were selected for clustering.

593

594 The optimal number of non-overlapping clusters with a correlation value below 0.85 was 3 and  
595 6 for *Pto AvrRpm1*-treated samples at the IN and OUT areas of infection, respectively.

596 Subsequently, two highly redundant clusters were merged for OUT samples, yielding 5 final  
597 clusters. Genes that integrated each cluster derived from *Pto AvrRpm1*-treated samples were  
598 re-clustered for mock-treated samples in order to inspect the differences and similarities of

599 trajectories between treatments over time. Between two and four mock-based sub-clusters were  
600 obtained for every infected-cluster. To avoid overlap, we reduced the number of sub-clusters  
601 to two in mock-treated samples. Each gene belonging to a cluster returned an associated  
602 membership score value (MSV) that ranged from 0 to 1 depending on how well it fitted the  
603 expression profile dictated by the overall genes comprising the cluster. Genes that integrate  
604 each cluster in Figure 3 area found in Tables S6-S7.

605

### 606 **Enriched Gene Ontology analysis.**

607 The set of genes that belonged to expression profile clusters or that exhibited differential  
608 expression were input into TAIR for Gene Ontology enrichment analysis for biological  
609 processes, which uses the PANTHER Classification system that contains up to date GO  
610 annotation data for Arabidopsis (Berardini et al., 2004). The most specific term belonging to a  
611 particular family of GO terms was always selected for plotting. Only those GO terms exhibiting  
612 an FDR < 0.05 after Bonferroni Correction for multiple testing and a fold enrichment above 2  
613 were selected for representation in dot plots.

614

### 615 **Identification of HR indicators**

616 For identification of HR indicators, we concatenated four pairwise comparisons using DESeq2,  
617 in which we set different thresholds of log<sub>2</sub>FC, while keeping a stringent cut-off of FDR <0.05  
618 throughout all comparisons. Briefly, we firstly selected genes that were upregulated (log<sub>2</sub>FC  
619 > 2) after *Pto AvrRpm1* infection at 4 or 6 hpi vs 0 hpi. From the genes that complied with this  
620 first filter, we selected those that were specifically upregulated in *Pto AvrRpm1*-infected vs  
621 mock-inoculated samples at 4 or 6 hpi (log<sub>2</sub>FC >2). From the genes that passed these two filters  
622 we kept those with a log<sub>2</sub>FC <1 at the OUT area in *Pto AvrRpm1*-infected vs mock-inoculated  
623 samples at 4 or 6 hpi. Since genes with log<sub>2</sub>FC near 0 do not usually have a low FDR, we kept

624 our stringent FDR threshold while setting the log<sub>2</sub>FC threshold below 1 in order to capture  
625 with statistical confidence downregulated and only mildly upregulated genes at this tissue area.  
626 Finally, from the genes that met those three criteria, we kept those that were differentially  
627 upregulated at the IN area compared to the OUT area in *Pto AvrRpm1*-infected plants.

628

### 629 **Validation of gene expression by real time quantitative PCR.**

630 The same experimental setup used for RNA-seq data generation was followed for experimental  
631 validation by RT-qPCR including infections with *Pto AvrRpt2*, *Pto AvrRps4*, *Pto hrpC*- and  
632 *Pto* EV. Briefly, tissue was snap frozen and RNA isolated with the Maxwell® RSC Plant RNA  
633 kit (Promega). 1 µg of RNA was reverse transcribed into cDNA with the High-Capacity cDNA  
634 Reverse Transcription Kit with RNase inhibitor (Applied Biosystems™). RT-qPCRs were  
635 performed with LightCycler® SYBRgreen I master (Roche) in a LightCycler® 480 System  
636 (Roche). Data was analyzed using the  $\Delta\Delta CT$  method and represented as fold enrichment of the  
637 time point tested (4 or 6 hpi) relative to 0 hpi. Primers for RT-qPCR used in this study are listed  
638 in **Table S12** along with primer concentrations. RT-qPCR results in numeric format along with  
639 Cp values of Targets and Cp values of reference housekeeping gene are listed in **Table S13**.

640

### 641 **Cell death analysis**

642 Trypan blue staining of Arabidopsis leaves was performed by collecting whole leaves in 50 ml  
643 tubes (each leaf in a separate tube) at the specified time-points after treatment and covered with  
644 a 1:3 dilution of the stain. Tubes were incubated in previously boiled water for 15 min, and  
645 then cleared overnight with chloral hydrate on an orbital shaker. After removal of staining  
646 solution, leaves were covered in a 50% glycerol solution and photographed using a Leica DM6  
647 microscope.

648



649 **Electrolyte leakage**

650 Whole leaves from four to five-weeks-old *Arabidopsis* Col-0, *rpm1-3* or *at5g17760* (GABI-  
651 KAT: 592F04) grown in short-day with a photoperiod of 9h light and 15h dark, were infiltrated  
652 with *Pto AvrRpm1* at a wavelength of 600 nm ( $OD_{600}$ ) of 0.05 using a 1-ml needleless syringe.  
653 Leaf discs were dried and subsequently collected with a 0.8-cm-diameter cork borer from  
654 infiltrated leaves. Discs were washed in deionized water for 1 h before being floated on 2 ml  
655 deionized water. Electrolyte leakage was measured as water conductivity with a pocket water  
656 quality meter (LAQUAtwin-EC-11; Horiba, Kyoto, Japan) at the indicated time points.

657 **Bacterial growth assay**

658 Whole leaves from four to five-weeks-old *Arabidopsis* Col-0, *rpm1-3* or *at5g17760* (GABI-  
659 KAT: 592F04) grown in short-day conditions (9h light and 15h dark) were infiltrated with *Pto*  
660 *AvrRpm1* at a wavelength of 600 nm ( $OD_{600}$ ) of 0.001 using a 1-ml needleless syringe. Two  
661 leaf discs from two different leaves were collected using a 6 mm-diameter cork borer (disc area  
662  $0.282\text{ cm}^2$ ). Samples at day 0 and day 3 post-infection were grounded in 10 mM  $MgCl_2$  and  
663 serially diluted 5, 50, 500, 5,000 and 50,000 times on a 96-well plate. Subsequently, dilutions  
664 were spotted (10  $\mu\text{l}$  per spot) on KB medium with antibiotics. The number of colony forming  
665 units (CFUs) per drop was calculated and bacterial growth represented as  $\log_{10}$  CFU per  $\text{cm}^2$   
666 of tissue.

667

668 **Chlorophyll fluorescence imaging**

669 An IMAGING-PAM (Pulse-Amplitude-Modulated) M-Series Chlorophyll Fluorometer  
670 system (Heinz Walz, Effeltrich, Germany) was used to investigate spatio-temporal changes in  
671 photosynthetic parameters at the IN and OUT areas of infection (Schreiber, 2004). Plants were  
672 kept in the dark for 30 minutes before measurement. Plants were exposed to 2 Hz frequency  
673 measuring light pulses for  $F_0$  (minimum fluorescence in the dark-adapted state) determination.

674 Saturating pulses (800 ms) of white light (2400 mmol photons.m<sup>-2</sup> s<sup>-1</sup>) were applied for Fm  
675 (maximum fluorescence in the dark-adapted state) determination. The photosynthetic  
676 efficiency or maximum quantum yield of PSII photochemistry (Fv/Fm) was determined as  
677 (Fm-Fo)/Fm. The relative PSII electron transport rate (ETR) was calculated by performing a  
678 kinetic analysis for 10 minutes with 60 second pulses (Schreiber et al., 2012). Areas of interest  
679 (AOI) included IN and OUT to evaluate spatial heterogeneity. The measurements were taken  
680 after 0, 1, 2, 4 and 6 hpi. Results are shown from 6 different AOI.

681

### 682 **Generation of transgenic promoter reporter lines**

683 Regions of approximately -2.5 kb upstream of the transcription starting site of *AT1G79710*,  
684 *AT4G18050*, *AT1G78380*, *AT4G24160*, *AT5G18480*, *AT4G30390*, *AT5G54650*, *AT5G16910*,  
685 *AT5G20000*, *AT2G36580*, *AT5G56350* and *AT5G17760* were amplified from Arabidopsis Col-  
686 0 genomic DNA by PCR and cloned into the pGGA (plasmid Green Gate A) entry vector to  
687 generate pGGA-pMarkerGene. A region of approximately -1.5 kb upstream of the transcription  
688 starting site of *AT1G30270* was synthesized by GENEWIZ, Inc. (South Plainfield, NJ) and  
689 subsequently cloned into the pGGA entry vector as well. (Lampropoulos et al., 2013). Each  
690 entry vector was then recombined with the following plasmids: pGGB-SV40-NLS, pGGC-  
691 3xGFP, pGGD-RBCSt (D-F), pGGF-AlliYFP (seed coat selection cassette for transgenic seed  
692 selection) and pGGZ-empty destination vector. Primers used for cloning and sequencing the  
693 final constructs are listed in **Table S12**. All plasmids were transfected by electroporation into  
694 *Agrobacterium tumefaciens* GV3101 strain containing the plasmid pSoup and then transformed  
695 into Arabidopsis Col-0 by the floral dipping method (Clough and Bent, 1998). Transgenic  
696 seeds from transformed plants were identified as those displaying a clear fluorescence signal  
697 under the stereo microscope Olympus SZX18.

698

## 699 **Pathogen inoculation and microscopy of reporter lines**

700 For microscopy of the reporter line pAT5G17760:NLS-3xGFP, plants were grown as  
701 previously described. Leaves of Col-0 pAT5G17760:NLS-3xGFP were infiltrated in the IN  
702 area with either a mock solution (10 mM MgCl<sub>2</sub>) or different *Pto* strains. *Pto* strains expressing  
703 the following effectors were used: *AvrRpm1*, *AvrRpt2* and *AvrRps4*. As controls, the *Pto* EV  
704 and *Pto hrcC*- strains were also used. All *Pto* strains were infiltrated at a wavelength of 600  
705 nm (OD<sub>600</sub>) of 0.01 for microscopy imaging. For *B. cinerea* infection, B05.10 strain  
706 was grown for 14 days in Potato Dextrose Agar (PDA) at 22°C under dark conditions. Spores  
707 collected, washed in 5 mL of PDA and filtered through two layers of Miracloth (Merck  
708 Millipore). Subsequently, number of spores per cm<sup>2</sup> were counted under the microscope and  
709 diluted to 1 x 10<sup>5</sup> spores per mL. For inoculation a 6 µl droplet was placed on the upper surface  
710 of the 7<sup>th</sup> or 8<sup>th</sup> leaf of an adult Arabidopsis plant grown in short day conditions. A dome  
711 covering the plants was placed throughout the course of *B. cinerea* infection.

712

713 Leaves were imaged at 16 hpi with *Pto* stains and 3 dpi with *B. cinerea*. Whole leaves were  
714 photographed using a Leica DM6 microscope (Leica Microsystems) equipped with DFC365  
715 FX 1.4 MP monochrome digital camera. Bright field and GFP filter pictures were taken of each  
716 leaf. Confocal images were obtained using a FV1000 Olympus confocal microscope with the  
717 following excitation/emission wavelengths for GFP: 488 nm/500 to 540 nm. Confocal  
718 microscopy images were taken of the epidermal layer (20 Z-stacks with stack size of 1 µm) and  
719 fluorescent nuclei were counted using ImageJ software.

720

## 721 **References**

722 **Abu-Qare, A. W., and Abou-Donia, M. B.** (2001). Biomarkers of apoptosis: Release of  
723 cytochrome c, activation of caspase-3, induction of 8-hydroxy-2'-deoxyguanosine,

724 increased 3-nitrotyrosine, and alteration of p53 gene. *Journal of Toxicology and*  
725 *Environmental Health-Part B-Critical Reviews* **4**:313–332.

726 **Alfano, J. R., Charkowski, A. O., Deng, W. L., Badel, J. L., Petnicki-Ocwieja, T., van**  
727 **Dijk, K., and Collmer, A.** (2000). The *Pseudomonas syringae* Hrp pathogenicity island  
728 has a tripartite mosaic structure composed of a cluster of type III secretion genes  
729 bounded by exchangeable effector and conserved effector loci that contribute to parasitic  
730 fitness and pathogenicity in pl. *Proc Natl Acad Sci U S A* **97**:4856–4861.

731 **Ausubel, F. M.** (2005). Are innate immune signaling pathways in plants and animals  
732 conserved? *Nature Immunology* **6**:973–979.

733 **Balint-Kurti, P.** (2019). The plant hypersensitive response: concepts, control and  
734 consequences. *Molecular Plant Pathology* **20**:1163–1178.

735 **Barragan, A. C., Collenberg, M., Wang, J., Lee, R. R. Q., Cher, W. Y., Rabanal, F. A.,**  
736 **Ashkenazy, H., Weigel, D., and Chae, E.** (2021). A Truncated Singleton NLR Causes  
737 Hybrid Necrosis in *Arabidopsis thaliana*. *Molecular Biology and Evolution* **38**:557–574.

738 **Benjamini, Y., and Hochberg, Y.** (1995). CONTROLLING THE FALSE DISCOVERY  
739 RATE - A PRACTICAL AND POWERFUL APPROACH TO MULTIPLE TESTING.  
740 *Journal of the Royal Statistical Society Series B-Statistical Methodology* **57**:289–300.

741 **Berardini, T. Z., Mundodi, S., Reiser, L., Huala, E., Garcia-Hernandez, M., Zhang, P.**  
742 **F., Mueller, L. A., Yoon, J., Doyle, A., Lander, G., et al.** (2004). Functional  
743 annotation of the *Arabidopsis* genome using controlled vocabularies. *Plant Physiology*  
744 **135**:745–755.

745 **Berger, S., Benediktyova, Z., Matous, K., Bonfig, K., Mueller, M. J., Nedbal, L., and**  
746 **Roitsch, T.** (2007). Visualization of dynamics of plant-pathogen interaction by novel  
747 combination of chlorophyll fluorescence imaging and statistical analysis: differential

748 effects of virulent and avirulent strains of *P-syringae* and of oxylipins on *A-thaliana*.  
749 *Journal of Experimental Botany* **58**:797–806.

750 **Betsuyaku, S., Katou, S., Takebayashi, Y., Sakakibara, H., Nomura, N., and Fukuda, H.**  
751 (2018). Salicylic Acid and Jasmonic Acid Pathways are Activated in Spatially Different  
752 Domains Around the Infection Site During Effector-Triggered Immunity in *Arabidopsis*  
753 *thaliana*. *Plant and Cell Physiology* **59**:8–16.

754 **Bi, G., Su, M., Li, N., Liang, Y., Dang, S., Xu, J., Hu, M., Wang, J., Zou, M., Deng, Y., et**  
755 **al.** (2021). The ZAR1 resistosome is a calcium-permeable channel triggering plant  
756 immune signaling. *Cell* **184**:3528+.

757 **Bilgin, D. D., Zavala, J. A., Zhu, J., Clough, S. J., Ort, D. R., and DeLucia, E. H.** (2010).  
758 Biotic stress globally downregulates photosynthesis genes. *Plant Cell and Environment*  
759 **33**:1597–1613.

760 **Bozso, Z., Ott, P. G., Kaman-Toth, E., Bognar, G. F., Pogany, M., and Szatmari, A.**  
761 (2016). Overlapping Yet Response-Specific Transcriptome Alterations Characterize the  
762 Nature of Tobacco-*Pseudomonas syringae* Interactions. *Frontiers in Plant Science* **7**.

763 **Chantarachot, T., Sorenson, R. S., Hummel, M., Ke, H., Kettenburg, A. T., Chen, D.,**  
764 **Aiyetiwa, K., Dehesh, K., Eulgem, T., Sieburth, L. E., et al.** (2020). DHH1/DDX6-  
765 like RNA helicases maintain ephemeral half-lives of stress-response mRNAs. *Nature*  
766 *Plants* **6**:675–685.

767 **Chung, H. S., Koo, A. J. K., Gao, X., Jayanty, S., Thines, B., Jones, A. D., and Howe, G.**  
768 **A.** (2008). Regulation and function of *Arabidopsis* JASMONATE ZIM-domain genes in  
769 response to wounding and herbivory. *Plant Physiology* **146**:952–964.

770 **Clough, S. J., and Bent, A. F.** (1998). Floral dip: a simplified method for *Agrobacterium*-  
771 mediated transformation of *Arabidopsis thaliana*. *Plant Journal* **16**:735–743.

772 **Couto, D., and Zipfel, C.** (2016). Regulation of pattern recognition receptor signalling in  
773 plants. *Nature Reviews Immunology* **16**:537–552.

774 **Dangl, J. L., and Jones, J. D. G.** (2019). A pentagonal plant inflammasome. *Science (1979)*  
775 **364**:31–32.

776 **Dangl, J. L., Horvath, D. M., and Staskawicz, B. J.** (2013). Pivoting the Plant Immune  
777 System from Dissection to Deployment. *Science (1979)* **341**:746–751.

778 **Dongus, J. A., and Parker, J. E.** (2021). EDS1 signalling: At the nexus of intracellular and  
779 surface receptor immunity. *Current Opinion in Plant Biology* **62**.

780 **Dorey, S., Baillieul, F., Pierrel, M. A., Saindrenan, P., Fritig, B., and Kauffmann, S.**  
781 (1997). Spatial and temporal induction of cell death, defense genes, and accumulation of  
782 salicylic acid in tobacco leaves reacting hypersensitively to a fungal glycoprotein  
783 elicitor. *Molecular Plant-Microbe Interactions* **10**:646–655.

784 **Duan, Y., Duan, S., Armstrong, M. R., Xu, J., Zheng, J., Hu, J., Chen, X., Hein, I., Li,**  
785 **G., and Jin, L.** (2020). Comparative Transcriptome Profiling Reveals Compatible and  
786 Incompatible Patterns of Potato Toward *Phytophthora infestans*. *G3-Genes Genomes*  
787 *Genetics* **10**:623–634.

788 **Enyedi, A. J., Yalpani, N., Silverman, P., and Raskin, I.** (1992). LOCALIZATION,  
789 CONJUGATION, AND FUNCTION OF SALICYLIC-ACID IN TOBACCO DURING  
790 THE HYPERSENSITIVE REACTION TO TOBACCO MOSAIC-VIRUS. *Proc Natl*  
791 *Acad Sci U S A* **89**:2480–2484.

792 **Förderer, A., Li, E., Lawson, A., Deng, Y.-N., Sun, Y., Logemann, E., Zhang, X., Wen,**  
793 **J., Han, Z., Chang, J., et al.** (2022). A wheat resistosome defines common principles of  
794 immune receptor channels. *bioRxiv Advance Access* published 2022,  
795 doi:10.1101/2022.03.23.485489.

796 **Gassmann, W., Hinsch, M. E., and Staskawicz, B. J.** (1999). The Arabidopsis RPS4  
797 bacterial-resistance gene is a member of the TIR-NBS-LRR family of disease-resistance  
798 genes. *Plant Journal* **20**:265–277.

799 **Giolai, M., Verweij, W., Lister, A., Heavens, D., Macaulay, I., and Clark, M. D.** (2019).  
800 Spatially resolved transcriptomics reveals plant host responses to pathogens. *Plant*  
801 *Methods* **15**.

802 **Grant, M. R., Godiard, L., Straube, E., Ashfield, T., Lewald, J., Sattler, A., Innes, R.**  
803 **W., and Dangl, J. L.** (1995). STRUCTURE OF THE ARABIDOPSIS RPM1 GENE  
804 ENABLING DUAL-SPECIFICITY DISEASE RESISTANCE. *Science (1979)* **269**:843–  
805 846.

806 **Hillmer, R. A., Tsuda, K., Rallapalli, G., Asai, S., Truman, W., Papke, M. D.,**  
807 **Sakakibara, H., Jones, J. D. G., Myers, C. L., and Katagiri, F.** (2017). The highly  
808 buffered Arabidopsis immune signaling network conceals the functions of its  
809 components. *Plos Genetics* **13**.

810 **Jacob, P., Kim, N. H., Wu, F., el Kasr, F., Chi, Y., Walton, W. G., Furzer, O. J.,**  
811 **Lietzan, A. D., Sunil, S., Kempthorn, K., et al.** (2021). Plant “helper” immune  
812 receptors are Ca<sup>2+</sup>-permeable nonselective cation channels. *Science (1979)* **373**:420+.

813 **Jones, J. D. G., and Dangl, J. L.** (2006). The plant immune system. *Nature* **444**:323–329.

814 **Jones, J. D. G., Vance, R. E., and Dangl, J. L.** (2016). Intracellular innate immune  
815 surveillance devices in plants and animals. *Science (1979)* **354**.

816 **Kachroo, P., Burch-Smith, T. M., and Grant, M.** (2021). An Emerging Role for  
817 Chloroplasts in Disease and Defense. *Annual Review of Phytopathology, Vol 59, 2021*  
818 **59**:423–445.

819 **Kumar, L., and Futschik, M.** (2007). Mfuzz: A software package for soft clustering of  
820 microarray data. *Bioinformatics* **2**:5–7.

821 **Lampropoulos, A., Sutikovic, Z., Wenzl, C., Maegele, I., Lohmann, J. U., and Forner, J.**  
822 (2013). GreenGate - A Novel, Versatile, and Efficient Cloning System for Plant  
823 Transgenesis. *Plos One* **8**.

824 **Lee, M.-H., Jeon, H. S., Kim, S. H., Chung, J. H., Roppolo, D., Lee, H.-J., Cho, H. J.,**  
825 **Tobimatsu, Y., Ralph, J., and Park, O. K.** (2019). Lignin-based barrier restricts  
826 pathogens to the infection site and confers resistance in plants. *Embo Journal* **38**.

827 **Lewis, L. A., Polanski, K., de Torres-Zabala, M., Jayaraman, S., Bowden, L., Moore, J.,**  
828 **Penfold, C. A., Jenkins, D. J., Hill, C., Baxter, L., et al.** (2015). Transcriptional  
829 Dynamics Driving MAMP-Triggered Immunity and Pathogen Effector-Mediated  
830 Immunosuppression in Arabidopsis Leaves Following Infection with *Pseudomonas*  
831 *syringae* pv tomato DC3000. *Plant Cell* **27**:3038–3064.

832 **Littlejohn, G. R., Breen, S., Smirnov, N., and Grant, M.** (2021). Chloroplast immunity  
833 illuminated. *New Phytologist* **229**.

834 **Liu, L. J., Sonbol, F. M., Huot, B., Gu, Y. N., Withers, J., Mwimba, M., Yao, J., He, S.**  
835 **Y., and Dong, X. N.** (2016). Salicylic acid receptors activate jasmonic acid signalling  
836 through a non-canonical pathway to promote effector-triggered immunity. *Nature*  
837 *Communications* **7**:10.

838 **Love, M. I., Huber, W., and Anders, S.** (2014). Moderated estimation of fold change and  
839 dispersion for RNA-seq data with DESeq2. *Genome Biology* **15**.

840 **Love, M. I., Anders, S., Kim, V., and Huber, W.** (2015). RNA-Seq workflow: gene-level  
841 exploratory analysis and differential expression. *F1000Res* **4**:1070.

842 **Lu, Y., and Yao, J.** (2018). Chloroplasts at the Crossroad of Photosynthesis, Pathogen  
843 Infection and Plant Defense. *International Journal of Molecular Sciences* **19**.

844 **Lu, J. v, Chen, H. C., and Walsh, C. M.** (2014). Necroptotic signaling in adaptive and  
845 innate immunity. *Seminars in Cell & Developmental Biology* **35**:33–39.



846 **Lukan, T., Pompe-Novak, M., Baebler, S., Tusek-Znidaric, M., Kladnik, A., Kriznik,**  
847 **M., Blejec, A., Zagorscak, M., Stare, K., Dusak, B., et al. (2020).** Precision  
848 transcriptomics of viral foci reveals the spatial regulation of immune-signaling genes  
849 and identifies RBOHD as an important player in the incompatible interaction between  
850 potato virus Y and potato. *Plant Journal* **104**:645–661.

851 **Ma, S., Lapin, D., Liu, L., Sun, Y., Song, W., Zhang, X., Logemann, E., Yu, D., Wang,**  
852 **J., Jirschitzka, J., et al. (2020).** Direct pathogen-induced assembly of an NLR immune  
853 receptor complex to form a holoenzyme. *Science (1979)* **370**:1184-+.

854 **Mackey, D., Holt, B. F., Wiig, A., and Dangl, J. L. (2002).** RIN4 interacts with  
855 *Pseudomonas syringae* type III effector molecules and is required for RPM1-mediated  
856 resistance in Arabidopsis. *Cell* **108**:743–754.

857 **Mackey, D., Belkhadir, Y., Alonso, J. M., Ecker, J. R., and Dangl, J. L. (2003).**  
858 Arabidopsis RIN4 is a target of the type III virulence effector AvrRpt2 and modulates  
859 RPS2-mediated resistance. *Cell* **112**:379–389.

860 **Martin, R., Qi, T., Zhang, H., Liu, F., King, M., Toth, C., Nogales, E., and Staskawicz,**  
861 **B. J. (2020).** Structure of the activated ROQ1 resistosome directly recognizing the  
862 pathogen effector XopQ. *Science (1979)* **370**:1185-+.

863 **Mine, A., Seyfferth, C., Kracher, B., Berens, M. L., Becker, D., and Tsuda, K. (2018).**  
864 The Defense Phytohormone Signaling Network Enables Rapid, High-Amplitude  
865 Transcriptional Reprogramming during Effector-Triggered Immunity. *Plant Cell*  
866 **30**:1199–1219.

867 **Misas-Villamil, J. C., Kolodziejek, I., Crabill, E., Kaschani, F., Niessen, S., Shindo, T.,**  
868 **Kaiser, M., Alfano, J. R., and van der Hoorn, R. A. L. (2013).** *Pseudomonas syringae*  
869 *pv. syringae* Uses Proteasome Inhibitor Syringolin A to Colonize from Wound Infection  
870 Sites. *Plos Pathogens* **9**.

871 **Muckenschnabel, I., Goodman, B. A., Williamson, B., Lyon, G. D., and Deighton, N.**  
872 (2002). Infection of leaves of *Arabidopsis thaliana* by *Botrytis cinerea*: Changes in  
873 ascorbic acid, free radicals and lipid peroxidation products. *Journal of Experimental*  
874 *Botany* **53**:207–214.

875 **Nagata, S., and Tanaka, M.** (2017). Programmed cell death and the immune system. *Nature*  
876 *Reviews Immunology* **17**:333–340.

877 **Narusaka, M., Shirasu, K., Noutoshi, Y., Kubo, Y., Shiraishi, T., Iwabuchi, M., and**  
878 **Narusaka, Y.** (2009). RRS1 and RPS4 provide a dual Resistance-gene system against  
879 fungal and bacterial pathogens. *Plant Journal* **60**:218–226.

880 **Navarro, L., Zipfel, C., Rowland, O., Keller, I., Robatzek, S., Boller, T., and Jones, J. D.**  
881 **G.** (2004). The transcriptional innate immune response to flg22. interplay and overlap  
882 with Avr gene-dependent defense responses and bacterial pathogenesis. *Plant*  
883 *Physiology* **135**:1113–1128.

884 **Ngou, B. P. M., Jones, J. D. G., and Ding, P.** (2021a). Plant immune networks. *Trends*  
885 *Plant Sci* Advance Access published 2021, doi:10.1016/j.tplants.2021.08.012.

886 **Ngou, B. P. M., Ahn, H. K., Ding, P., and Jones, J. D. G.** (2021b). Mutual potentiation of  
887 plant immunity by cell-surface and intracellular receptors. *Nature* **2021** 592:7852  
888 **592**:110–115.

889 **Olsen, J. v, Blagoev, B., Gnäd, F., Macek, B., Kumar, C., Mortensen, P., and Mann, M.**  
890 (2006). Global, in vivo, and site-specific phosphorylation dynamics in signaling  
891 networks. *Cell* **127**:635–648.

892 **Olvera-Carrillo, Y., van Bel, M., van Hautegeem, T., Fendrych, M., Huysmans, M.,**  
893 **Simaskova, M., van Durme, M., Buscaill, P., Rivas, S., Coll, N. S., et al.** (2015). A  
894 Conserved Core of Programmed Cell Death Indicator Genes Discriminates

895 Developmentally and Environmentally Induced Programmed Cell Death in Plants. *Plant*  
896 *Physiology* **169**:2684–2699.

897 **Patro, R., Duggal, G., Love, M. I., Irizarry, R. A., and Kingsford, C.** (2017). Salmon  
898 provides fast and bias-aware quantification of transcript expression. *Nature Methods*  
899 **14**:417-+.

900 **Pitsili, E., Phukan, U. J., and Coll, N. S.** (2020). Cell Death in Plant Immunity. *Cold Spring*  
901 *Harbor Perspectives in Biology* **12**.

902 **Pruitt, R. N., Locci, F., Wanke, F., Zhang, L., Saile, S. C., Joe, A., Karelina, D., Hua, C.,**  
903 **Frohlich, K., Wan, W.-L., et al.** (2021). The EDS1-PAD4-ADR1 node mediates  
904 Arabidopsis pattern-triggered immunity. *Nature* Advance Access published 2021,  
905 doi:10.1038/s41586-021-03829-0.

906 **RStudio | Open source & professional software for data science teams** (2021). Advance  
907 Access published 2021.

908 **Salguero-Linares, J., and Coll, N. S.** (2019). Plant proteases in the control of the  
909 hypersensitive response. *Journal of Experimental Botany* **70**:2087–2095.

910 **Savage, Z., Duggan, C., Toufexi, A., Pandey, P., Liang, Y., Eugenia Segretin, M., Yuen,**  
911 **L. H., Gaboriau, D. C. A., Leary, A. Y., Tumas, Y., et al.** (2021). Chloroplasts alter  
912 their morphology and accumulate at the pathogen interface during infection by  
913 *Phytophthora infestans*. *Plant Journal* Advance Access published 2021,  
914 doi:10.1111/tpj.15416.

915 **Savatin, D. v, Gramegna, G., Modesti, V., and Cervone, F.** (2014). Wounding in the plant  
916 tissue: the defense of a dangerous passage. *Frontiers in Plant Science* **5**.

917 **Schreiber, U.** (2004). Pulse-amplitude-modulation (PAM) fluorometry and saturation pulse  
918 method: An overview. *Chlorophyll a Fluorescence: Signature of Photosynthesis*  
919 **19**:279-+.

920 **Schreiber, U., Klughammer, C., and Kolbowski, J.** (2012). Assessment of wavelength-  
921 dependent parameters of photosynthetic electron transport with a new type of multi-  
922 color PAM chlorophyll fluorometer. *Photosynthesis Research* **113**:127–144.

923 **Soneson, C., Love, M. I., and Robinson, M. D.** (2015). Differential analyses for RNA-seq:  
924 transcript-level estimates improve gene-level inferences. *F1000Res* **4**:1521.

925 **Spoel, S. H., Johnson, J. S., and Dong, X.** (2007). Regulation of tradeoffs between plant  
926 defenses against pathogens with different lifestyles. *Proc Natl Acad Sci U S A*  
927 **104**:18842–18847.

928 **Tao, Y., Xie, Z. Y., Chen, W. Q., Glazebrook, J., Chang, H. S., Han, B., Zhu, T., Zou, G.**  
929 **Z., and Katagiri, F.** (2003). Quantitative nature of Arabidopsis responses during  
930 compatible and incompatible interactions with the bacterial pathogen *Pseudomonas*  
931 *syringae*. *Plant Cell* **15**:317–330.

932 **Tian, H., Wu, Z., Chen, S., Ao, K., Huang, W., Yaghmaiean, H., Sun, T., Xu, F., Zhang,**  
933 **Y., Wang, S., et al.** (2021). Activation of TIR signalling boosts pattern-triggered  
934 immunity. *Nature Advance Access* published 2021, doi:10.1038/s41586-021-03987-1.

935 **Ustun, S., Sheikh, A., Gimenez-Ibanez, S., Jones, A., Ntoukakis, V., and Bornke, F.**  
936 (2016). The Proteasome Acts as a Hub for Plant Immunity and Is Targeted by  
937 *Pseudomonas* Type III Effectors. *Plant Physiology* **172**:1941–1958.

938 **Ustun, S., Hafren, A., Liu, Q. S., Marshall, R. S., Minina, E. A., Bozhkov, P. v, Vierstra,**  
939 **R. D., and Hofius, D.** (2018). Bacteria Exploit Autophagy for Proteasome Degradation  
940 and Enhanced Virulence in Plants. *Plant Cell* **30**:668–685.

941 **van Doorn, W. G.** (2011). Classes of programmed cell death in plants, compared to those in  
942 animals. *Journal of Experimental Botany* **62**:4749–4761.

943 **van Doorn, W. G., Beers, E. P., Dangl, J. L., Franklin-Tong, V. E., Gallois, P., Hara-**  
944 **Nishimura, I., Jones, A. M., Kawai-Yamada, M., Lam, E., Mundy, J., et al.** (2011).

945 Morphological classification of plant cell deaths. *Cell Death and Differentiation*  
946 **18**:1241–1246.

947 **Vega-Munoz, I., Duran-Flores, D., Fernandez-Fernandez, A. D., Heyman, J., Ritter, A.,**  
948 **and Stael, S.** (2020). Breaking Bad News: Dynamic Molecular Mechanisms of Wound  
949 Response in Plants. *Frontiers in Plant Science* **11**.

950 **Wang, J., Hu, M., Wang, J., Qi, J., Han, Z., Wang, G., Qi, Y., Wang, H.-W., Zhou, J.-**  
951 **M., and Chai, J.** (2019a). Reconstitution and structure of a plant NLR resistosome  
952 conferring immunity. *Science (1979)* **364**:44-+.

953 **Wang, J. Z., Wang, J., Hu, M. J., Wu, S., Qi, J. F., Wang, G. X., Han, Z. F., Qi, Y. J.,**  
954 **Gao, N., Wang, H. W., et al.** (2019b). Ligand-triggered allosteric ADP release primes a  
955 plant NLR complex. *Science (1979)* **364**:43-+.

956 **Ward, T., Cummings, J., Dean, E., Greystoke, A., Hou, J. M., Backen, A., Ranson, M.,**  
957 **and Dive, C.** (2008). Biomarkers of apoptosis. *British Journal of Cancer* **99**:841–846.

958 **Wu, C. H., Abd-El-Haliem, A., Bozkurt, T. O., Belhaj, K., Terauchi, R., Vossen, J. H.,**  
959 **and Kamoun, S.** (2017). NLR network mediates immunity to diverse plant pathogens.  
960 *Proc Natl Acad Sci U S A* **114**:8113–8118.

961 **Wu, C.-H., Derevnina, L., and Kamoun, S.** (2018). Receptor networks underpin plant  
962 immunity. *Science (1979)* **360**:1300–1301.

963 **Yang, L., Chen, X., Wang, Z., Sun, Q., Hong, A., Zhang, A., Zhong, X., and Hua, J.**  
964 (2020). HOS15 and HDA9 negatively regulate immunity through histone deacetylation  
965 of intracellular immune receptor NLR genes in Arabidopsis. *New Phytologist* **226**:507–  
966 522.

967 **Yu, D., Song, W., Yong, E., Tan, J., Liu, L., Cao, Y., Jirschitzka, J., Li, E., Logemann,**  
968 **E., Xu, C., et al.** (2021). TIR domains of plant immune receptors are 2',3'-cAMP/cGMP

969 synthetases mediating cell death. *bioRxiv* Advance Access published November 10,  
970 2021, doi:10.1101/2021.11.09.467869.

971 **Yuan, M., Jiang, Z., Bi, G., Nomura, K., Liu, M., Wang, Y., Cai, B., Zhou, J.-M., Yang**  
972 **He, S., Xin, X.-F., et al.** (2021a). Pattern-recognition receptors are required for NLR-  
973 mediated plant immunity Check for updates. *Nature* **592**:105.

974 **Yuan, M., Ngou, B. P. M., Ding, P., and Xin, X.-F.** (2021b). PTI-ETI crosstalk: an  
975 integrative view of plant immunity. *Curr Opin Plant Biol* **62**:102030.

976 **Zheng, X., Zhou, M., Yoo, H., Pruneda-Paz, J. L., Spivey, N. W., Kay, S. A., and Dong,**  
977 **X.** (2015). Spatial and temporal regulation of biosynthesis of the plant immune signal  
978 salicylic acid. *Proc Natl Acad Sci U S A* **112**:9166–9173.

979

#### 980 **Author Contribution Statement**

981 JS-L designed and performed experiments, analyzed and interpreted data and wrote the  
982 manuscript

983 IS designed and performed experiments and analyzed and interpreted data and helped writing  
984 the manuscript

985 NR-S designed and performed experiments, analyzed and interpreted data and helped writing  
986 the manuscript

987 MS performed experiments

988 UP performed experiments

989 VMG performed analysis and interpreted data

990 MB-F performed analysis and interpreted data

991 MV interpreted data and helped writing the manuscript

992 DR performed experiments, analyzed and interpreted data, and helped writing the manuscript.

993 NSC conceptualized the research, designed the experiments, interpreted data and wrote the  
994 manuscript.

995

## 996 **Acknowledgements**

997 The authors would like to thank Susana Rivas, who conceived and initiated the project, but  
998 declined to be author on the manuscript. Likewise, we thank Susana Rivas's team for their help  
999 with the preliminary experiments and the plant tissue harvest for the RNA-Seq. We thank  
1000 Sebastien Carrère from the Bioinformatics facility at the LIPM, for his bioinformatics  
1001 preliminary analysis. We also thank Simon Stael (VIB) for helpful comments and inspiring  
1002 discussions and all members from the Bacterial plant diseases and cell death lab for their  
1003 insights and suggestions. We thank José Luis Riechman (CRAG) and Miguel Ángel Moreno-  
1004 Risueño for help with the analysis, Antoni Garcia-Molina for help with *B. cinerea* infections  
1005 and Montse Amenós for help with microscopy. We would like to thank Kenichi Tsuda for  
1006 sharing his RNA-seq data of previously published transcriptomic studies (Mine *et al.*, 2018)  
1007 and Ignacio Rubio-Somoza for providing us with the green gate plasmid pGGD-RBCSt (D-F).

1008

## 1009 **Conflict of Interest Statement**

1010 The authors declare no conflict of interest.

1011

## 1012 **Ethics Statement**

1013 The present study did not require ethical approval.

1014

## 1015 **Funding Statement**

1016 Research at CRAG was funded with grants PID2019-108595RB-I00 funded by MCIN/AEI/  
1017 10.13039/501100011033 and AGL2016-78002-R funded by MCIN/AEI/  
1018 10.13039/501100011033 and by “ERDF A way of making Europe” (NSC, MV), fellowship  
1019 PID2019-108595RB-I00 funded by Spanish MCIN/AEI/ 10.13039/501100011033 (NSC,  
1020 MV) and fellowships BES-2017-080210 funded by MCIN/AEI/ 10.13039/501100011033 and  
1021 by “ESF Investing in your future” (JS-L) and FPU19/03778 funded by MU (o Ministerio de  
1022 Universidades) (NR-S); and through the “Severo Ochoa Programme for Centres of Excellence  
1023 in R&D” (SEV-2015-0533 and CEX2019-000902-S funded by MCIN/AEI/  
1024 10.13039/501100011033) and by the CERCA Programme / Generalitat de Catalunya. Work at  
1025 the LIPM was supported by the INRA SPE department (AAP2014), the Région Midi-Pyrénées  
1026 (grant 13050322) and the French Laboratory of Excellence project “TULIP” (ANR-10-LABX-  
1027 41; ANR-11-IDEX-0002-02). IS was supported by an AgreeSkills fellowship within the EU  
1028 Marie-Curie FP7 COFUND People Programme (grant agreement no. 267196).

1029

### 1030 **Data Availability Statement**

1031 RNA-seq raw and processed data generated in this study can be found in GEO (GSE198022).

1032 All code used for analysis can be found at

1033 <https://doi.org/10.34810/data174>

1034

1035

1036

1037

1038

1039

1040



1041

1042

1043 **Figure legends**

**Figure 1. HR in plants can be spatio-temporally dissected.** (A) Experimental design of the study. A limited area (3-4 mm) at the side edge of four-week-old *Arabidopsis thaliana* Col-0 leaves was syringe-infiltrated with either *Pto AvrRpm1* at  $2.5 \times 10^7$  cfu/ml (INFECTED) or a 10 mM  $MgCl_2$  solution (MOCK) and samples were collected at 5 different time points after infection: 0, 1, 2, 4 and 6 hpi. Upon infiltration, the edge of the infiltrated area was marked, and the total area infiltrated designated as “IN”. A 1 mm buffer zone right next to the IN zone ensured proper separation between the IN and “OUT” area, which was the parallel region that expanded from the edge of the buffer zone to 1-2 mm towards the vein. Three biological replicates per area, treatment and time point were collected and subjected for RNA-seq analysis. (B) Analysis of macroscopic cell death upon infection with either *Pto AvrRpm1* or 10 mM  $MgCl_2$  solution. Leaves were infected as described in (a) and subsequently stained with trypan blue. Scale bar 3 mm (C) Representative images of mock or *Pto AvrRpm1*-treated plants subjected to pulse-amplitude modulated (PAM) chlorophyll fluorescence measurement to monitor photosynthesis. Scale bar 3 mm. Photosynthetic efficiency (Fv/Fm ratio) and electron transport rate (ETR) were measured in the infiltrated area (IN) and the neighboring tissue (OUT). Measurements were taken at 0, 1, 2, 4 and 6 hpi. Results are representative of 6 different measurements of each tissue area from 6 different plants. Letters indicate statistically significant differences in either Fv/Fm ratio or ETR values following a two-way ANOVA with Tukey’s HSD test ( $\alpha = 0.05$ ). Exact p values are provided in **Table S5**.

**Figure 2. Spatio-temporal dynamics of the transcriptome reveal time and zone-dependent gene expression signatures upon infection.** (A) Differentially expressed genes (FDR < 0.05 and  $|\log_2FC| > 2$ ) in *Pto AvrRpm1*-infected plants compared to mock-treated plants at each time point at the IN (left) and OUT (right) areas. Red color denotes upregulated genes whereas blue color indicates downregulated genes. Yellow color shows genes with FDR < 0,05 but  $|\log_2FC| < 2$ , whereas grey indicates genes not complying with neither FDR nor  $\log_2FC$  criteria. (B-C) Genes exclusively upregulated (FDR < 0.05 and  $\log_2FC > 2$ ) at either IN or OUT areas of infection at 4 and 6 hpi. (B) Venn diagrams shows sizes of gene sets that are upregulated (FDR < 0.05 and  $\log_2FC > 2$ ) upon bacterial infection at 4 and/or 6 hpi at either IN, OUT or both areas. (C) GO terms representing enriched biological processes derived from genes exclusively upregulated at either IN or OUT areas at 4 and/or 6 hpi. The most specific term from each family term provided by PANTHER was plotted along with their corresponding gene number, fold enrichment (FE) and FDR (Bonferroni Correction for multiple testing) represented as  $\log_{10}$ . Only GO Terms with a FE above 2 and FDR below 0.05 were plotted.

**Figure 3. Gene expression profile clustering reveals three distinctive expression patterns at the IN and OUT areas of infection.** Non-overlapping clusters derived from *Pto AvrRpm1*- and mock-treated plants for IN (A) and OUT (B) areas. Standardized expression to Z-scores (Y-axis) is calculated by subtracting the mean and normalizing to standard deviation. The trajectory that defines the overall expression profile of each cluster through the course of the infection is shown in red for *Pto AvrRpm1*-treated plants. Genes derived from *Pto AvrRpm1*-treated samples were re-clustered for mock-treated samples and their trajectories are

represented in grey. Since the expression profile of these genes in mock-treated samples was very distinct among the overall number of genes, they were divided into two sub-clusters represented either in dotted or dashed grey lines. The number of genes that constitute each cluster is indicated below each cluster. Genes comprising each cluster along with their MSV can be found in **Table S6-S7**.

**Figure 4. Identification of HR markers specific for the IN area of infection.** (A) Schematic representation of the sequence of filters applied to identify indicators. Four filters were concatenated considering the three variables of our experimental design: time, treatment and tissue area. Briefly, in the first filter, we selected genes differentially upregulated from 0 to 4/6 hpi (FDR < 0.05 and  $\log_2FC > 2$ ) at the IN area (colored in red) upon bacterial infection. From the genes that passed this first filter, we selected those that were exclusively upregulated (FDR < 0.05 and  $\log_2FC > 2$ ) due to bacterial infection at the IN area at 4/6 hpi. Subsequently, from the genes that made it into the third filter, we selected those that were not highly upregulated in the OUT area (colored in blue) upon bacterial infection at 4/6 hpi (FDR < 0.05 and  $\log_2FC < 1$ ). Finally, we applied a fourth filter to discard genes that could potentially be basally upregulated at the OUT area upon pathogen treatment at 4/6 hpi (FDR < 0.05 and  $\log_2FC > 2$ ). The starting number of genes and the genes passing the different filtering criteria are indicated. (B) RT-qPCR and RNA-seq expression profiles of marker genes that behave as *bona fide* HR indicators. Relative expression levels to the housekeeping gene *EIF4a* were represented as fold enrichment between 4/6 and 0 hpi. Error bars represent standard error of the mean from three independent experiments. Letters indicate statistically significant differences between treatments following one-way ANOVA with Tukey's HSD test ( $\alpha = 0.05$ ) performed independently at IN and OUT. NS (non-significant after one-way ANOVA). Exact p values

are provided in **Table S5**. (C) List of HR indicators along with their gene ID, gene name and description.

**figure 5. *AT5G17760* encodes an AAA-ATPase and is a reliable HR indicator**

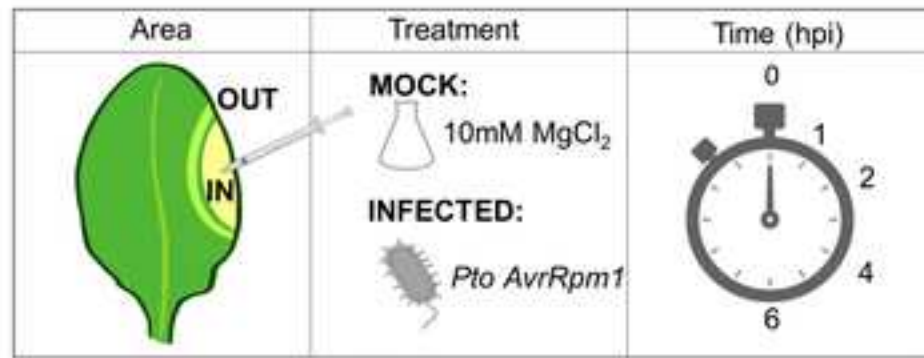
**specifically induced at the IN area by activation of different classes of NLR receptors. (A)**

Representative images of trypan blue-stained leaves, epifluorescence microscope and confocal microscope from *pAT5G17760:NLS-3xGFP* Arabidopsis transgenics. A small region of 4-week-old *pAT5G17760::NLS-3xGFP* leaves was syringe-infiltrated with *Pto* expressing the effectors *AvrRpm1*, *AvrRpt2* or *AvrRps4* at  $1 \times 10^7$  colony-forming units (CFU)/ml (O.D<sub>600</sub> = 0.01). Besides mock treatment, the non-cell death-causing bacterial strains *Pto* DC3000 EV and *Pto* DC3000 *hrcC*- were included as negative controls. Images were taken 16 hpi. Scale bar 3 mm. Images were taken 16 hpi on a Leica DM6 microscope and a confocal microscope prior to trypan blue staining. Scale bar 3 mm. Expression of *pAT5G17760* is detected as green dots corresponding to nuclei with positive GFP signal. Scale bar 100  $\mu$ m. **A** representative close-up magnified image of a *Pto AvrRpm1*-infected leaf expressing *pAT5G17760:NLS-3xGFP* at 16 hpi is shown. Scale bar 3 mm. **(B)** Quantification of fluorescent nuclei from confocal microscopy pictures in **(A)**. Nuclei count was performed using ImageJ software. Data is representative of three independent experiments each one of them containing 4 leaves. Letters indicate statistically significant differences in number of nuclei following one-way ANOVA with Tukey's HSD test ( $\alpha = 0.05$ ). Exact p values are provided in **Table S5**. **(C)** Activation of *pAT5G17760* occurred upon drop inoculation infection with the necrotrophic pathogen *B. cinerea* or a mock solution. Four- to 5-week-old leaves from *pAT5G17760::3xGFP* transgenics were drop inoculated with *B. cinerea* at concentration of  $1 \times 10^5$  spores per mL. Images in left panels represent trypan blue stained leaves and right panels represent leaves imaged under the epifluorescent microscope at 3 dpi. Scale bars 3 mm.

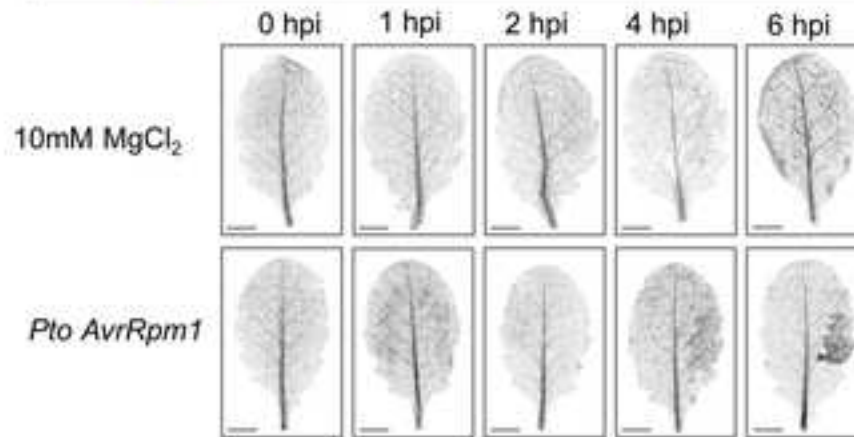


Figure 1

A



B



C

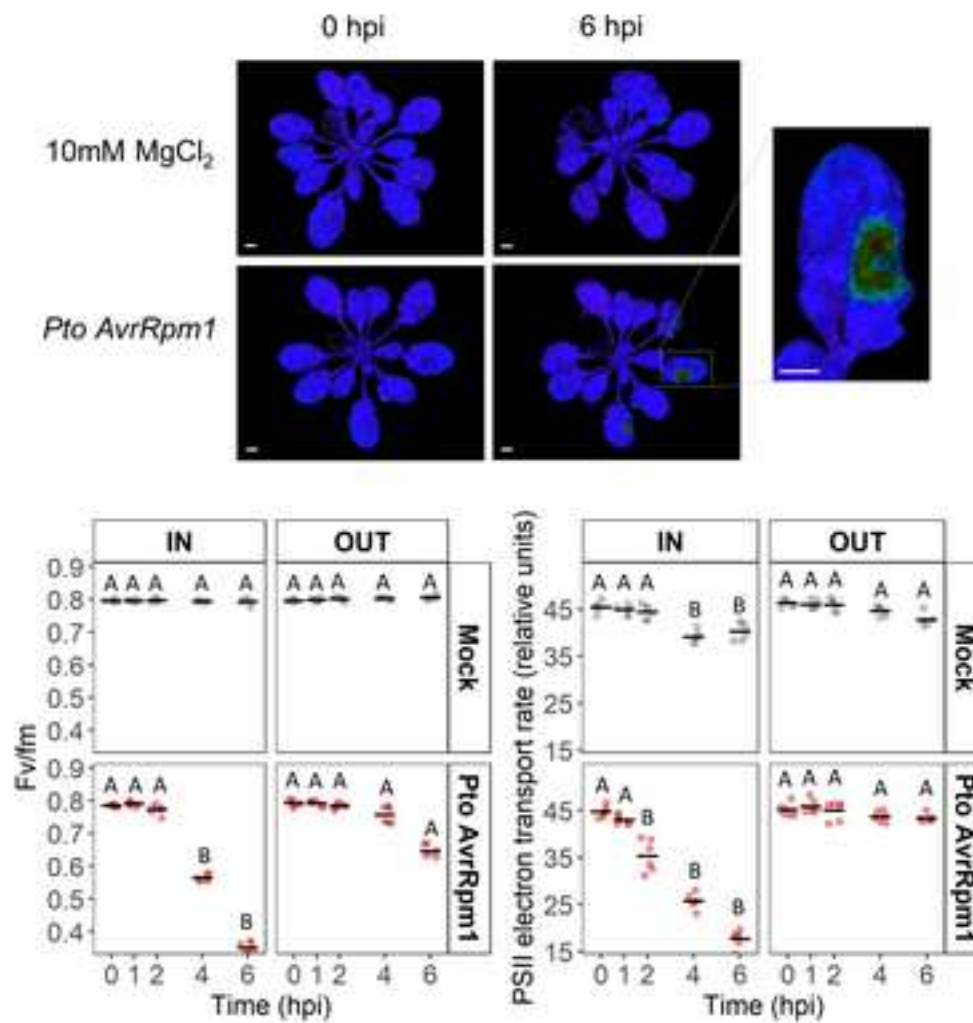
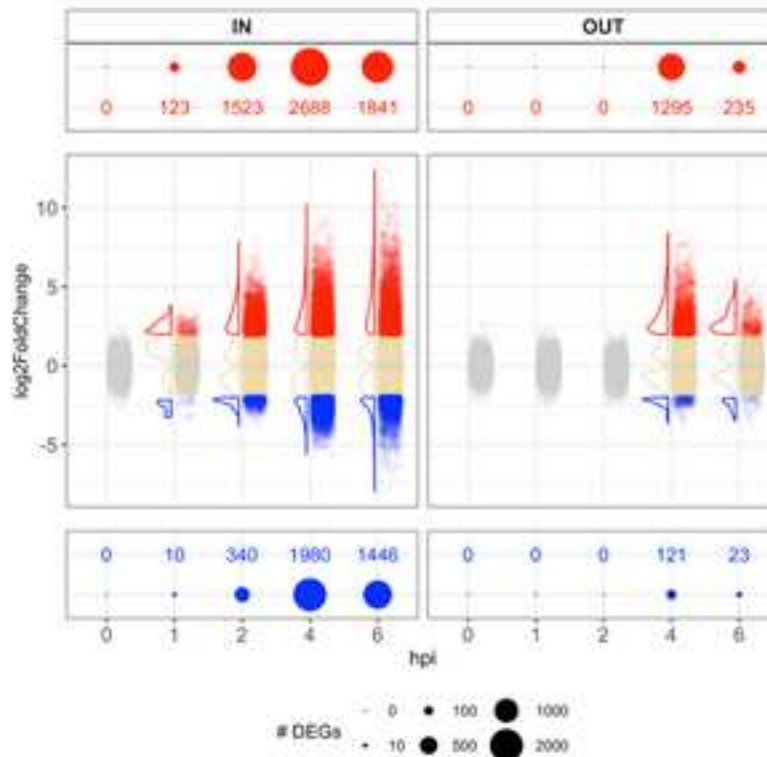
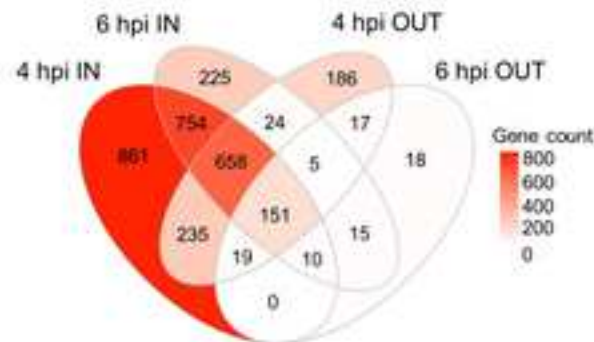


Figure 2

A



B



C

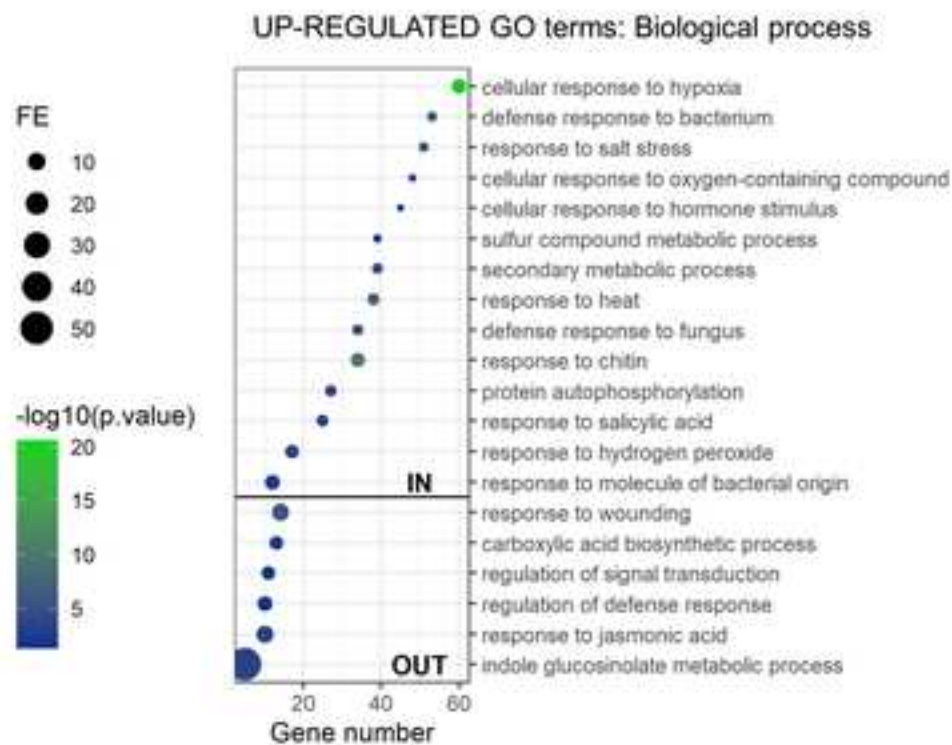




Figure 3

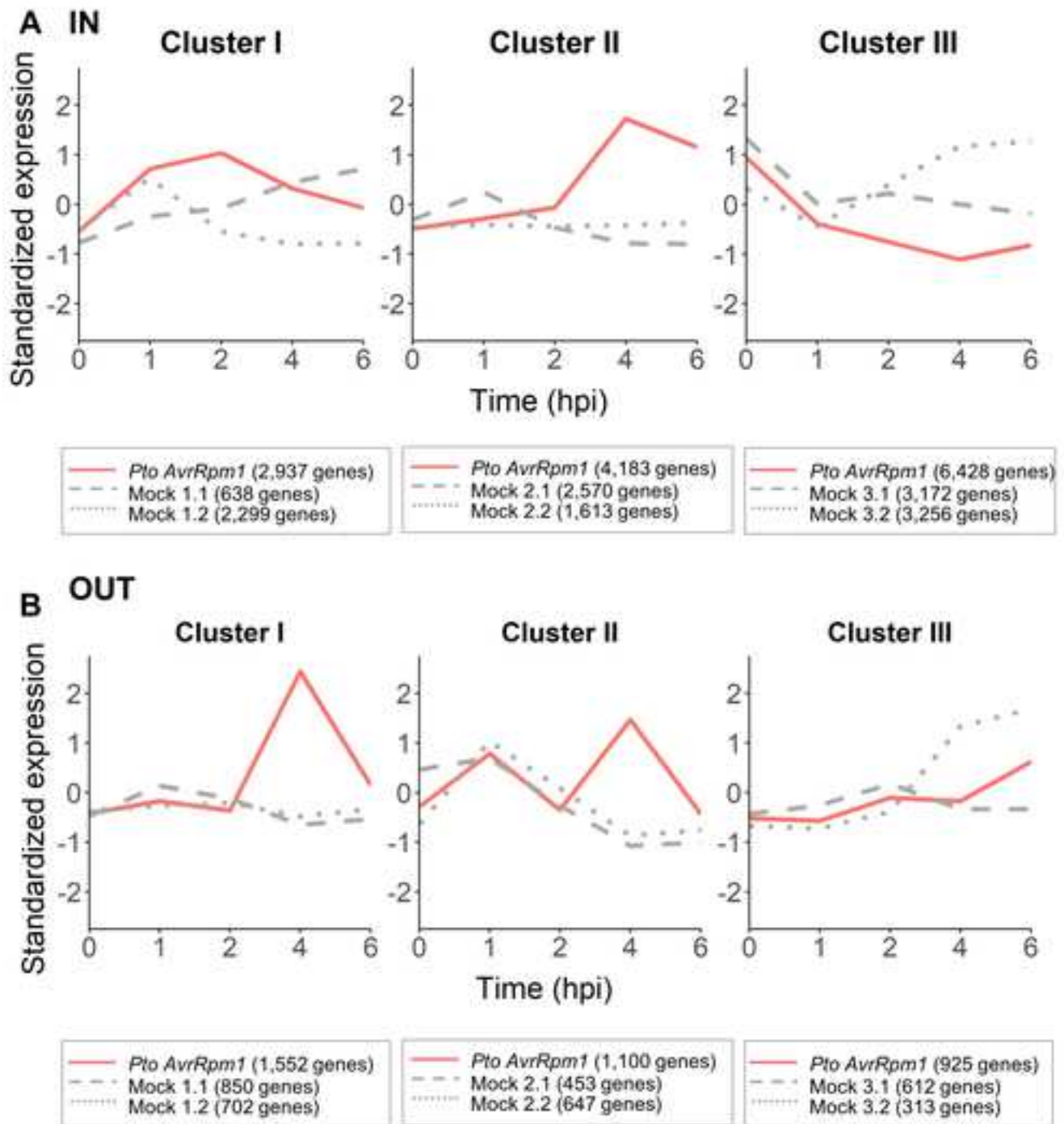
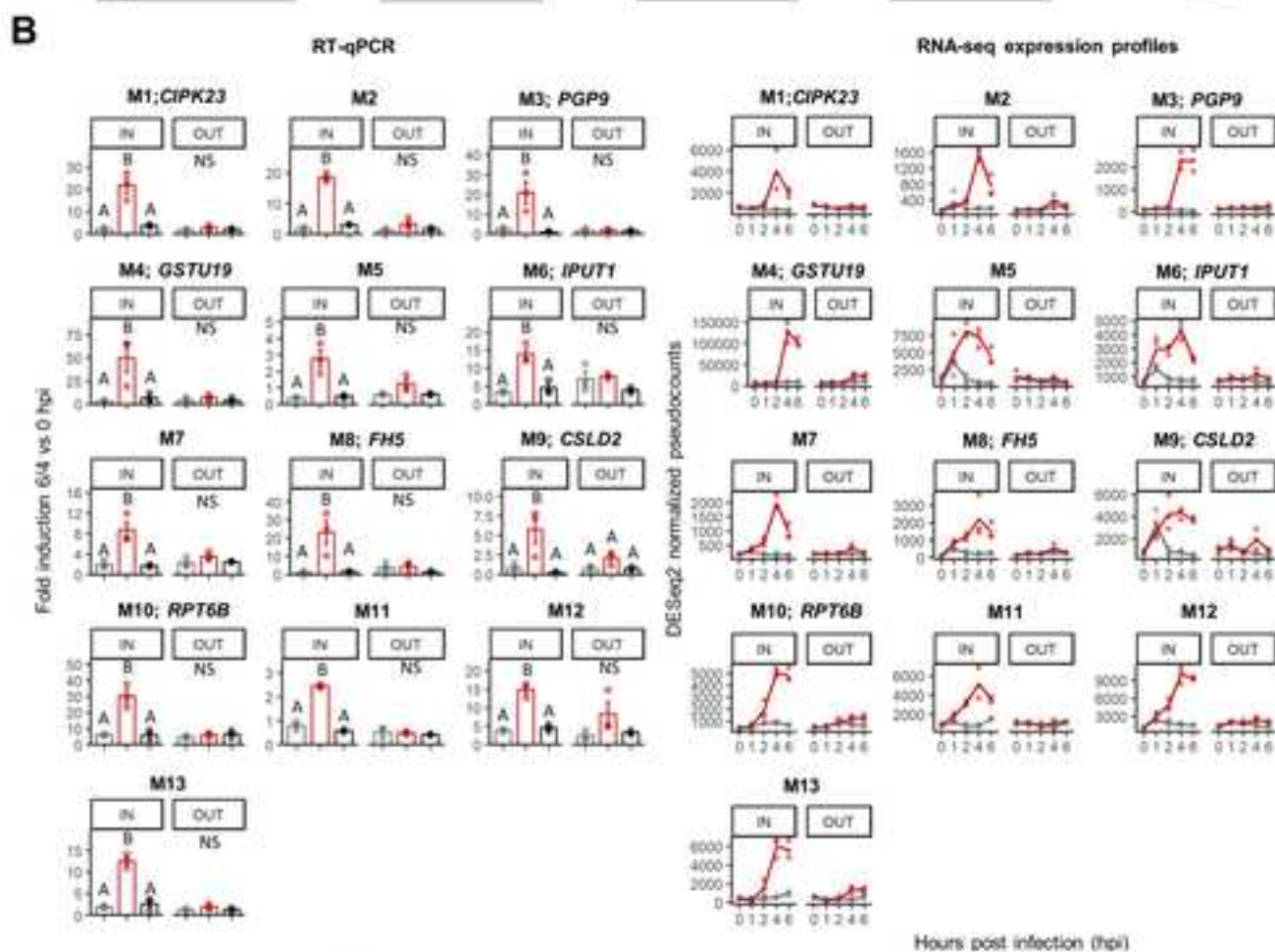
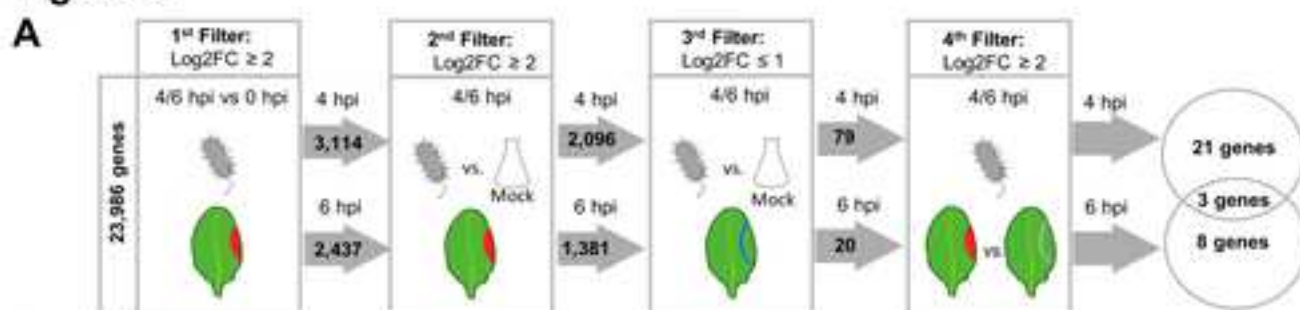


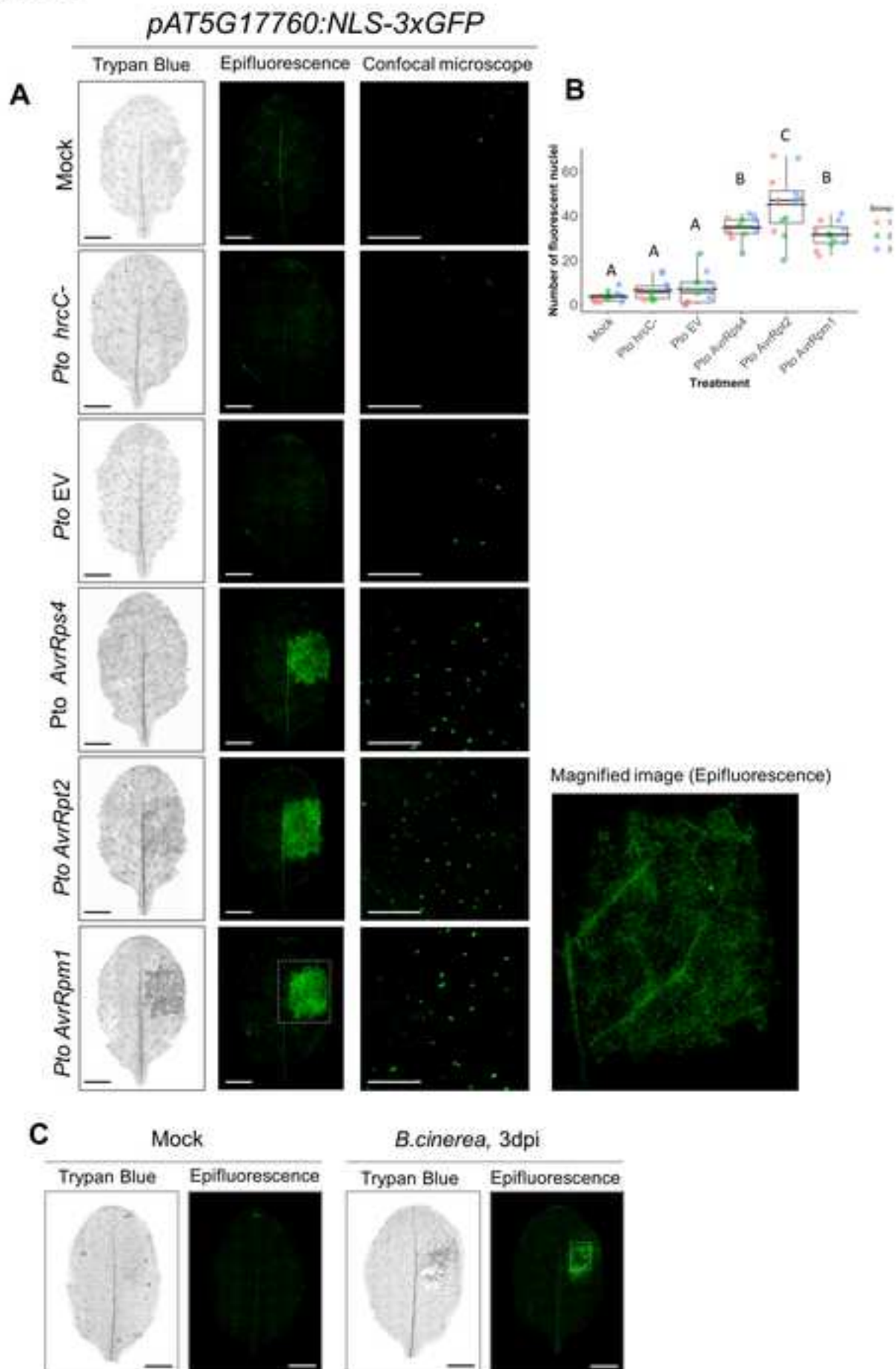
Figure 4



C

| Marker ID | Gene ID   | Gene   | Description  | Time point | Process              |
|-----------|-----------|--------|--|------------|----------------------|
| M1        | AT1G30270 | CIPK23 | CBL-interacting serine/threonine-protein kinase 23   | 4 hpi      | Ion transport PM     |
| M2        | AT1G79710 |        | Probable folate-biopterin transporter 3              | 4 hpi      |                      |
| M3        | AT4G18050 | PGP9   | P-glycoprotein 9                                     | 4 hpi      | Cell detoxification  |
| M4        | AT1G78380 | GSTU19 | Glutathione S-transferase U19                        | 6 hpi      |                      |
| M5        | AT4G24160 |        | 1-acylglycerol-3-phosphate O-acyltransferase         | 4 hpi      | Lipid metabolism     |
| M6        | AT5G18480 | IPUT1  | Inositol phosphoryceramide glucuronosyltransferase 1 | 4 hpi      |                      |
| M7        | AT4G30390 |        | UDP-arabinopyranose mutase                           | 4 hpi      |                      |
| M8        | AT5G54650 | FH5    | Formin-like protein 5                                | 4 hpi      | Cell wall remodeling |
| M9        | AT5G16910 | CSLD2  | Cellulose synthase-like protein D2                   | 6 hpi      |                      |
| M10       | AT5G20000 | RPT6B  | 26S proteasome regulatory subunit 8 homolog B        | 4 hpi      | Protein degradation  |
| M11       | AT2G36580 |        | Pyruvate kinase                                      | 4 hpi      |                      |
| M12       | AT5G56350 |        | Pyruvate kinase                                      | 4/6 hpi    | Uncharacterized      |
| M13       | AT5G17760 |        | AAA-ATPase   | 6 hpi      |                      |

Figure 5



# **Robust transcriptional indicators of immune cell death revealed by spatio-temporal transcriptome analyses**

Jose Salguero-Linares<sup>a,#</sup>, Irene Serrano<sup>b, #,†</sup>, Nerea Ruiz-Solani<sup>a</sup>, Marta Salas-Gómez<sup>a</sup>, Ujjal

Jyoti Phukan<sup>a</sup>, Victor Manuel González<sup>a</sup>, Martí Bernardo-Faura<sup>a</sup>, Marc Valls<sup>a,b</sup>, David

Rengel<sup>b,c,¥,§,\*</sup>, Nuria S. Coll<sup>a,d,§,\*</sup>

## **Supplemental Information**

### **Supplementary figures and supplementary tables**

**Figure S1:**

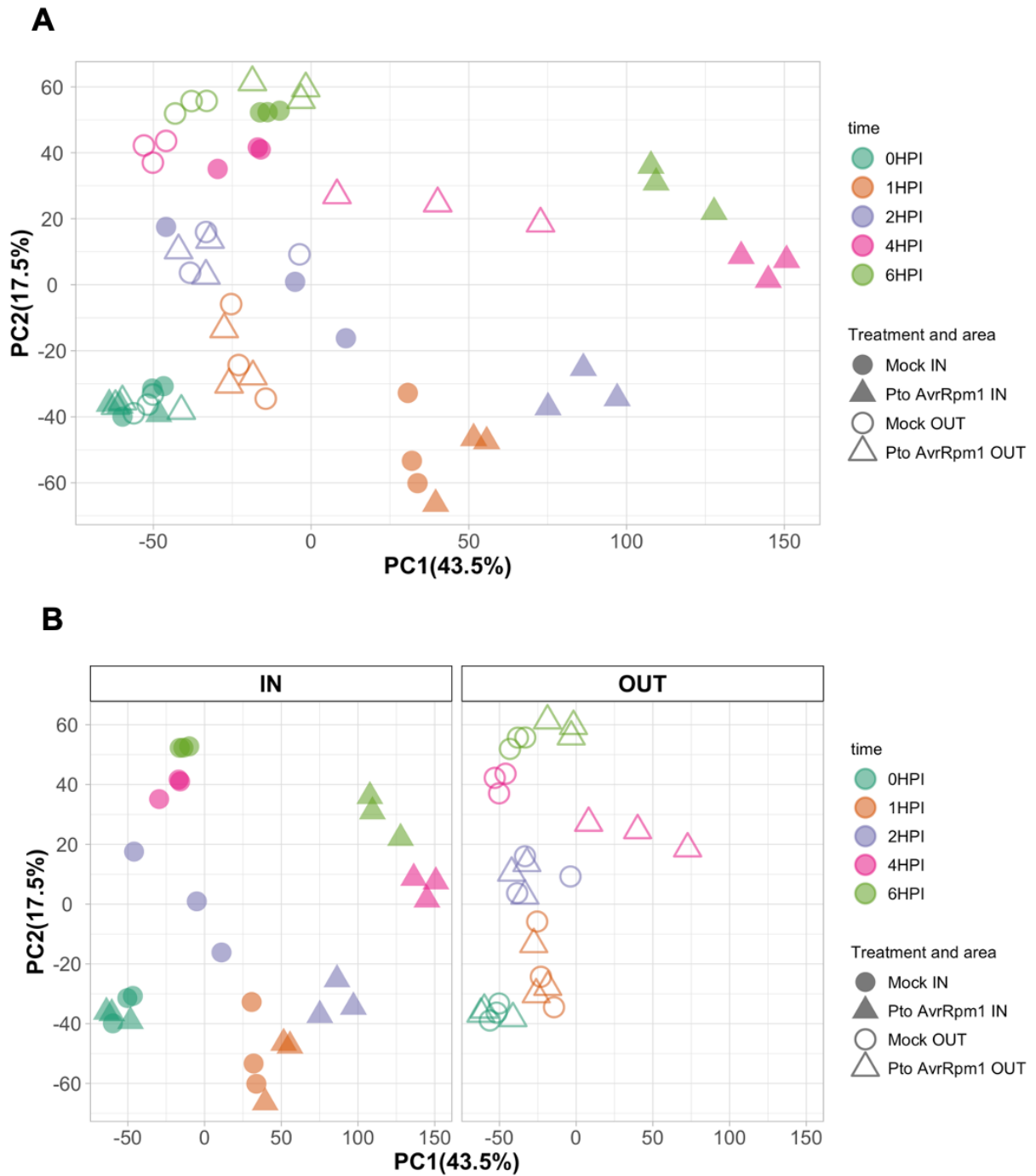
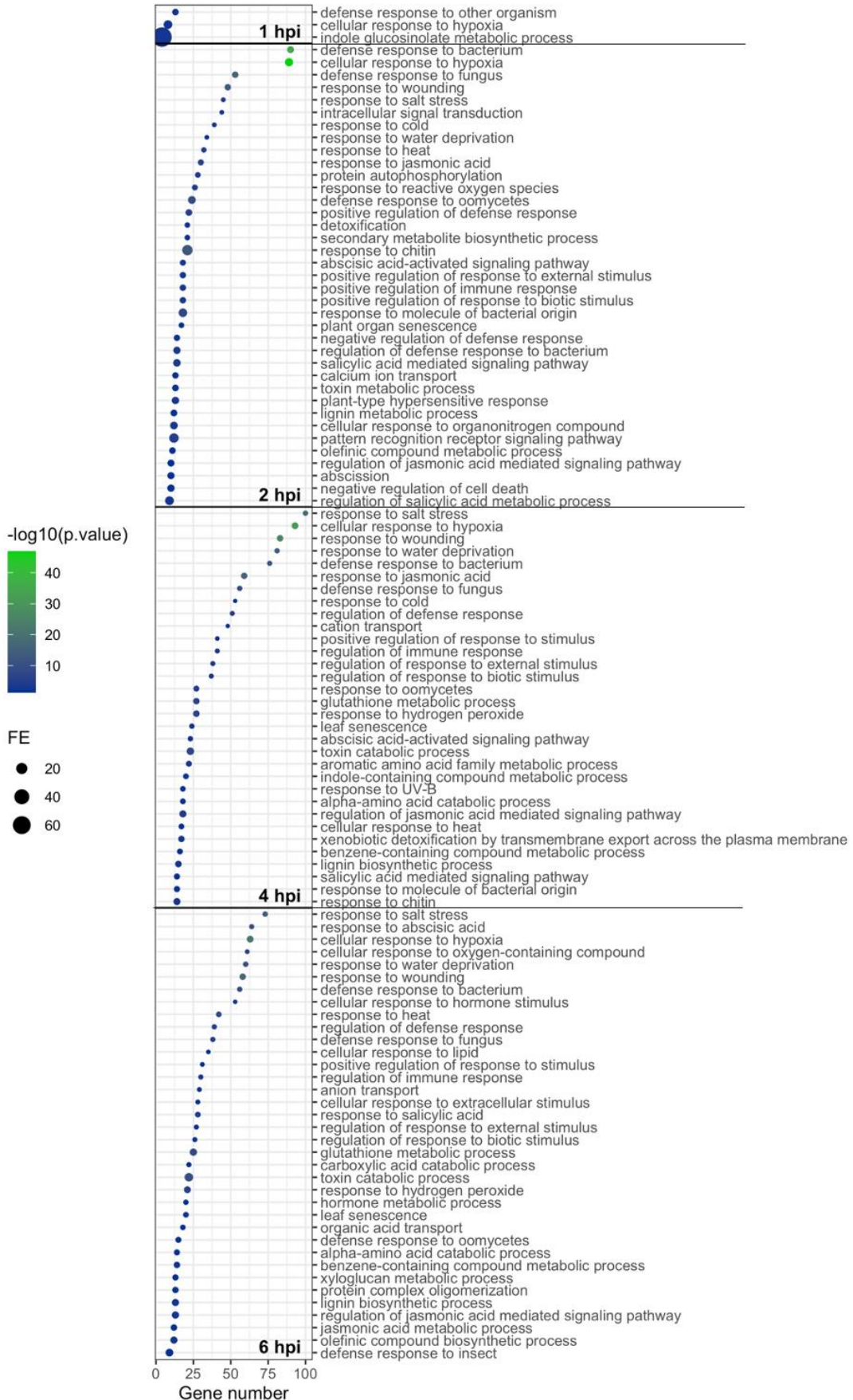


**Figure S1.** Principal component analysis (PCA) from the RNA seq-data. Circles represent mock-treated plants and triangles represent *Pto AvrRpm1*-infected plants. Different colors are assigned for each time point. **(A)** PCA comprising all data sets in our study (IN and OUT samples together). **(B)** PCA with IN and OUT data sets separated in order to ease visualization of the data.

**Figure S2:**

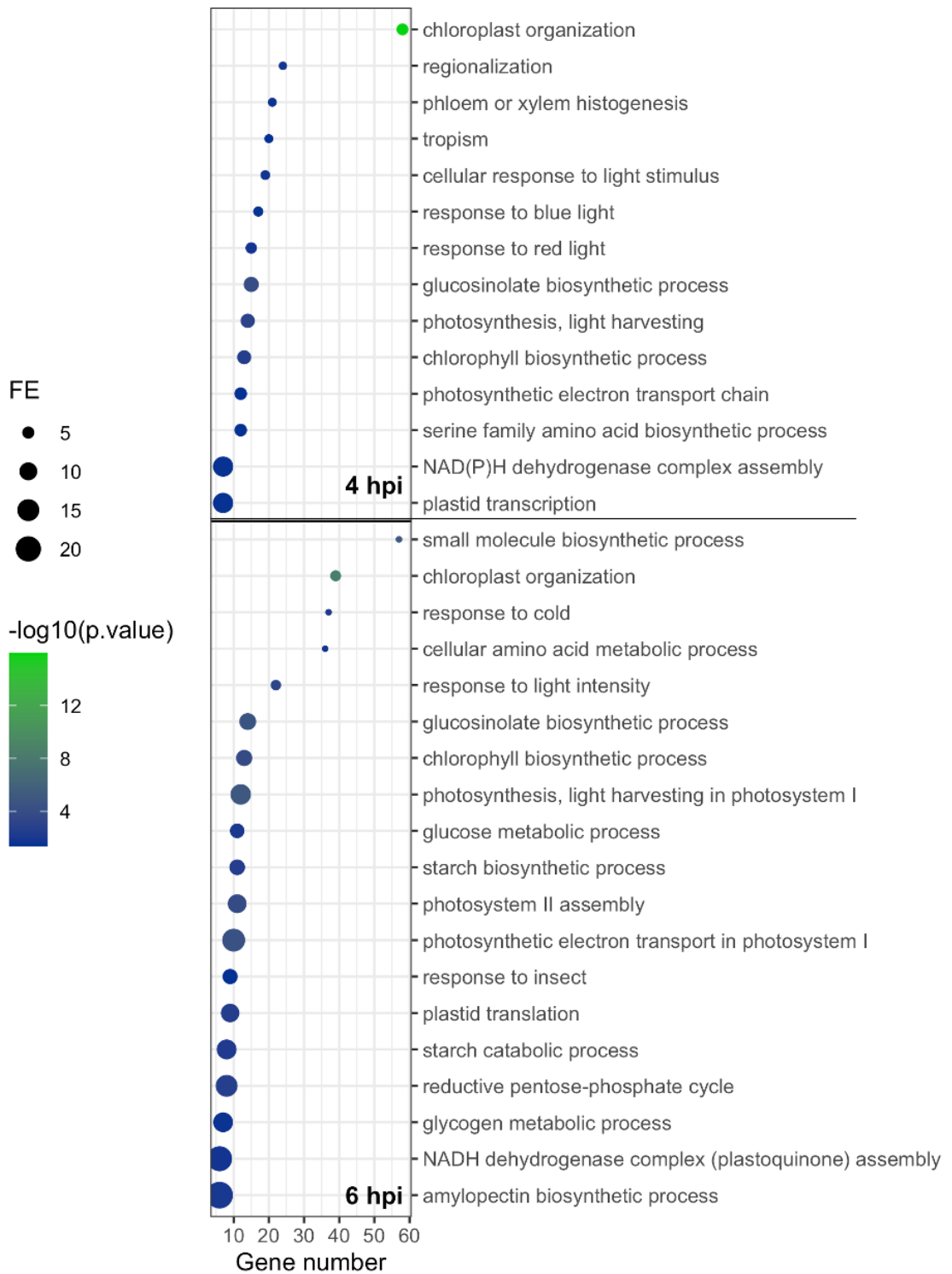
**A**

**IN area UP-REGULATED GO terms: Biological process**



**B**

**IN area DOWN-REGULATED GO terms: Biological process**



C

OUT area UP-REGULATED GO terms: Biological process

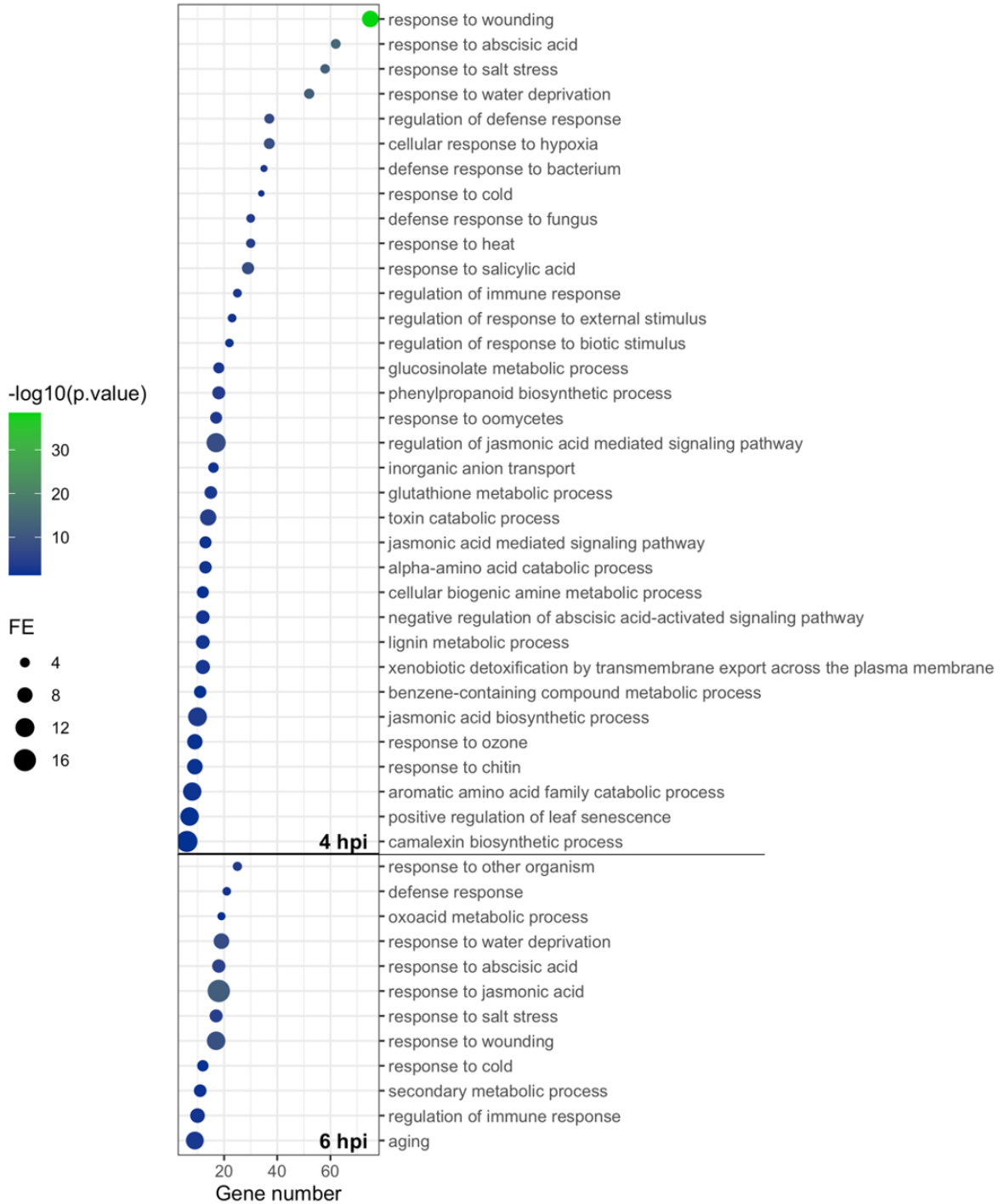




**Figure S2.** GO term enrichment analysis of upregulated and downregulated genes at each time after infection at the IN (**A-B**) and OUT (**C**) areas. The most specific term from each family term provided by PANTHER was plotted along with their corresponding gene number, fold enrichment and adj p value (Bonferroni Correction for multiple testing) represented as  $\log_{10}$ . Only GO terms with a fold enrichment above 2 and adj p value below 0.05 were plotted.

**Figure S3:**

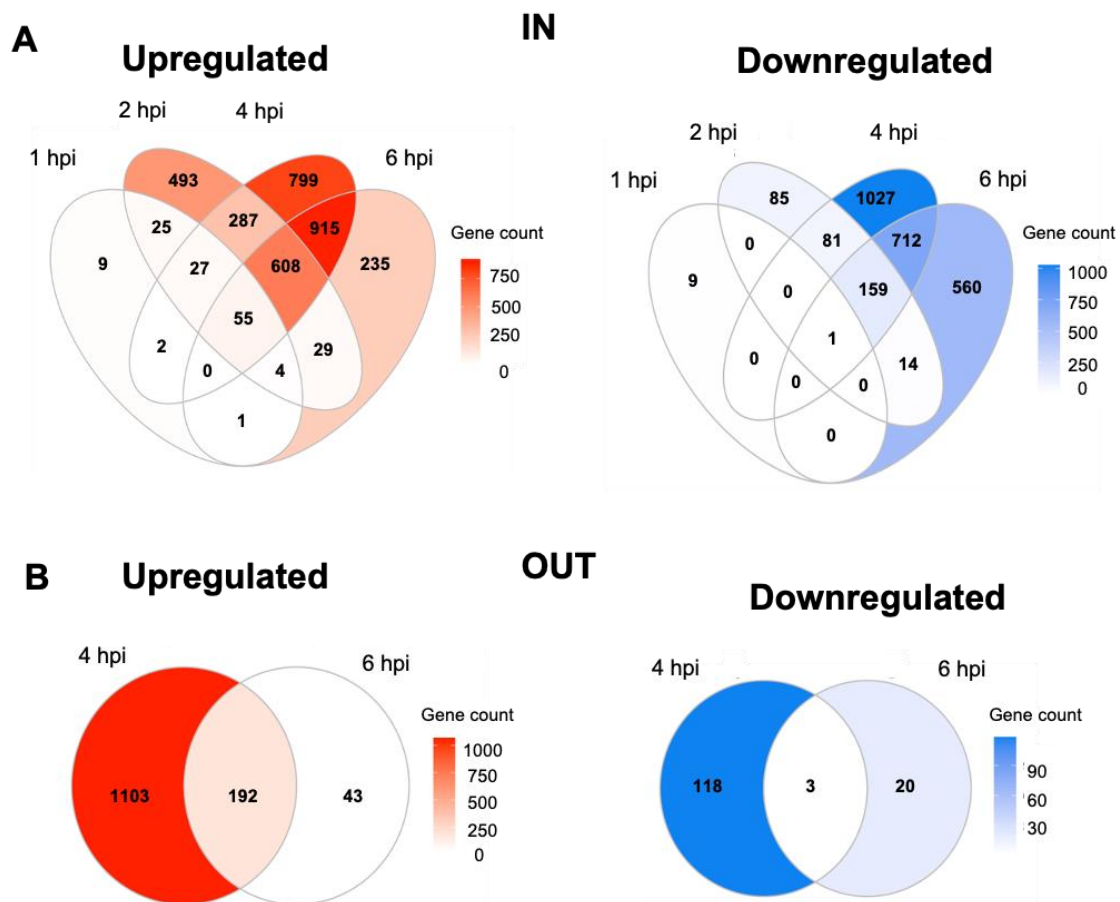


**Figure S3.** The majority of differentially expressed genes at both IN and OUT are specific to 4 and 6 hpi. Venn diagrams showing sizes of gene sets that are differentially expressed (red: upregulated and blue: downregulated) at IN (**A**) or OUT (**B**) at each time point.

**Figure S4**

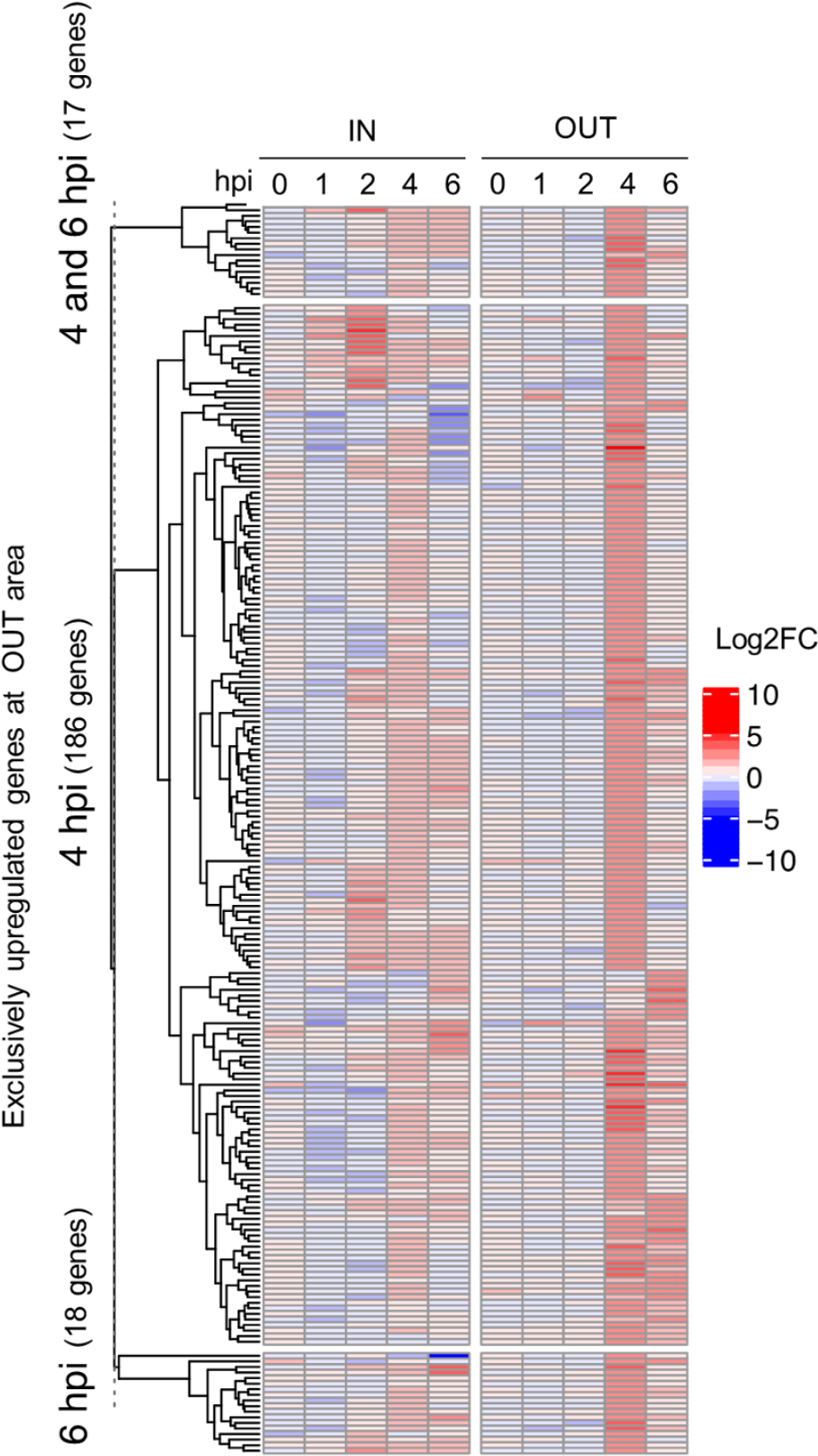


**Figure S4.** Heatmap representing differential expression of genes exclusively upregulated at 4 and/or 6 hpi at the OUT area ( $\log_2FC > 2$  and  $BTH < 0.05$ ) throughout the course of the infection (0,1,2,4 and 6 hpi) at IN and OUT areas.

## Figure S5

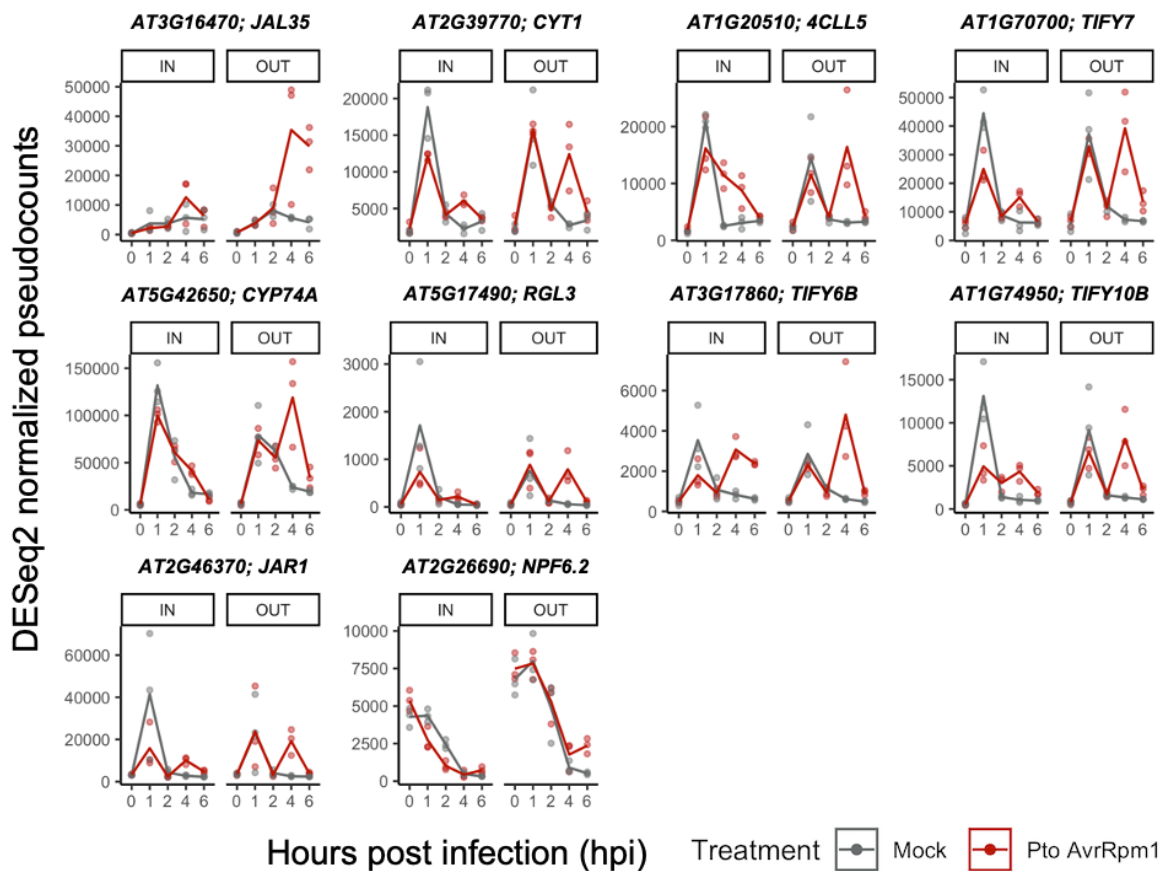


**Figure S5.** RNA-seq expression profiles of JA responsive genes exclusively upregulated at the OUT area upon *Pto AvrRpm1* infection. Gene expression of genes from *Pto-AvrRpm1* or mock-infected plants is represented as DESeq2 pseudocounts.

*JAL35*, Jacalin-related lectin 35; *CYT1*, Mannose-1-phosphate guanylyltransferase 1; *4CLL5*, 4-coumarate--CoA ligase-like 5; *TIFY7*, Protein TIFY 7; *CYP74A*, Allene oxide synthase, chloroplastic; *RGL3*, DELLA protein RGL3; *TIFY6B*, Protein TIFY 6B; *TIFY10B*, Protein

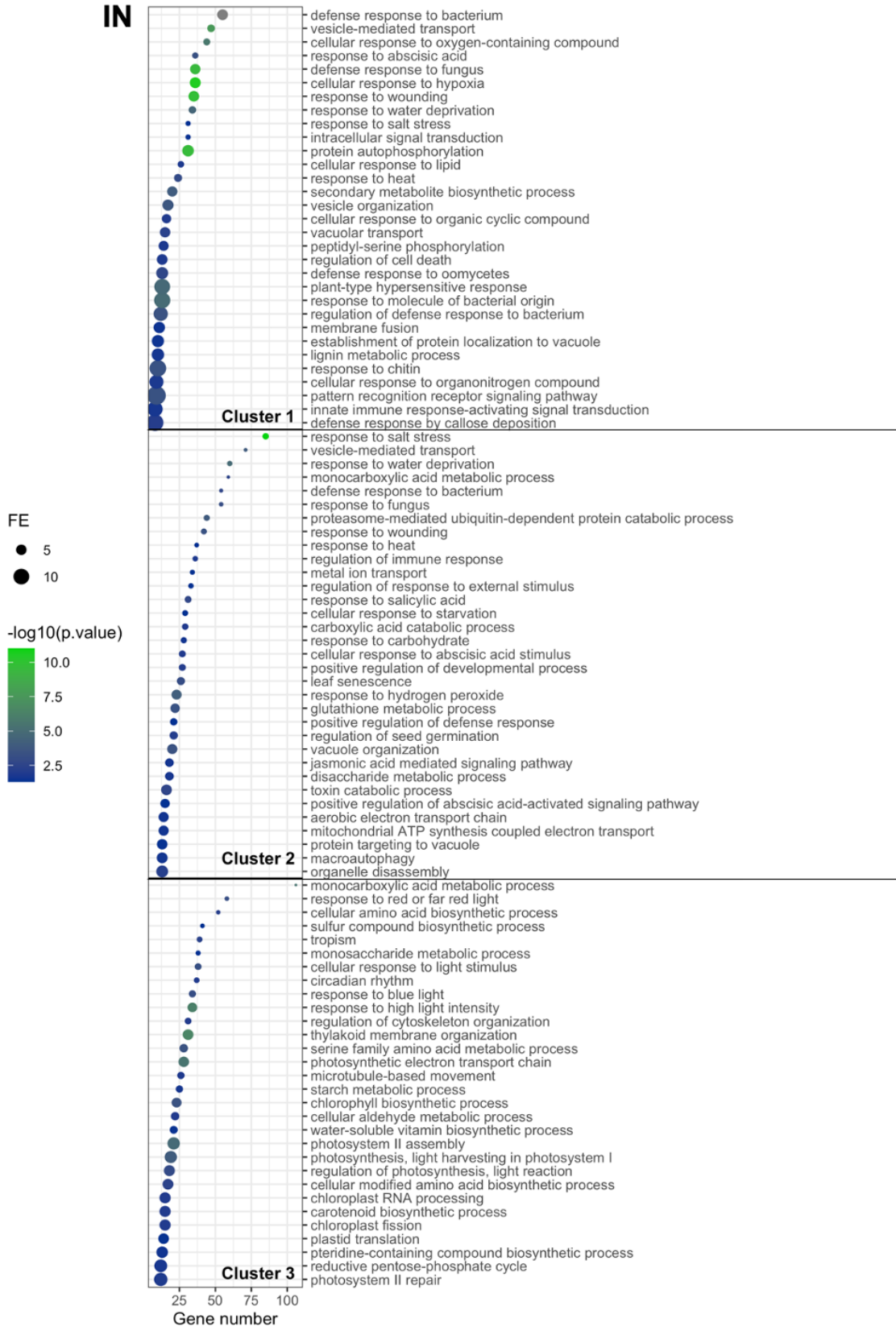
TIFY 10B; *JAR1*, Jasmonoyl--L-amino acid synthetase JAR1; *NPF6.2*, Protein NRT1/ PTR

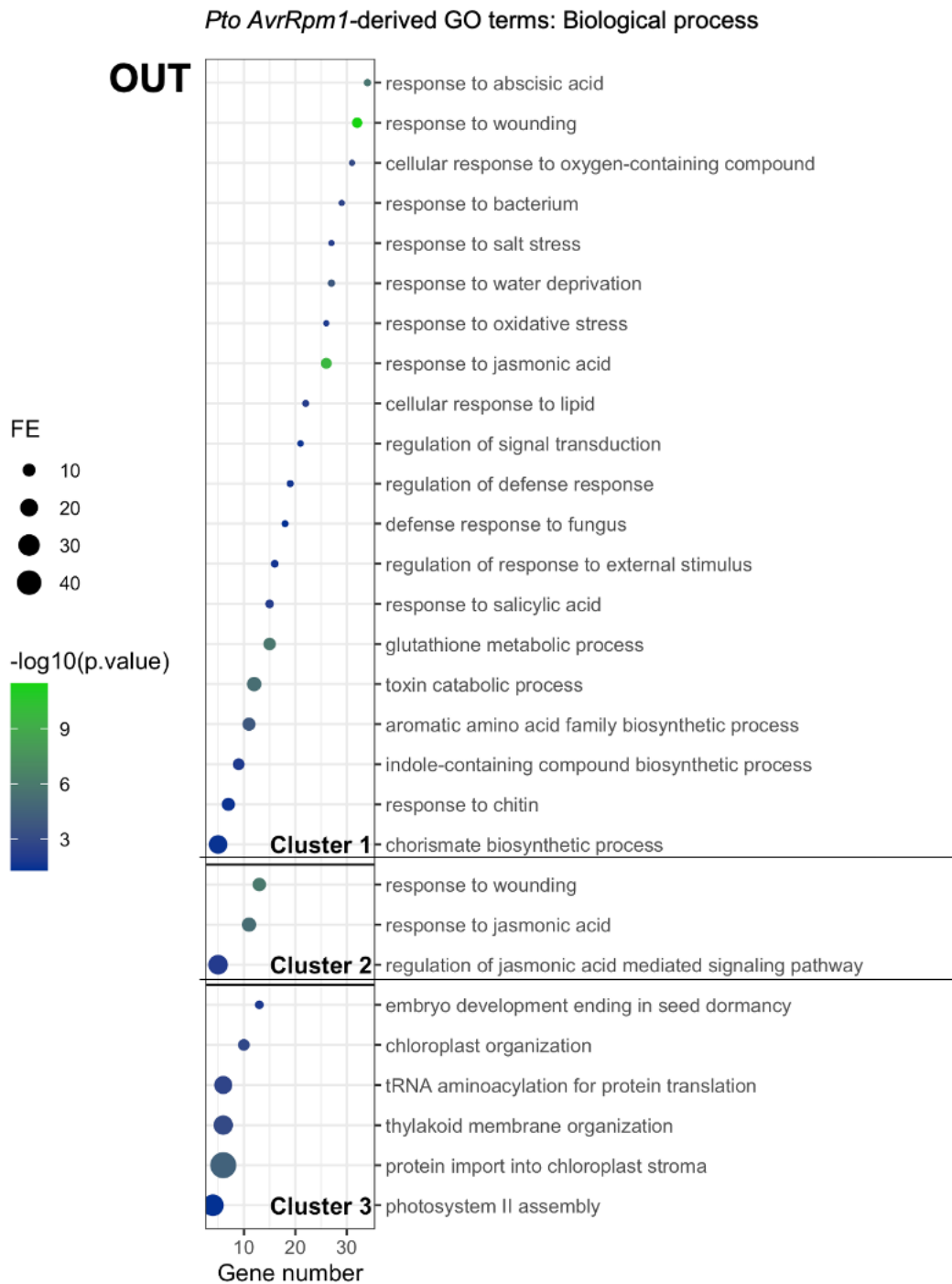
FAMILY 6.2

**Figure S6.**

**A**

*Pto AvrRpm1*-derived clusters GO terms: Biological process



**B**

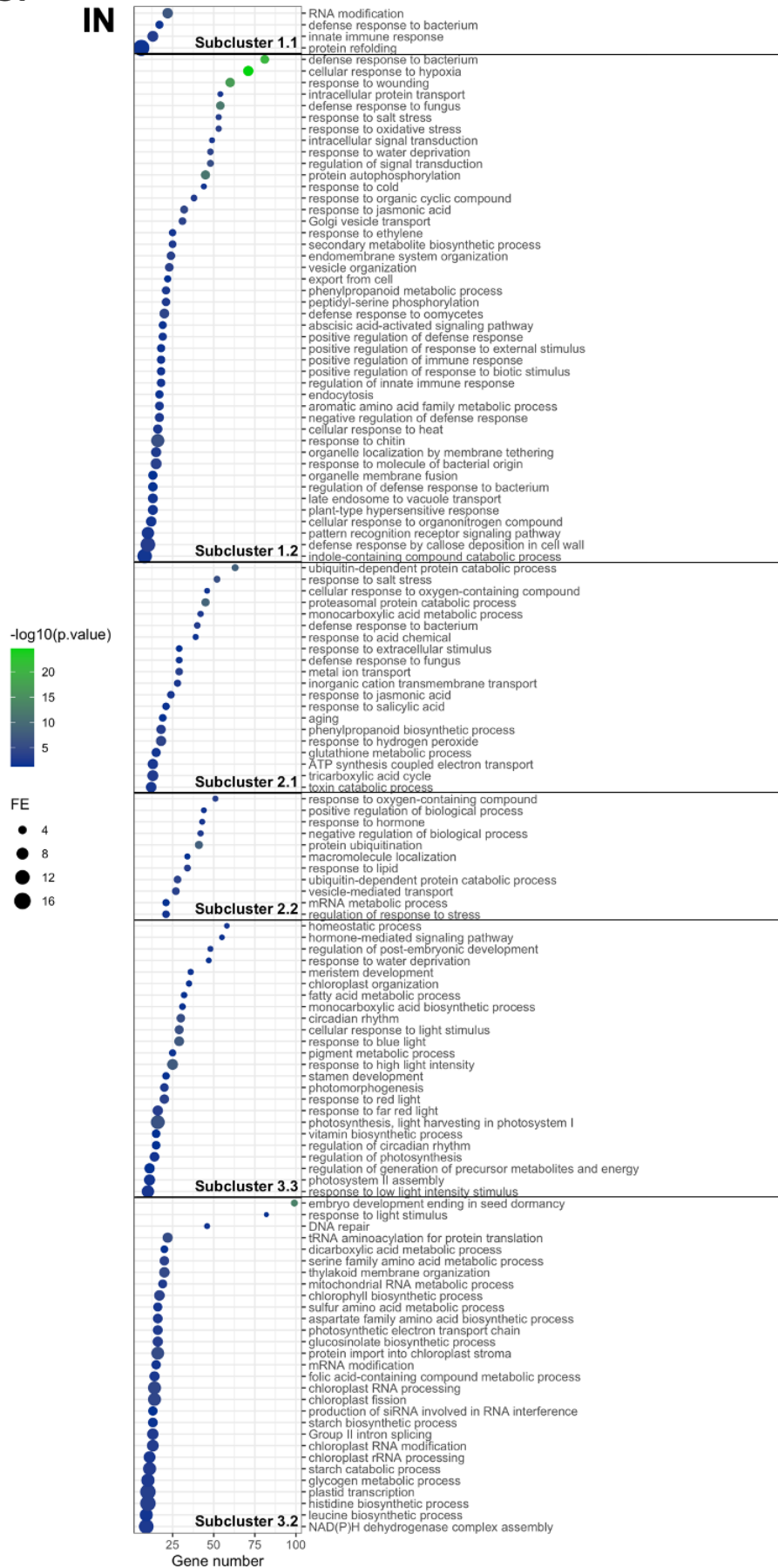
**Figure S6.** GO terms representing enriched biological processes derived from each cluster in *Pto AvrRpm1*-treated plants. GO term enrichment analysis was performed on those genes that had a membership score value (MSV) above or equal to 0.7 (see Materials and Methods). The most specific term from each family provided by PANTHER was plotted along with their corresponding gene number, fold enrichment (FE) and adj p value (Bonferroni Correction for

multiple testing) represented as  $\log_{10}$ . Only GO Terms with a FE above 2 and adj p value below 0.05 were plotted. Enriched GO terms from cluster I (2,937 genes; MSV > 0.7 → 1069 genes), cluster II (4,183 genes; MSV > 0.7 → 2613 genes) and cluster III (6,428 genes; MSV > 0.7 → 4885 genes) at the IN area (**A**) in *Pto AvrRpm1*-treated plants were predominantly linked to processes related to immunity, protein turnover and photosynthesis, respectively. At the OUT area (**B**), enriched GO terms from cluster I (1,552 genes; MS > 0.7 → 747 genes) and II (1,100 genes; MS > 0.7 → 184) suggest the importance of processes related to hormonal regulation in by-stander cells, whereas genes comprising cluster III (925 genes; MS > 0.7 → 181 genes) infer that photosynthesis and rearrangements in the chloroplast occur similarly compared to mock-treated samples at the OUT area

**Figure S7**

**Mock-derived clusters GO terms: Biological process**

**A**





B

Mock-derived clusters GO terms: Biological process

OUT

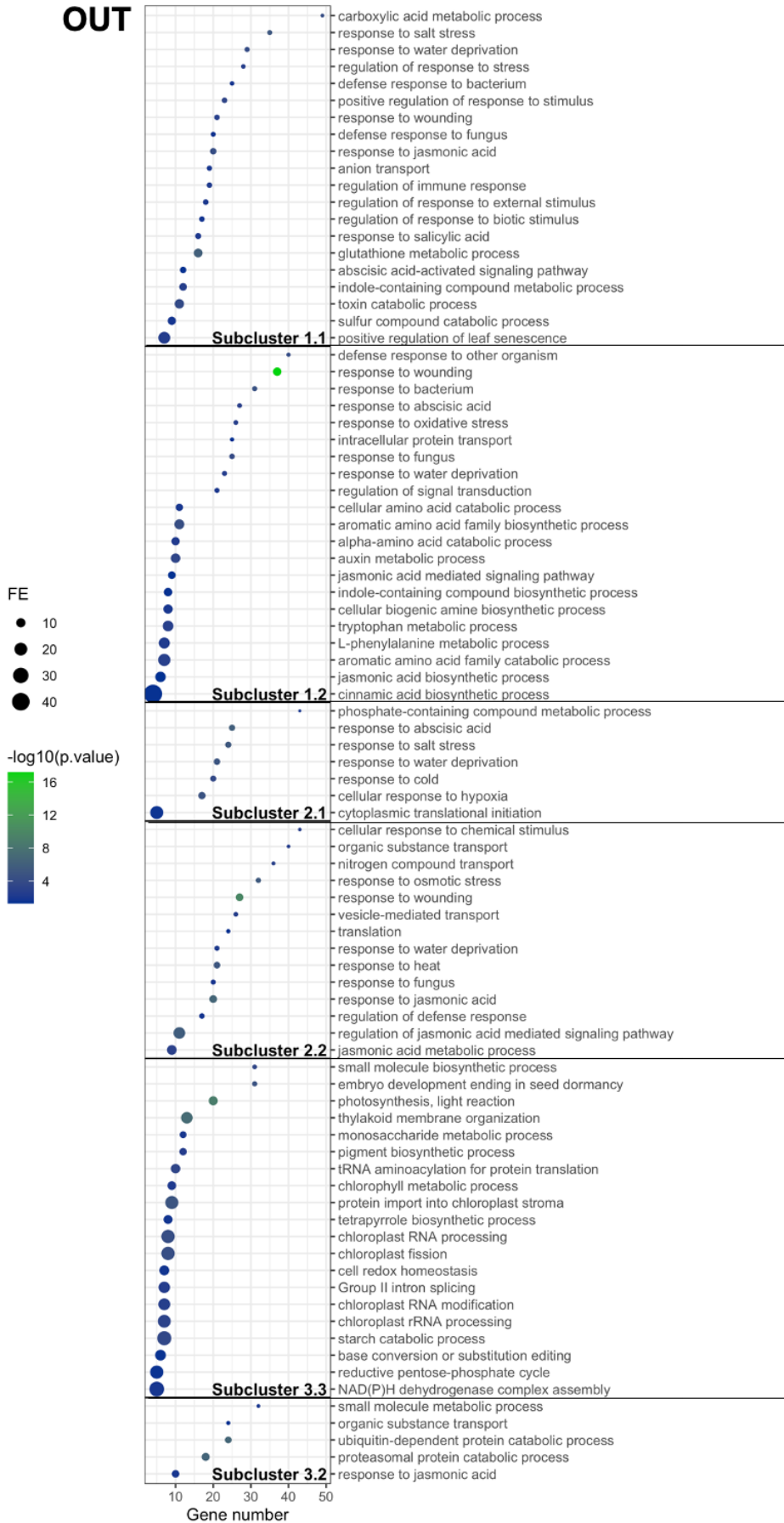


**Figure S7.** GO terms representing enriched biological processes derived from each sub-cluster in mock-treated plants at the IN and OUT areas. From each cluster belonging to mock-treated samples, GO term enrichment analysis was performed on those genes that had a membership score value (MSV) above or equal to 0.7 at the IN (a) and OUT areas (b). The most specific term from each family term provided by PANTHER was plotted along with their corresponding gene number, fold enrichment and adj p value (Bonferroni Correction for multiple testing) represented as  $\log_{10}$ . Only GO Terms with a fold enrichment above 2 and adj p value below 0.05 were plotted. **(A)** Sub-cluster 1.1 (638 genes; MSV  $\geq 0.7 \rightarrow$  467 genes), sub-cluster 1.2 (2299 genes; MSV  $\geq 0.7 \rightarrow$  1942 genes), sub-cluster 2.1 (2570 genes; MSV  $\geq 0.7 \rightarrow$  1573 genes), sub-cluster 2.2 (1613 genes; MSV  $\geq 0.7 \rightarrow$  649 genes), sub-cluster 3.1 (3172 genes; MSV  $\geq 0.7 \rightarrow$  2391 genes), sub-cluster 3.2 (3256 genes; MSV  $\geq 0.7 \rightarrow$  2557 genes). **(B)** Sub-cluster 1.1 (850 genes; MSV  $\geq 0.7 \rightarrow$  319 genes), sub-cluster 1.2 (702 genes; MSV  $\geq 0.7 \rightarrow$  183 genes), sub-cluster 2.1 (453 genes; MSV  $\geq 0.7 \rightarrow$  286 genes), sub-cluster 2.2 (647 genes; MSV  $\geq 0.7 \rightarrow$  389 genes), sub-cluster 3.1 (612 genes; MSV  $\geq 0.7 \rightarrow$  555 genes), sub-cluster 3.2 (313 genes; MSV  $\geq 0.7 \rightarrow$  257 genes).

## Figure S8

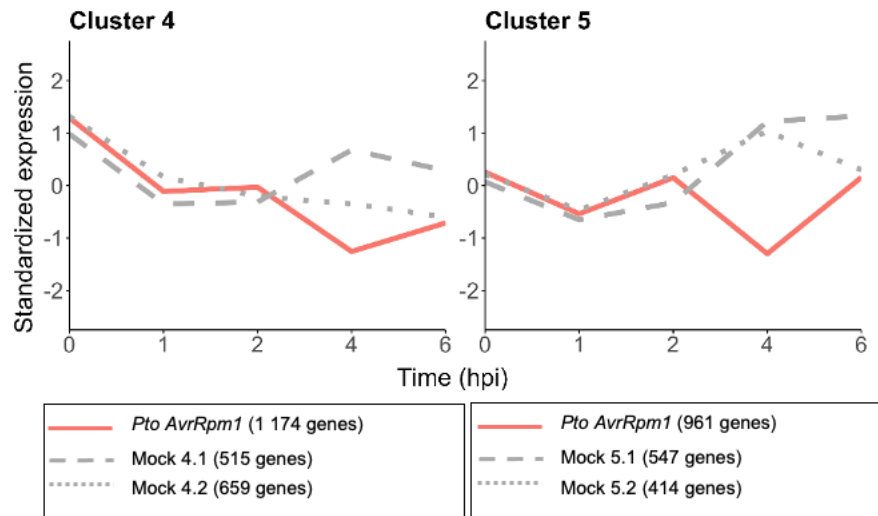
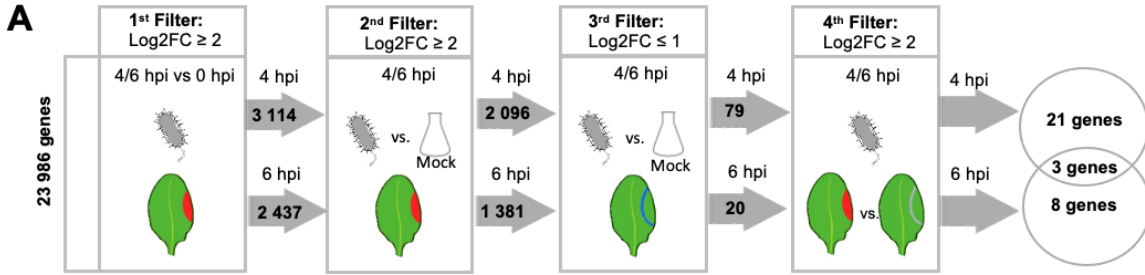


**Figure S8.** Clusters 4 (1,174 genes; MSV  $\geq 0.7 \rightarrow 57$  genes ) and 5 (961 genes; MSV  $\geq 0.7 \rightarrow 314$  genes) from *Pto AvrRpm1*-treated plants at the OUT area share similar expression profiles and do not contain any relevant enriched GO terms associated with biological processes, possibly due to low gene number.

**Figure S9**



**B**

|           | Gene ID   | 1 <sup>st</sup> Filter | 2 <sup>nd</sup> Filter | 3 <sup>rd</sup> Filter | 4 <sup>th</sup> Filter                    | Gene description  |
|-----------|-----------|------------------------|------------------------|------------------------|---|---|
| 4 hpi     | AT1G24095 | 4.03                   | 2.49                   | 0.77                   | 2.36                                      | Putative thiol-disulfide oxidoreductase DCC                 |
|           | AT1G27720 | 3.51                   | 3.01                   | 0.94                   | 2.55                                      | Transcription initiation factor TFIID subunit 4 (TAF4)      |
|           | AT1G30270 | 2.59                   | 3.07                   | 0.67                   | 2.54                                      | CBL-interacting serine/threonine-protein kinase 23 (CIPK23) |
|           | AT1G31880 | 3.00                   | 3.27                   | 0.84                   | 2.56                                      | DZC domain containing protein (NLM9)                        |
|           | AT1G74810 | 3.70                   | 3.09                   | 0.90                   | 2.51                                      | Putative boron transporter 5 (BOR5)                         |
|           | AT1G79710 | 3.50                   | 2.94                   | 0.85                   | 2.11                                      | Probable folate-biopterin transporter 3                     |
|           | AT2G33120 | 2.74                   | 2.71                   | 0.86                   | 2.13                                      | Vesicle-associated membrane protein 722 (SAR1/VAMP722)      |
|           | AT2G39400 | 3.46                   | 2.38                   | -1.08                  | 3.61                                      | Alpha/beta-Hydrolases superfamily protein                   |
|           | AT3G04120 | 2.24                   | 2.29                   | 0.50                   | 2.01                                      | Glyceraldehyde-3-phosphate dehydrogenase (GAPC1)            |
|           | AT3G13782 | 3.38                   | 2.95                   | 0.83                   | 2.85                                      | Nucleosome assembly protein 1;4 (NAP 1;4)                   |
|           | AT3G28850 | 2.72                   | 2.16                   | 0.79                   | 2.14                                      | Glutaredoxin family protein                                 |
|           | AT3G60680 | 2.03                   | 2.87                   | 0.70                   | 2.05                                      | DUF641 family protein                                       |
|           | AT4G18050 | 4.47                   | 4.57                   | 0.79                   | 3.56                                      | P-glycoprotein 9 (PGP9)                                     |
|           | AT4G24160 | 2.66                   | 3.43                   | 0.99                   | 2.68                                      | 1-acylglycerol-3-phosphate O-acyltransferase                |
|           | AT4G30390 | 3.33                   | 3.42                   | 0.98                   | 2.54                                      | UDP-arabinopyranose mutase                                  |
|           | AT5G10820 | 3.55                   | 2.01                   | 0.72                   | 2.05                                      | Probable folate-biopterin transporter 6                     |
|           | AT5G18480 | 2.86                   | 2.54                   | 0.94                   | 2.04                                      | Inositol phosphorylceramide glucuronosyltransferase1(IPUT1) |
|           | AT5G20000 | 3.67                   | 2.50                   | 0.79                   | 2.25                                      | 26S proteasome regulatory subunit 8 homolog B (RPT6B)       |
|           | AT2G36580 | 2.51                   | 2.58                   | 0.77                   | 2.36                                      | Pyruvate kinase   |
| AT5G37710 | 2.14      | 2.29                   | 0.56                   | 2.02                   | alpha/beta-Hydrolases superfamily protein |   |
| AT5G54650 | 4.05      | 3.21                   | 0.99                   | 2.21                   | Formin-like protein 5 (FH5)               |   |
| 6 hpi     | AT1G78380 | 3.88                   | 3.45                   | 0.96                   | 3.88                                      | Glutathione S-transferase U19 (GSTU19)                      |
|           | AT3G02875 | 3.35                   | 2.92                   | 0.93                   | 3.35                                      | IAA-amino acid hydrolase (ILR1)                             |
|           | AT3G06420 | 3.41                   | 3.14                   | 0.83                   | 3.41                                      | Autophagy-related protein 8h (ATG8H)                        |
|           | AT3G17420 | 2.75                   | 2.63                   | 0.72                   | 2.75                                      | Probable receptor-like protein kinase (GPK1)                |
|           | AT5G05730 | 4.10                   | 2.90                   | 0.96                   | 4.10                                      | Anthranilate synthase alpha subunit 1 (ASA1)                |
|           | AT5G14730 | 3.47                   | 3.17                   | -1.41                  | 3.47                                      | Unknown protein   |
|           | AT5G16910 | 2.26                   | 2.83                   | 0.96                   | 2.26                                      | Cellulose synthase-like protein D2 (CSLD2)                  |
| AT5G17760 | 3.64      | 2.54                   | 0.98                   | 3.64                   | AAA-ATPase                                |   |
| 4/6 hpi   | AT5G20910 | 2.78                   | 2.59                   | 0.74                   | 2.06                                      | E3 ubiquitin-protein ligase (AIP2)                          |
|           | AT2G31390 | 2.55                   | 2.73                   | 0.84                   | 2.04                                      | Probable fructokinase-1                                     |
|           | AT5G56350 | 3.20                   | 2.55                   | 0.79                   | 2.22                                      | Pyruvate kinase   |

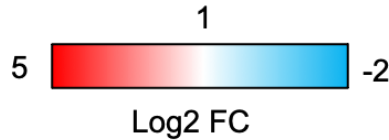
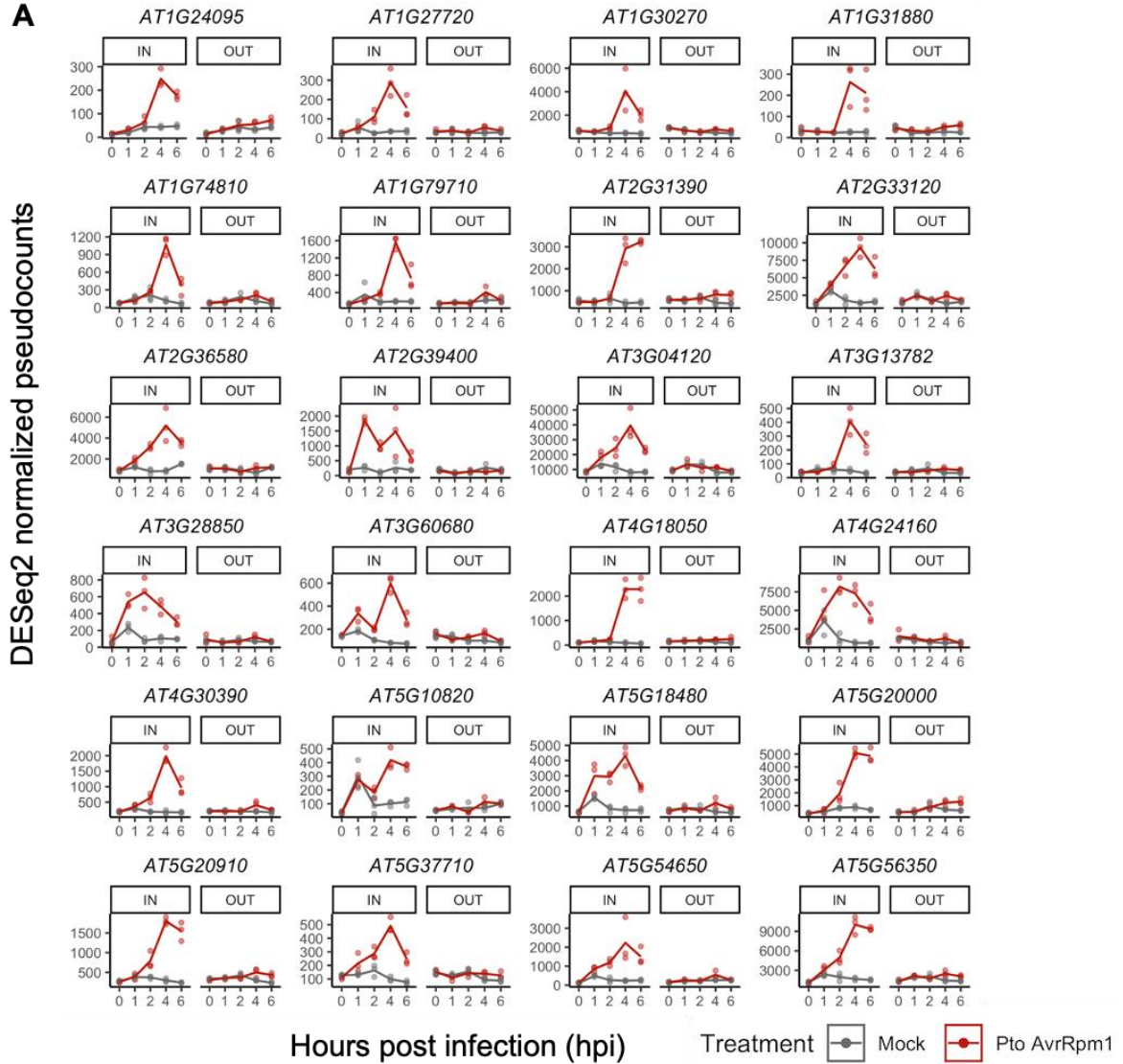


**Figure S9.** List of *in silico* HR indicators obtained after filtering at 4 and 6 hpi. **(A)** Briefly, we firstly selected genes that were upregulated ( $\log_2FC > 2$ ) after *Pto AvrRpm1* infection at 4 or 6 hpi vs 0 hpi. From the genes that complied with this first filter, we selected those that were specifically upregulated in *Pto AvrRpm1*-infected vs mock-inoculated samples at 4 or 6 hpi ( $\log_2FC > 2$ ). From the genes that complied these criteria, we kept those with a  $\log_2FC < 1$  at the OUT area in *Pto AvrRpm1*-infected vs mock-inoculated samples at 4 or 6 hpi. Finally, from the genes that met those three criteria, we kept those that were differentially upregulated at the IN area compared to the OUT area in *Pto AvrRpm1*-infected plants. **(B)**  $\log_2FC$ s resulting from pairwise comparisons in the 1<sup>st</sup>, 2<sup>nd</sup>, 3<sup>rd</sup> and 4<sup>th</sup> filters applied are indicated for each gene marker along with its corresponding gene description.

**Figure S10**

**A**



**B**

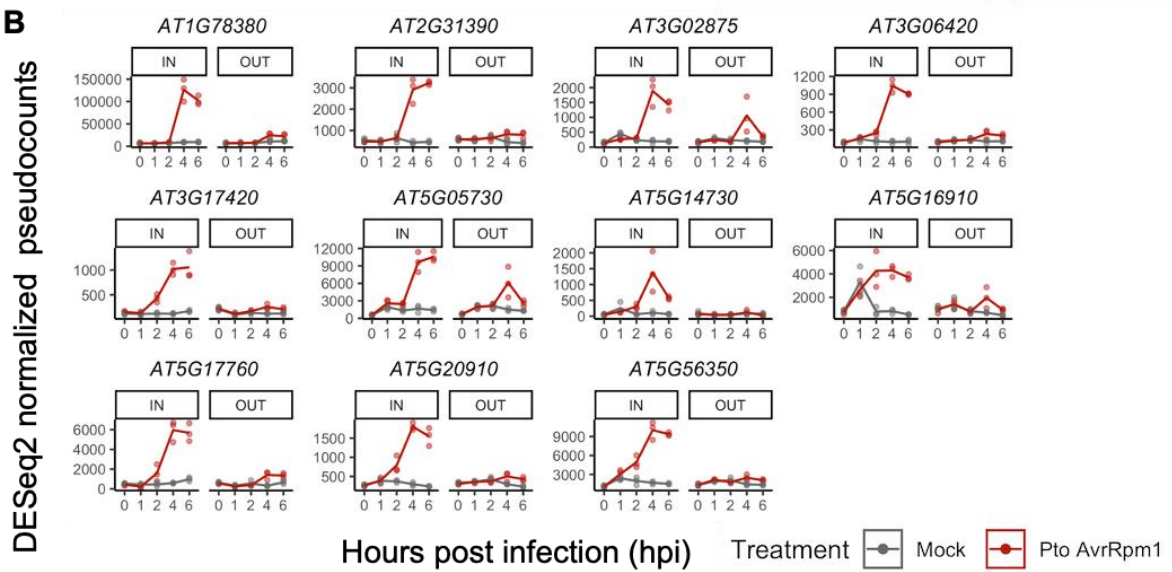
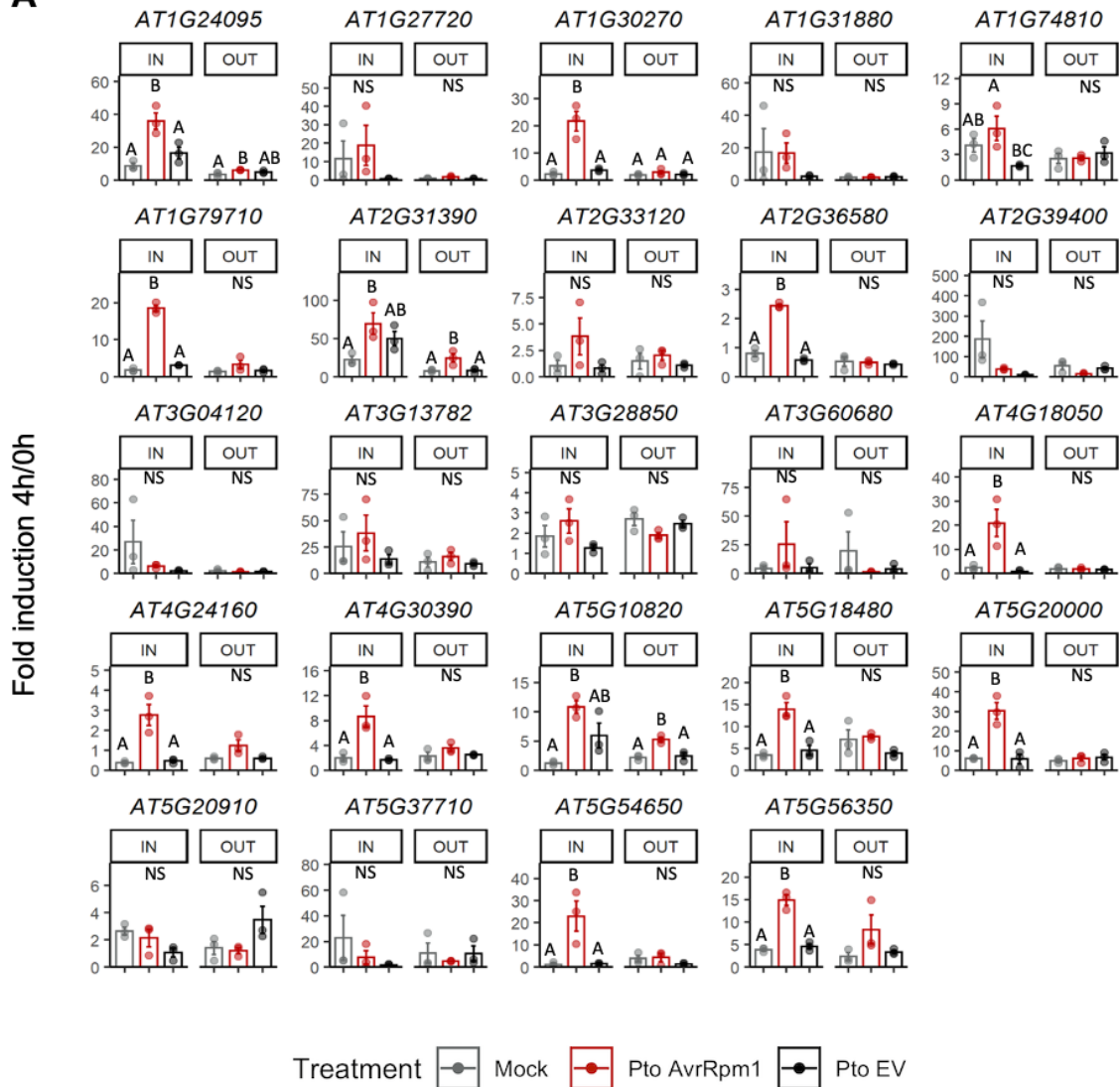


**Figure S10.** RNA-seq expression profiles of 4 (**A**) and 6 (**B**) hour candidate HR indicators at the IN and OUT areas of infection. Gene expression of genes from *Pto-AvrRpm1* or mock-infected plants is represented as DESeq2 pseudocounts.

**Figure S11**

**A**



**B**

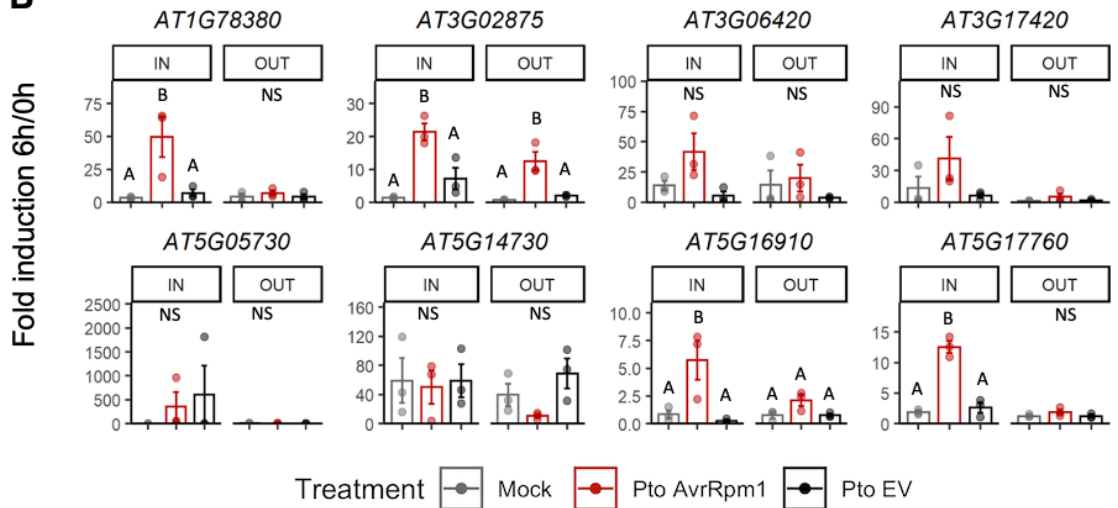




**Figure S11.** RT-qPCR of 4- and 6-hour transcriptional HR indicators at IN and OUT areas upon treatment with either mock, *Pto AvrRpm1* or *Pto* DC3000 EV. Relative expression levels to the housekeeping gene *EIF4a* were represented as fold induction between 4 (**A**) or 6 (**B**) and 0 hpi. Error bars represent standard error of the mean from three independent experiments. Letters indicate statistically significant differences between treatments following one-way ANOVA with Tukey's HSD test ( $\alpha = 0.05$ ) performed independently at IN and OUT. NS (non-significant after one-way ANOVA). Exact p values are provided in **Table S5**.

**Figure S12**

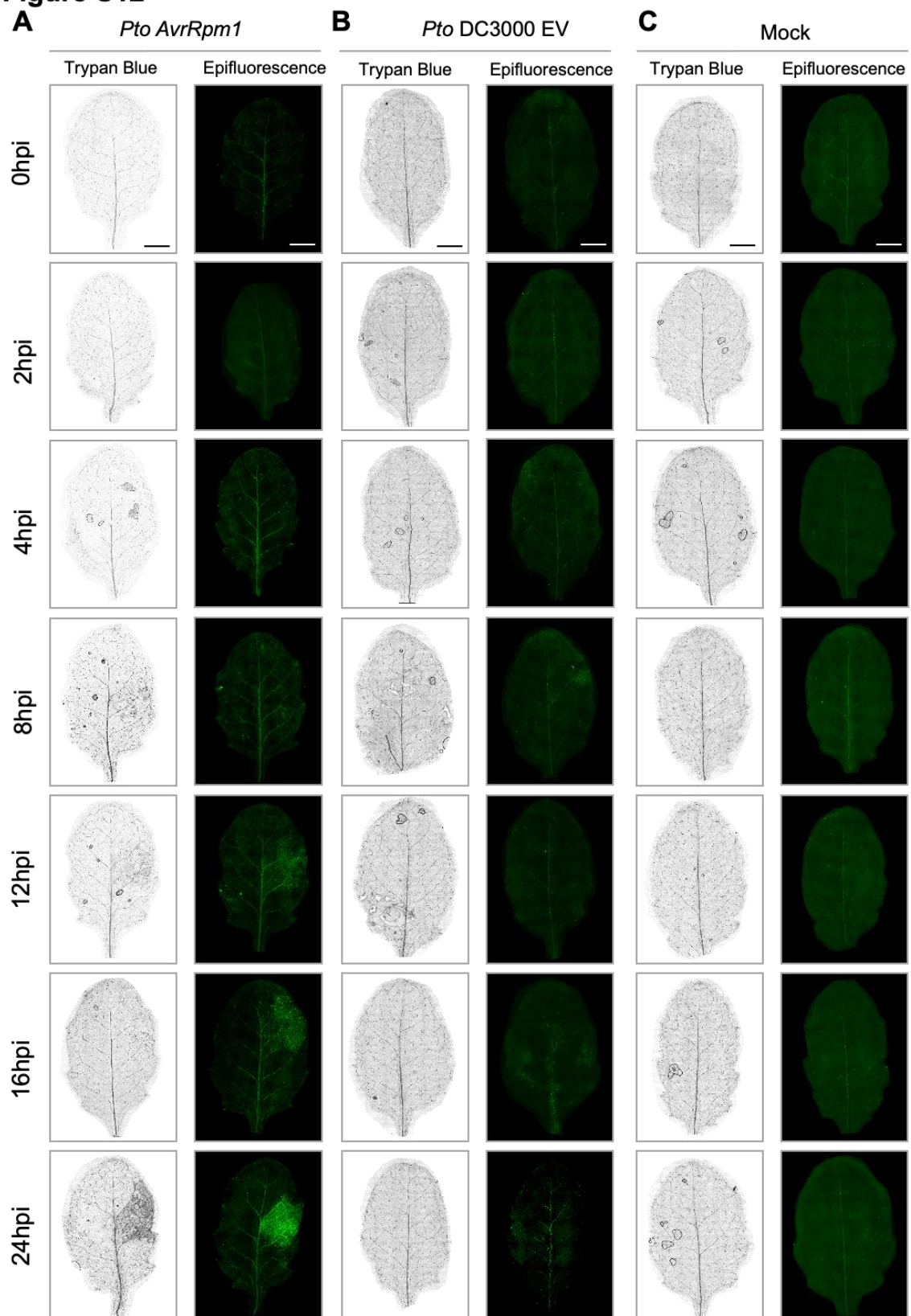


**Figure S12.** Time course imaging of *pAT5G17760::NLS-3xGFP* Arabidopsis transgenic leaves infected with *Pto AvrRpm1* (**A**), *Pto DC3000 EV* (**B**) or mock solution (10 mM MgCl<sub>2</sub>) (**C**). A small region of 4-week-old *pAT5G17760::NLS-3xGFP* leaves was syringe-infiltrated with *Pto* strains at  $1 \times 10^7$  colony-forming units (CFU)/ml (O.D<sub>600</sub> = 0.01). Fluorescent microscopy images were taken at 0, 2, 4, 8, 12, 16 and 24 hpi (right panels). Afterwards, leaves were subjected to trypan blue staining (left panels). Scale bar 3 mm.

**Figure S13**

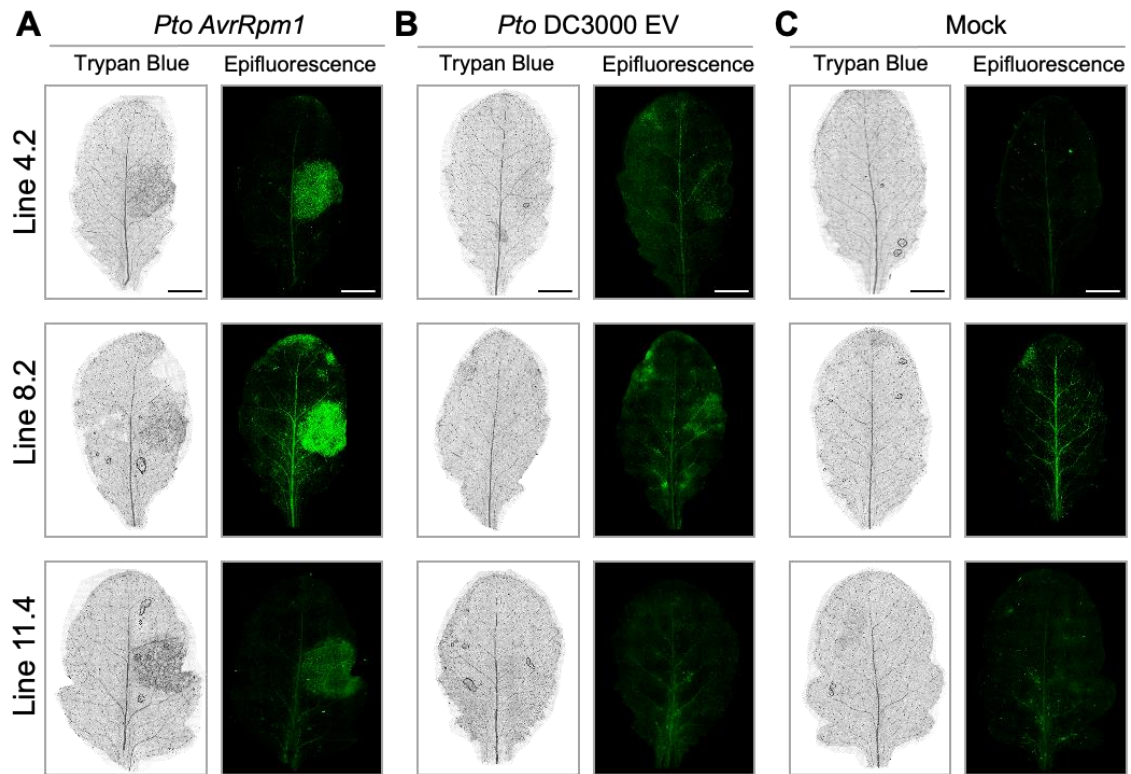
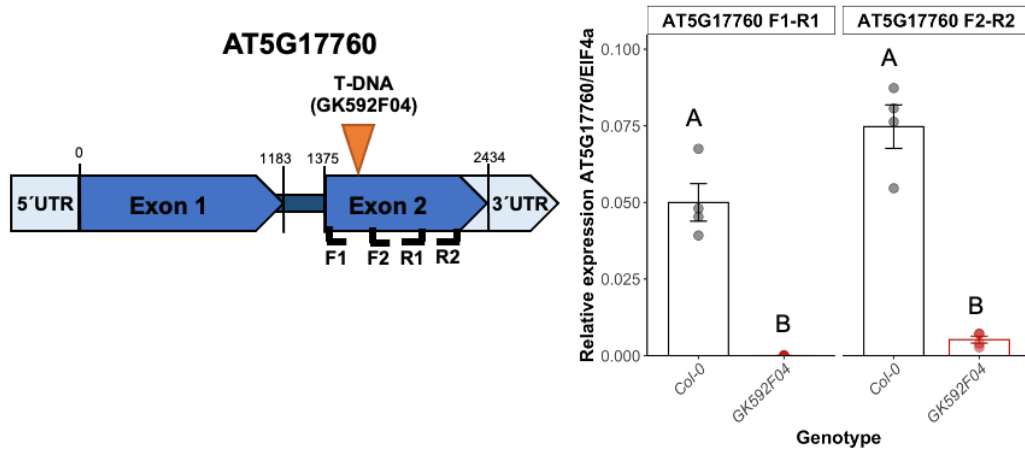


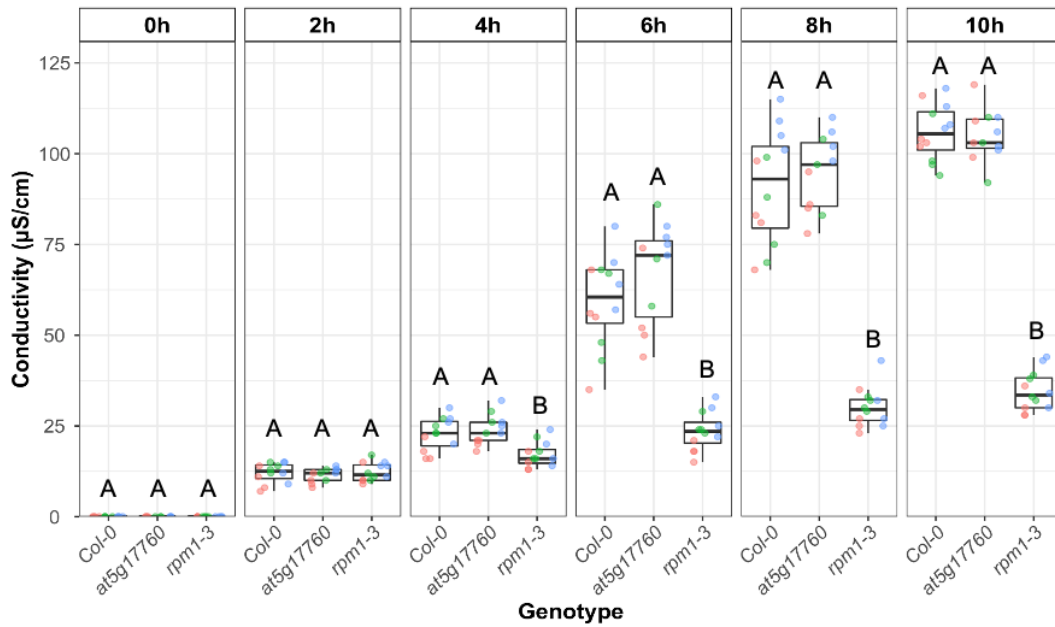
**Figure S13.** Activation of *pAT5G17760* in the syringe-infiltrated area occurred in several independent *pAT5G17760::3xGFP* transgenic lines. Leaves of Arabidopsis transgenics in the T2 generation were syringe infiltrated with *Pto AvrRpm1* (**A**), *Pto DC3000 EV* (**B**) at  $1 \times 10^7$  colony-forming units (CFU)/ml ( $O.D_{600} = 0.01$ ) and imaged at 16 hpi. Mock solution was used as a control (**C**). Images in left panels are leaves stained with trypan blue whereas images in right panels are leaves under the epifluorescence microscope. Scale bars 3 mm.

**Figure S14**

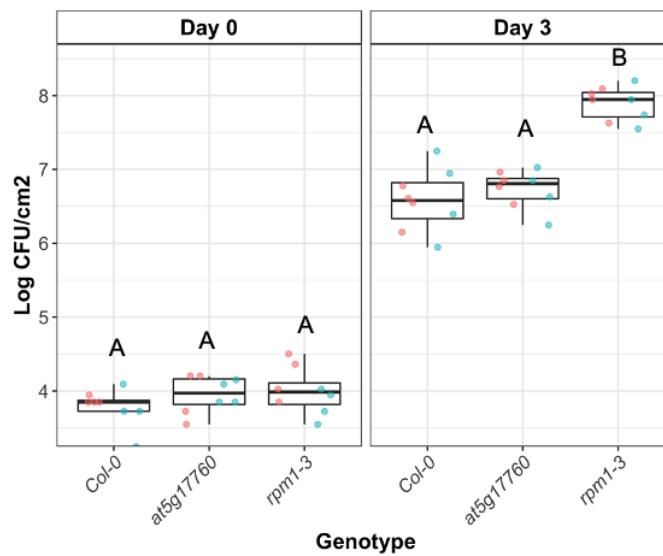
**A**



**B**



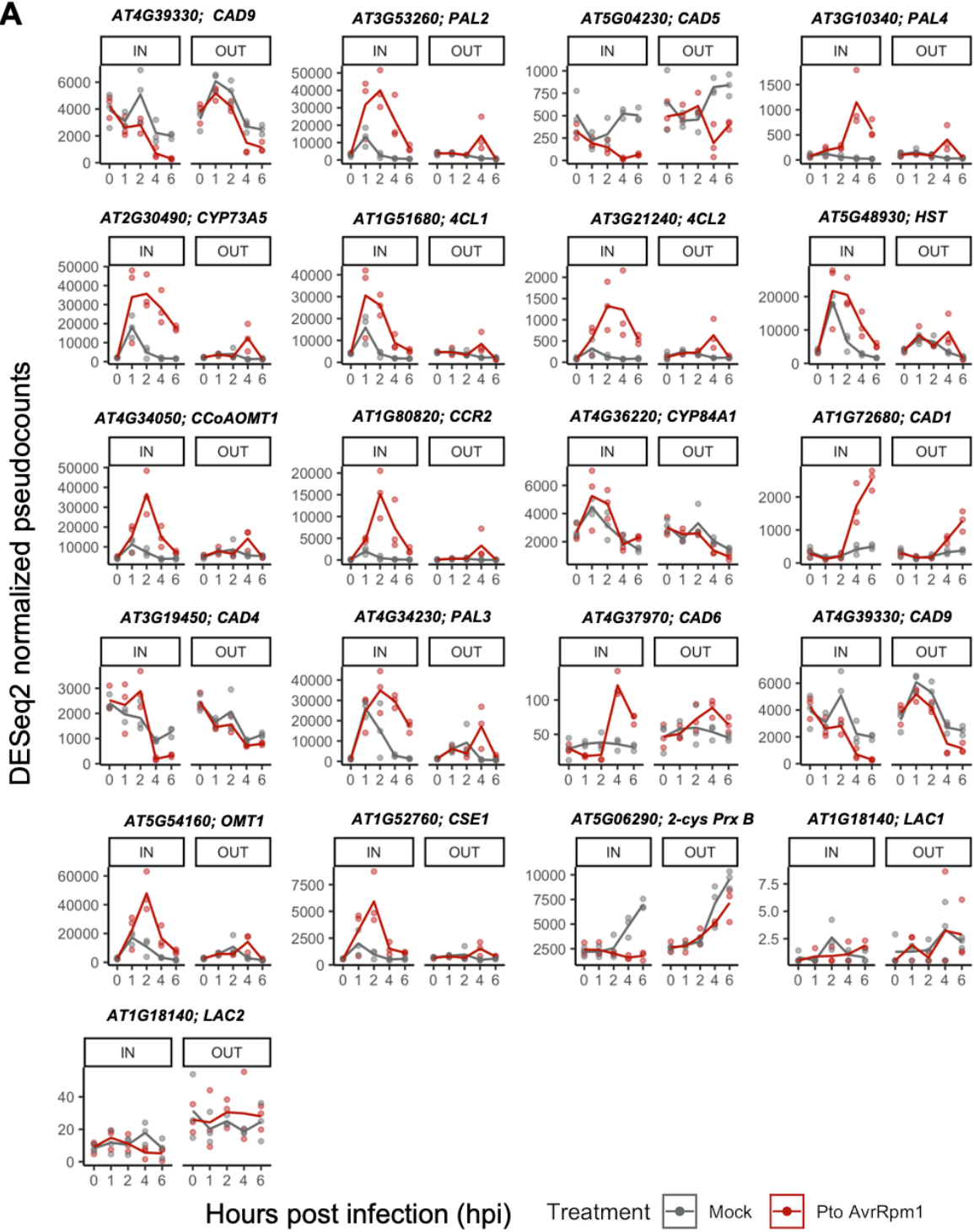
**C**



**Figure S14. Disease resistance and cell death triggered by avirulent *Pto AvrRpm1* strain is not compromised in *Arabidopsis* mutant lacking AT5G17760.** (A) Scheme of AT5G17760 gene indicating the position of the T-DNA insertion in GK-59F04 mutant line (left panel) and RT-qPCR of two regions (F1-R1 and F2-R2) of exon 2 in Col-0 and GK-59F04 plants. RT-qPCR data is represented as relative expression levels of *AT5G17760* to the housekeeping gene *EIF4a* (right panel). Error bars represent standard error of the mean from four biological replicates. Letters indicate statistically significant differences between treatments following a Welch Two Sample t-test. Exact p values are provided in **Table S5**. (B-C) Four to 5 week-old Col-0, *at5g17760* and *rpm1-3* plants were syringe-infiltrated with *Pto* DC3000 *AvrRpm1* at O.D<sub>600</sub>=0.05 for electrolyte leakage (b) and O.D<sub>600</sub>=0.001 for bacterial growth assays (C), *rpm1-3* mutant is used as a negative control since it is defective in the cognate NLR that recognizes the effector AvrRpm1. (B) Conductivity measurements of electrolyte leakage from dying cells were recorded at 0, 4, 6, 8 and 10 hpi. Dots represent data from 3 biological replicates (represented in different colors) consisting of 4 technical replicates each with 2 leaf discs measured per replicate. Letters indicate statistically significant differences between genotypes following one-way ANOVA with Tukey's HSD test performed at each time point. Exact p values are provided in **Table S5**. (C) Bacterial growth at 0 and 3 days post-infection (dpi) was measured in Col-0, *at5g17760* and *rpm1-3*. Dots represent bacterial CFU (colony-forming units) per cm<sup>2</sup> from 2 biological replicates (represented in different colors) consisting of 4 technical replicates each with 2 leaf discs measured per replicate. Letters indicate statistically significant differences between genotypes following one-way ANOVA with Tukey's HSD test performed at 0 and 3 days post infection. Exact p values are provided in **Table S5**.

**Figure S15**

**A**



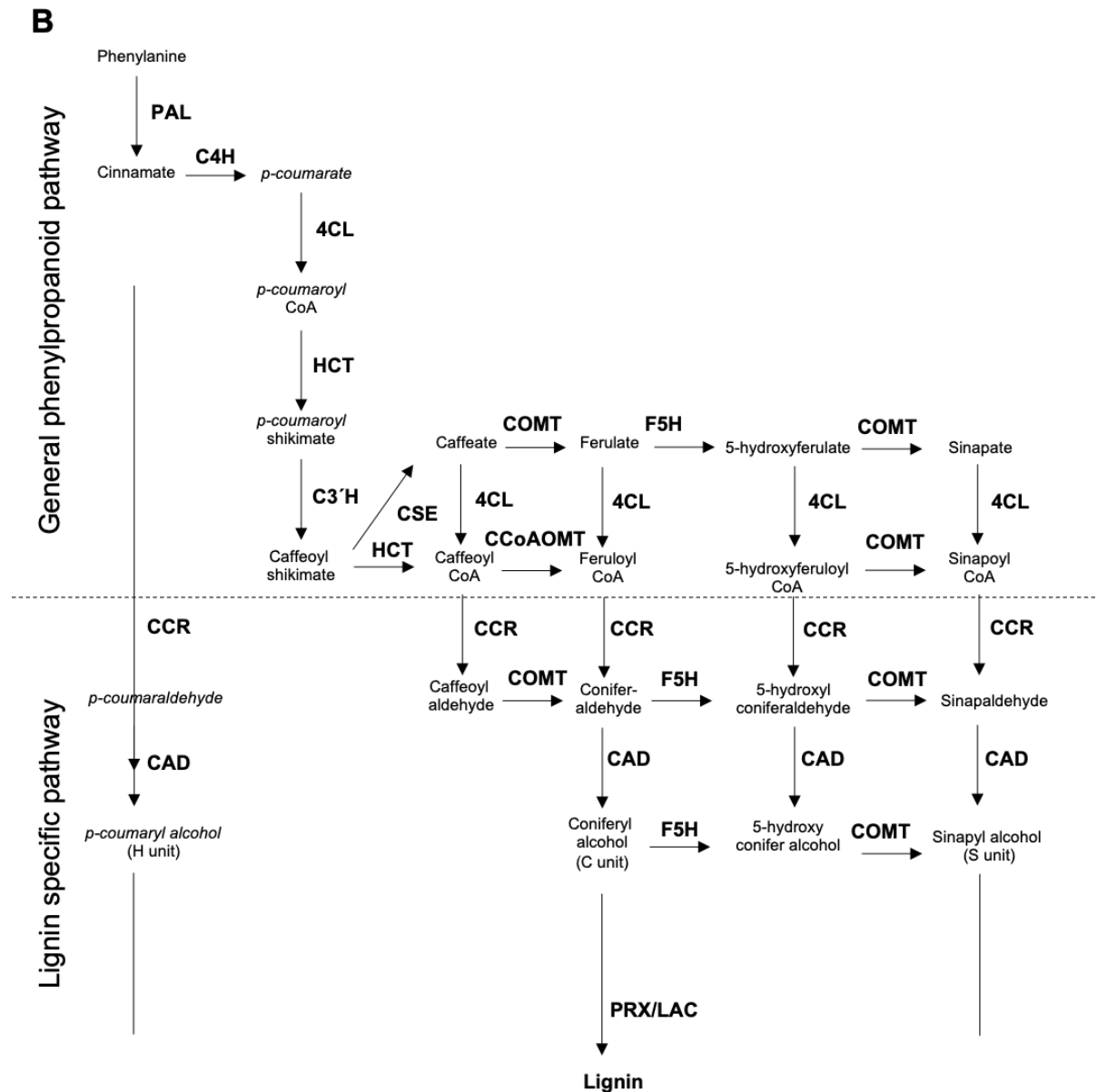


**Figure S15. RNA-seq expression profiles of genes involved in lignin biosynthesis.**

(A) Gene expression of genes from *Pto-AvrRpm1* or mock-infected plants is represented as DESeq2 pseudocounts. (B) Scheme of lignin biosynthesis in plants. Black arrow indicates the canonical lignin biosynthesis in plants. Bold font indicates enzymes involved in the different steps of the pathway. PAL, phenylalanine ammonia-lyase; C4H, cinnamate 4-hydroxylase; 4CL, 4-coumarate: CoA ligase; HCT, quinate shikimate *p*-hydroxycinnamoyltransferase;



C3'H, *p*-coumaroylshikimate 3'-hydroxylase; CCoAOMT, caffeoyl-CoA *O*-methyltransferase; CCR, cinnamoyl-CoA reductase; F5H, ferulate 5-hydroxylase; CAD, cinnamyl alcohol dehydrogenase; COMT, caffeic acid *O*-methyltransferase; CSE, caffeoyl shikimate esterase; PRX, peroxidase; LAC, laccase (Adapted from Meng Chie et al., 2018)

**Figure S16**

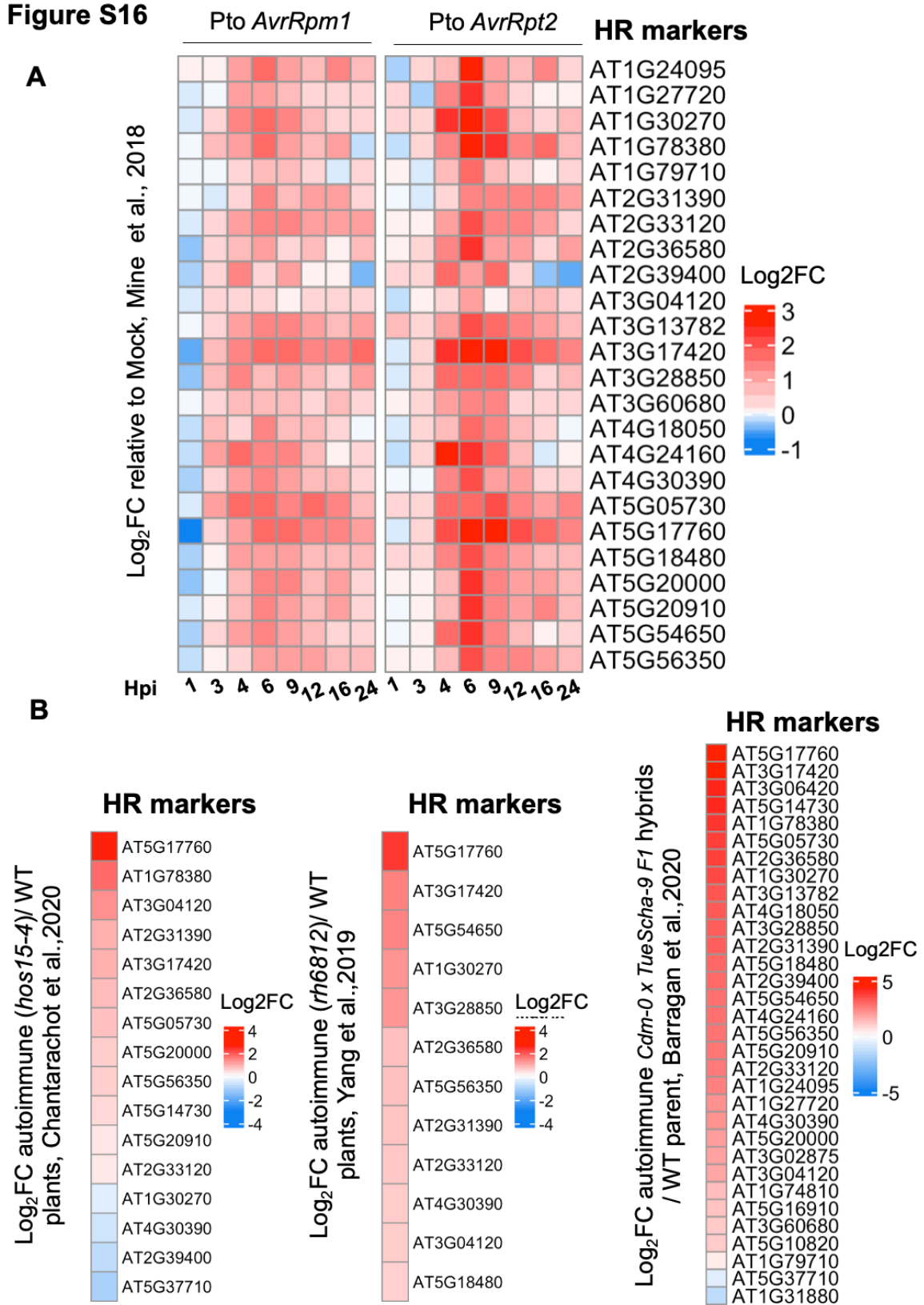


**Figure S16. Transcriptional regulation of HR markers found in this study compared to RNA-seq data sets from plants undergoing ETI and autoimmunity.** (A) HR markers found in this study were searched in Mine et al., 2018. In pairwise comparisons between infection with ETI-causing bacteria (*Pto AvrRpm1* and *Pto AvrRpt2*) and mock, only genes with high statistical confidence ( $q$  value  $\leq 0,01$ ) in at least one time point were plotted on a heatmap indicating  $\text{Log}_2\text{FC}$  for the different times tested in their study. (B) HR markers found in this study were searched in RNA-seq data sets of Arabidopsis *hos15-4* (Yang et al.,2019), *rh6812* autoimmune plants (Chantarachot et al., 2020) and *Cdm-0 x TueScha-9 F1* hybrids (Barragan et al., 2020). Genes with high statistical confidence in their data sets (FDR  $<0.05$ ) were plotted on a heatmap indicating  $\text{Log}_2\text{FC}$  between expression of WT (Col-0) and autoimmune plants.

**Supplementary tables/dataset legends.**

**Table S1 (Associated to Figure 2A).** List of differentially expressed genes upon *Pto AvrRpm1* infection at each time point and tissue area.

**Table S2 (Associated to Figure S2).** List of genes constituting each GO term in Figure S2. GO term enrichment analysis of upregulated and downregulated genes at either IN or OUT areas. Only those GO terms exhibiting an FDR  $< 0.05$  after Bonferroni Correction for multiple testing and a fold enrichment above 2 are shown.

**Table S3 (Associated to Figure 2B).** List of genes that are upregulated upon *Pto AvrRpm1* at 4 and 6 hpi exclusively at IN, both at IN and OUT or exclusively at OUT.

**Table S4 (Associated to Figure 2C).** List of genes constituting each GO term in Figure 2C. GO term enrichment analysis of genes that are exclusively upregulated at either the IN or OUT area

upon *Pto AvrRpm1* infection. Only those GO terms exhibiting an FDR < 0.05 after Bonferroni Correction for multiple testing and a fold enrichment above 2 are shown.

**Table S5 (Associated to Figure 1C, Figure 4, Figure 5, Figure S11 and Figure S14).** Tukey HSD p-values and Welch two sample t-test p-values obtained from statistical tests applied in the study.

**Table S6 (Associated to Figure 3A).** List of genes comprising each cluster derived from *Pto AvrRpm1* and mock-treated plants along with their corresponding MSV at IN.

**Table S7 (Associated to Figure 3B).** List of genes comprising each cluster derived from *Pto AvrRpm1* and mock-treated plants along with their corresponding MSV at OUT.

**Table S8 (Associated to Figure S6A).** List of genes constituting each GO term in Figure S6A. GO term enrichment analysis of genes from clusters of *Pto AvrRpm1*-inoculated plants at the IN area with a MSV of 0.7 or above. Only those GO terms exhibiting an FDR < 0.05 after Bonferroni Correction for multiple testing and a fold enrichment above 2 are shown.

**Table S9 (Associated to Figure S6B).** List of genes constituting each GO term in Figure S6B. GO term enrichment analysis of genes from clusters of *Pto AvrRpm1*-inoculated plants at the OUT area with a MSV of 0.7 or above. Only those GO terms exhibiting an FDR < 0.05 after Bonferroni Correction for multiple testing and a fold enrichment above 2 are shown.

**Table S10 (Associated to Figure S7A).** List of genes constituting each GO term in Figure S5. GO term enrichment analysis of genes from clusters of mock-inoculated plants at the IN area

with a MSV of 0.7 or above. Only those GO terms exhibiting an FDR < 0.05 after Bonferroni Correction for multiple testing and a fold enrichment above 2 are shown.

**Table S11 (Associated to Figure S7B).** List of genes constituting each GO term in Figure S6. GO term enrichment analysis of genes from clusters of mock-inoculated plants at the OUT area with a MSV of 0.7 or above. Only those GO terms exhibiting an FDR < 0.05 after Bonferroni Correction for multiple testing and a fold enrichment above 2 are shown.

**Table S12.** Primers used in this study and primer concentration for RT-qPCRs.

**Table S13.** RT-qPCR results in numeric format along with Cp values of Targets and Cp value of Reference housekeeping gene.

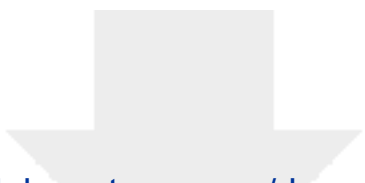


[Click here to access/download](#)

**Dataset**

**Table S1\_Primers.xlsx**





Click here to access/download  
**Dataset**  
Table S2\_Statistics.xlsx

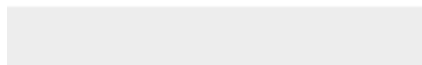
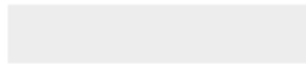




[Click here to access/download](#)

**Dataset**

**Table S3\_DEGs.xlsx**



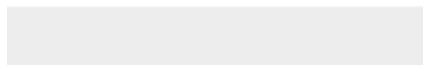




[Click here to access/download](#)

**Dataset**

**Table S4\_DEGsINvsOUT.xlsx**

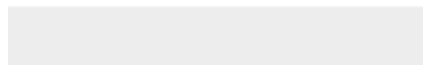




[Click here to access/download](#)

**Dataset**

**Table S5\_GOsINvsOUT.xlsx**





[Click here to access/download](#)

**Dataset**

Table S6\_GeneListClusters\_IN.xlsx





[Click here to access/download](#)

**Dataset**

[Table S7\\_GOsClusters\\_IN\\_PtoAvrRpm1.xlsx](#)





[Click here to access/download](#)

**Dataset**

[Table S8\\_GOsClusters\\_OUT\\_PtoAvrRpm1.xlsx](#)





[Click here to access/download](#)

**Dataset**

Table S9\_GOsDEGs.xlsx

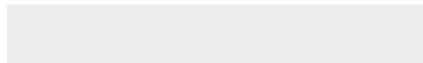




[Click here to access/download](#)

**Dataset**

[Table S10\\_GOsCluster\\_IN\\_Mock.xlsx](#)

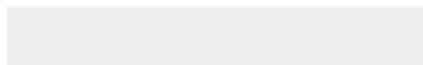




[Click here to access/download](#)

**Dataset**

[Table S11\\_GOsCluster\\_OUT\\_Mock.xlsx](#)



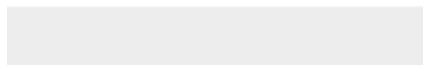




[Click here to access/download](#)

**Dataset**

**Table S12\_Primers.xlsx**





[Click here to access/download](#)

**Dataset**

Table S13\_qPCR\_RawData.xlsx

